ALFRED-WEGENER-INSTITUT
HELMHOLTZ-ZENTRUM FÜR POLAR- UND MEERESFORSCHUNG

757
2021

Berichte
zur Polar- und Meeresforschung

Reports on Polar and Marine Research

The Expedition PS126 of the Research Vessel POLARSTERN to the Fram Strait in 2021

Edited by

Thomas Soltwedel
with contributions of the participants

HELMHOLTZ

Die Berichte zur Polar- und Meeresforschung werden vom Alfred-Wegener-Institut, Helmholtz-Zentrum für Polar- und Meeresforschung (AWI) in Bremerhaven, Deutschland, in Fortsetzung der vormaligen Berichte zur Polarforschung herausgegeben. Sie erscheinen in unregelmäßiger Abfolge.

Die Berichte zur Polar- und Meeresforschung enthalten Darstellungen und Ergebnisse der vom AWI selbst oder mit seiner Unterstützung durchgeführten Forschungsarbeiten in den Polargebieten und in den Meeren.

Die Publikationen umfassen Expeditionsberichte der vom AWI betriebenen Schiffe, Flugzeuge und Stationen, Forschungsergebnisse (inkl. Dissertationen) des Instituts und des Archivs für deutsche Polarforschung, sowie Abstracts und Proceedings von nationalen und internationalen Tagungen und Workshops des AWI.

Die Beiträge geben nicht notwendigerweise die Auffassung des AWI wider.

Herausgeber
Dr. Horst Bornemann

Redaktionelle Bearbeitung und Layout
Susan Amir Sawadkuhi

Alfred-Wegener-Institut
Helmholtz-Zentrum für Polar- und Meeresforschung
Am Handelshafen 12
27570 Bremerhaven
Germany

www.awi.de
www.awi.de/reports

The Reports on Polar and Marine Research are issued by the Alfred Wegener Institute, Helmholtz Centre for Polar and Marine Research (AWI) in Bremerhaven, Germany, succeeding the former Reports on Polar Research. They are published at irregular intervals.

The Reports on Polar and Marine Research contain presentations and results of research activities in polar regions and in the seas either carried out by the AWI or with its support.

Publications comprise expedition reports of the ships, aircrafts, and stations operated by the AWI, research results (incl. dissertations) of the Institute and the Archiv für deutsche Polarforschung, as well as abstracts and proceedings of national and international conferences and workshops of the AWI.

The papers contained in the Reports do not necessarily reflect the opinion of the AWI.

Editor
Dr. Horst Bornemann

Editorial editing and layout
Susan Amir Sawadkuhi

Alfred-Wegener-Institut
Helmholtz-Zentrum für Polar- und Meeresforschung
Am Handelshafen 12
27570 Bremerhaven
Germany

www.awi.de
www.awi.de/en/reports

Titel: Meeresboden der Station HG-III des LTER Observatoriums HAUSGARTEN (2.000 m Wassertiefe, OFOS) vor Spitzbergen; Besiedlung des steinigen Untergrunds eines untermeerischen Riffs mit Schwämmen (Phakellia ventilabrum) und darauf ruhenden Garnelen (Bythocaris ssp.)
(Foto: AWI-Forschungsgruppe Tiefsee)

Cover: Seafloor of station HG-III of the LTER observatory HAUSGARTEN (2,000 m water depth, OFOS) off Spitsbergen; colonisation of the stony substrate of a submarine reef with sponges (Phakellia ventilabrum) and shrimps (Bythocaris ssp.) resting on them
(Photo: AWI Deep-Sea research group)

The Expedition PS126 of the Research Vessel POLARSTERN to the Fram Strait in 2021

Edited by

Thomas Soltwedel
with contributions of the participants

Please cite or link this publication using the identifiers

https://hdl.handle.net/10013/epic.d5d25704-4f74-4f60-827b-01988dace432
https://doi.org/10.48433/BzPM_0757_2021

ISSN 1866-3192

PS126

24 May 2021 – 27 June 2021

Bremerhaven – Bremerhaven

LTER HAUSGARTEN 2021
Long-Term Ecological Research at an Arctic marine Observatory

Chief scientist
Thomas Soltwedel

Coordinator
Ingo Schewe

Contents

1. ÜBERBLICK UND FAHRTVERLAUF

Thomas Soltwedel DE.AWI

Am Montag, den 24. Mai 2021 verließ die *Polarstern* Bremerhaven zur Expedition PS126, die sie in die Framstraße zwischen Grönland und Spitzbergen führte. Die insgesamt 7-wöchige Expedition wurde genutzt, um Beiträge zu verschiedenen nationalen und internationalen Forschungs- und Infrastrukturprojekten des AWI (FRAM, INTAROS, ICOS, SIOS, ARCHES) sowie dem Forschungsprogramm „Changing Earth – Sustaining our Future“ („Erde im Wandel – Unsere Zukunft nachhaltig gestalten“) zu leisten. Im Rahmen des Topic 6 “Marine and Polar Life: Sustaining Biodiversity, Biotic Interactions and Biogeochemical Functions” (Subtopics 6.1 “Future ecosystem functionality” und 6.3 “The future biological carbon pump”) des neuen Forschungsprogramms wurden die mit steigenden Wassertemperaturen und dem Rückgang des Meereises verbundenen Ökosystemverschiebungen im Pelagial und im tiefen Ozean ermittelt und quantifiziert und Rückkopplungsprozesse auf ozeanographische Prozesse untersucht. Diese Untersuchungen beinhalteten die Identifizierung räumlicher und zeitlicher Entwicklungen in der Funktion ausgewählter Plankton- und Benthos-Gemeinschaften. Im Rahmen des Subtopics 6.4 „Use and misuse of the ocean: Consequences for marine ecosystems“ wurden darüber hinaus der Eintrag von Plastikmüll in den Ozean, vertikale Plastikflüsse von der Meeresoberfläche zum Meeresboden und die Wechselwirkungen zwischen Plastik und marinen Organismen untersucht.

Die Arbeiten stellten einen weiteren Beitrag zur Sicherstellung der Langzeitbeobachtungen am LTER Observatorium HAUSGARTEN dar, in denen der Einfluss von Umweltveränderungen auf ein arktisches Tiefseeökosystem dokumentiert wird. Diese Arbeiten wurden in enger Zusammenarbeit der HGF-MPG Brückengruppe für Tiefsee-Ökologie und -Technologie der Arbeitsgruppe PEBCAO („Phytoplankton Ecology and Biogeochemistry in the Changing Arctic Ocean“) des AWI und der Helmholtz-Nachwuchsgruppe SEAPUMP („Seasonal and regional food web interactions with the biological pump“) durchgeführt.

Die Expedition wurde darüber hinaus genutzt, um weitere Installationen im Rahmen der HGF Infrastrukturmaßnahme FRAM (Frontiers in Arctic marine Monitoring) vorzunehmen. Das FRAM Ocean Observing System ermöglicht kontinuierliche Untersuchungen von der Meeresoberfläche bis in die Tiefsee und liefert zeitnah Daten zur Erdsystem-Dynamik sowie zu Klima- und Ökosystem-Veränderungen. Daten des Observatoriums werden zu einem besseren Verständnis der Veränderungen in der Ozeanzirkulation, den Wassermassen-Eigenschaften und des Meereisrückgangs sowie deren Auswirkungen auf das arktische, marine Ökosystem beitragen. FRAM führt Sensoren in Observationsplattformen zusammen, die sowohl die Registrierung von Ozeanvariablen, als auch physiko-chemischer und biologischer Prozesse im Ozean erlauben. Experimentelle und ereignisgesteuerte Systeme ergänzen diese Beobachtungsplattformen. Produkte der Infrastruktur umfassen hochaufgelöste Langzeitdaten sowie Basisdaten für Modelle und die Fernerkundung.

Die wissenschaftlichen Arbeiten während der *Polarstern* Expedition PS126 wurden in erheblichen Maßen durch die vorherrschenden Eisbedingungen beeinträchtigt. In der östlichen Framstraße waren es riesige Eisfelder kleinerer, einjähriger Eischollen mit bis zu 100 % Eisbedeckung, in der westlichen Framstraße waren es z.T. riesige, mehrjährige Eisschollen,

die ungewöhnlich schnell (1-2 Knoten) Richtung Süden gezogen sind, die speziell den Einsatz von geschleppten Geräten, den Austausch von Verankerungen und den sicheren Einsatz unseres Autonomen Unterwasserfahrzeugs zeitweise unmöglich gemacht haben. Aufgrund der Eisverhältnisse konnte das Schiff nur mit der im Eis gebotenen Geschwindigkeit von maximal 7 Knoten operieren, so dass das Forschungsprogramm nicht voll umfänglich durchgeführt werden konnte und einzelne Geräteeinsätze gestrichen werden mussten. Nichtsdestotrotz sind wir mit dem Erreichten insgesamt zufrieden. So konnten zwei sehr komplexe und teure Großgeräte der Tiefseegruppe des AWI, die Meeresboden-Kettenfahrzeuge (Benthic Crawler) TRAMPER und NOMAD, die beide auf einer zwei Jahre zurückliegenden *Polarstern*-Reise ausgebracht wurden, während der PS126 erfolgreich geborgen werden. Darüber hinaus konnten sämtliche in 2019 ausgebrachten Verankerungen erfolgreich ausgetauscht werden. Die *Polarstern* Expedition PS126 endete am Sonntag, den 27. Juni 2021 in Bremerhaven.

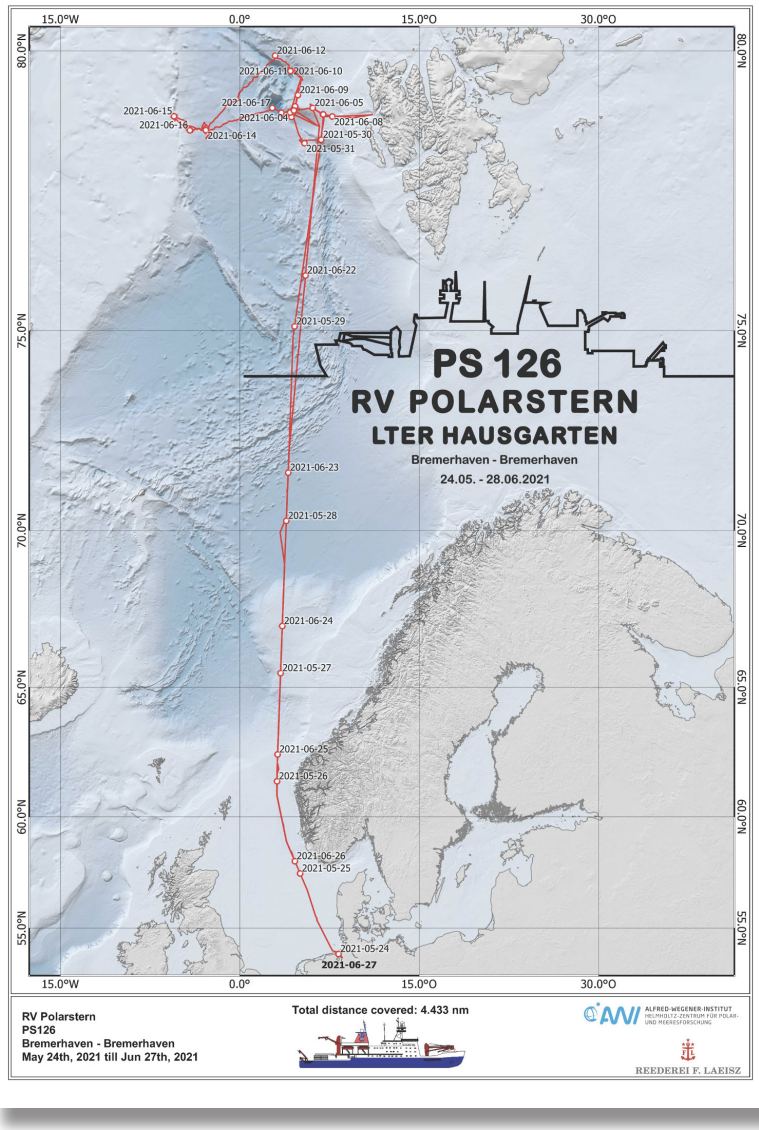

Abb. 1.1: Fahrtverlauf der Expedition PS126 von und nach Bremerhaven; siehe https://doi.pangaea.de/10.1594/PANGAEA.935582 für eine Darstellung des master tracks in Verbindung mit der Stationsliste der Expedition PS126

Fig. 1.1: Cruise track of expedition PS126 from and to Bremerhaven; see https://doi.pangaea.de/10.1594/PANGAEA.935582 to display the master track in conjunction with the station list of expedition PS126

SUMMARY AND ITINERARY

The *Polarstern* expedition PS126 started on Monday 24 May 2021 in Bremerhaven and lead to the Fram Strait between Greenland and the Svalbard archipelago. The expedition contributed to various large national and international research and infrastructure projects (FRAM, INTAROS, ICOS, SIOS, ARCHES) as well as to the new research programme „Changing Earth – Sustaining our Future" of the AWI. Within Topic 6 "Marine and Polar Life: Sustaining Biodiversity, Biotic Interactions and Biogeochemical Functions" (Subtopics 6.1 "Future ecosystem functionality" and 6.3 "The future biological carbon pump") of the new research programme, ecosystem shifts in the pelagic and deep ocean associated with water temperature increase and sea ice retreat were identified and quantified, and feedback processes on oceanographic processes were investigated. These studies included the identification of spatial and temporal developments in the function of selected pelagic and benthic communities. Within Subtopic 6.4 "Use and misuse of the ocean: Consequences for marine ecosystems", the input of plastic waste into the ocean, the vertical fluxes of plastic from the sea surface to the seafloor, and the interaction between plastic and marine biota were investigated.

The work supported the time-series studies at the LTER (Long-Term Ecological Research) observatory HAUSGARTEN, where we document Global Change induced environmental variations on a polar deep-water ecosystem. This work was carried out in close co-operation between the HGF-MPG Research Group on Deep-Sea Ecology and Technology, the Working Group PEBCAO ("Phytoplankton Ecology and Biogeochemistry in the Changing Arctic Ocean") at AWI and the Helmholtz Young Investigators Group SEAPUMP ("Seasonal and regional food web interactions with the biological pump"), representing a joint effort between the AWI, the MARUM – Center for Marine Environmental Sciences and the University of Bremen.

The expedition was further used to accomplish installations for the HGF infrastructure project FRAM (Frontiers in Arctic marine Monitoring). The FRAM Ocean Observing System aims at permanent presence at sea, from surface to depth, for the provision of near real-time data on Earth system dynamics, climate variability and ecosystem change. It serves national and international tasks towards a better understanding of the effects of change in ocean circulation, water mass properties and sea-ice retreat on Arctic marine ecosystems and their main functions and services. FRAM implements existing and next-generation sensors in observatory platforms, allowing synchronous observation of relevant ocean variables as well as the study of physical, chemical and biological processes in the ocean. Experimental and event-triggered platforms complement the observational platforms. Products of the infrastructure are continuous long-term data with appropriate resolution in space and time, as well as ground-truthing information for ocean models and remote sensing.

The scientific work during *Polarstern* expedition PS126 was severely affected by extreme ice conditions. In the eastern Fram Strait there were vast ice fields of smaller, one-year ice floes with up to 100 % ice coverage, in the western Fram Strait there were partly huge, perennial ice floes that moved unusually fast (1-2 knots) towards the south, which especially impaired the use of towed scientific equipment, the exchange of moorings and the safe use of our Autonomous Underwater Vehicle (AUV) very much and sometimes made it impossible. Due

to the ice conditions, the ship could only operate at the maximum allowed speed of 7 knots in the ice, so that the research programme could not be fully carried out as usual and individual equipment deployments had to be cancelled. Nevertheless, overall we are satisfied with what we were able to achieve during the expedition. Two larger, complex and expensive instruments of the AWI Deep-sea Research Group, the Benthic Crawlers TRAMPER and NOMAD, both deployed during a *Polarstern* cruise in 2019, were successfully recovered during PS126. In addition, all moorings deployed two years ago were successfully replaced. The cruise ended on Sunday 27 June 2021 in Bremerhaven.

2. WEATHER CONDITIONS DURING PS126

Julia Wenzel[1], Patrick Suter[1] [1]DE.DWD

Grant-No. AWI_PS126_00

Transit from Bremerhaven to the Fram Strait

On 24 May 2021 at 11:30, *Polarstern* left the port of Bremerhaven and relatively quickly entered the area of the occlusion front of a low-pressure system over Scotland, which moved towards Denmark until 26 May. At the beginning, a fresh to strong southerly wind was prevailing, which shifted to the Northeast in the night to 25 May and decreased to 4 Bft. The significant wave height was around 1 m. On 25 May, at the height of the Skagerrak, the wind shifted to the East for a few hours due to the coastal effect and increased to 6 Bft. In the night to 26 May the wind shifted to Northeast again and increased to 7 Bft in the course of the day, because *Polarstern* reached a strong wind band between the low-pressure complex over Denmark and a high-pressure area over the Norwegian Sea. The swell rose successively to 4 metres.

On 27 May, *Polarstern* moved north along the eastern flank of the aforementioned high-pressure system and reached its northern flank on 28 May. The wind decreased steadily from 27 May and at the same time shifted back, so that on the evening of 28 May it was blowing from the West with 3 Bft. The swell also decreased to 1 m. In the night to 29 May, the westerly wind increased to 6 Bft, so that the swell also increased temporarily to nearly 2 m.

Fram Strait

A shallow low over Northeast Greenland moved into Fram Strait on 30 May and subsequently filled rapidly. When reaching the working area in the eastern Fram Strait in the morning of 30th May, the wind shifted to the Southeast and decreased to 3 Bft, so that the swell also dropped below 0.5 m. By the evening, the wind shifted further back to the Northeast, slowly increasing to 4 to 5 Bft, and in the following night to 31 May, at times weak winds from variable directions were prevailing in the centre of the low.

On 31 May, *Polarstern* came under the influence of a new stronger low-pressure system which moved north along the east coast of Greenland and reached the western Fram Strait on 1st June. The wind shifted to the Southeast on 31 May and increased steadily during the day. With the crossing of the frontal system in the night to 1st June, wind speeds of 7 Bft occurred and the wind shifted to the South.

The strong southerly to south-westerly flow continued in the following days, as a strong blocking high-pressure system over Scandinavia repeatedly directed low-pressure systems to the Northeast into the Fram Strait. Thus, after a short phase of weak high pressure, a gale approached from the Southwest on 1 June. On the following day, the gale crossed the Fram Strait from southwest to northeast, with its frontal system causing intermittent drizzle and rain. The wind from southeast to south slowly increased from 5 to 7 Bft and, with the passage of the front, temporarily shifted to northwest during the evening. In the night to 3 June it weakened and returned to southwest.

On 3 June, the research area remained between low pressure in the North and high pressure over northern Scandinavia in the area of a fresh to moderate south-westerly air flow. The sea from southwest reached almost 3 m in the morning and then slowly decreased.

On 4 June, a trough embedded in the westerly flow reached the research area and subsequently moved eastwards over the Fram Strait. A second short-wave trough followed in the afternoon. The troughs were accompanied by snow showers. While the south-westerly wind on the front side of the first trough decreased to around 4 Bft, the wind on the rear side shifted to northwest, and after the passage of the second shortwave trough shifted to west with 4 to 5 Bft.

On 5 June, *Polarstern* approached the eastern flank of a high-pressure ridge extending north-westwards from a high over Scandinavia. Afterwards, this ridge slowly moved eastwards across the Fram Strait. The wind blew from northwest to west with 4 to 5 Bft. In the night to 6 June, the wind shifted to south when the axis of the ridge crossed and temporarily decreased to 2 to 3 Bft, before increasing to 5 to 6 Bft again during the day. The cloud coverage decreased and dissipated in the course of 5 June. On 6 June, mostly sunny conditions prevailed with very good visibility. Due to this weather development, the more than 100 nmi transport flight by helicopter to Longyearbyen could already be carried out on 6 June, instead of 8 June, as originally planned.

Subsequently, a small-scale low-pressure system moved from the Southwest into the western Fram Strait. This brought mild and humid air from the South on 7 June, which caused rain, drizzle and fog. The southerly wind with initially 5 Bft slowly decreased and turned to northwest in the evening.

A strong low between the North Pole and Severnaya Zemlya brought cooler and drier air with a weak north-westerly current from the night of 8 June. On 8 June *Polarstern* reached the easternmost point of the HAUSGARTEN research area, directly in the entrance area of the Kongsfjorden on Svalbard. The wind was mostly weak from variable directions and the sea state decreased below 0.5 m. The low moved under weakening towards Svalbard until 10 June, and filled north of it by 12 June. During this period, *Polarstern* was in the central to northern part of the HAUSGARTEN research area, surrounded by ice.

Further on, from 11 June, a powerful low-pressure system moved northeast from Iceland over Jan Mayen and the southern tip of Svalbard. On the cold front of this depression, a secondary low developed over northern Scandinavia on 12 June. While developing into a gale, this secondary low moved to the East coast of Svalbard until 14 June. As a result, the northerly wind increased successively from 4 to 7 Bft in the period from 12 June to 15 June. From 15 June onwards, the low weakened temporarily and moved off towards Franz-Josef-Land. Due to this development and the steady winds from north to northwest, an unstable weather character prevailed in the period from 10 to 15 June. An often-broken cloud layer took turn with small episodes of sunshine. In addition, snow showers occurred repeatedly during this period due to the unstable boundary layer. Meanwhile, *Polarstern* reached the westernmost point of the HAUSGARTEN research area on 15 June and returned to the central area from 17 June on.

From 16 June, a high-pressure ridge extended into the western Fram Strait and moved eastwards over the Fram Strait by 17 June. In contrast, a strong low-pressure system remained in the vicinity of Franz-Josef-Land. Between the pressure areas, *Polarstern* was situated in a north-westerly and at times moist air current of moderate to fresh strength.

The aforementioned low subsequently moved north-westwards, and at the same time a surface trough formed on the northeast coast of Greenland starting on 18 June. This trough further amplified, but remained quasi-stationary. In the meantime, the aforementioned low-pressure system again approached the research area from the North. With simultaneously

higher air pressure in the Southeast, the pressure gradient over the Fram Strait increased in the course of 20 June. As a result, the wind shifted from west to southwest and reached 6 to 7 Bft in the night to 21 June. Within larger ice-free areas, the wind sea reached 1 to 1.5 m. Afterwards, the low in the North of Svalbard turned towards the Northeast again, which made the wind decrease to 5 to 6 Bft in the second half of the night to 21 June. Meanwhile, the trough developed into an independent small low over the western Fram Strait. On the last day of research in the central Fram Strait, the sky was grey with very low-lying stratus all day and light freezing drizzle at times in the afternoon.

Transit from Fram Strait to Bremerhaven

Only when leaving the HAUSGARTEN working area and thus beginning the transit to the South in the night to 22 June *Polarstern* did finally leave the ice-covered and thus protected-from-waves-area. However, the sea only reached 1 to 1.5 m outside the ice, as *Polarstern* moved away from the weak low over the western Fram Strait. Shortly after, the transit area was influenced by a high-pressure ridge and thus decreasing south-westerly winds. The high subsequently moved further north-eastwards into the Barents Sea.

Continuing South, on 23 June, *Polarstern* crossed a low-pressure system with an associated occluded front which was moving from Iceland to the East. On the north side of the low, the wind shifted to east to southeast and increased to 6 Bft. Later in the afternoon, the wind shifted to south, slightly weakened, and in the following night to 24 June it shifted to west as *Polarstern* reached the southern flank of the low. Due to the swell from southwest to south and the simultaneous wind sea from east to southeast, there was a temporary cross sea with increasing wave heights of 2 to 2.5 m. With the wind shift to west, wind sea and swell came in again from a similar direction.

Further south, the influence of the low slowly decreased on 24 June. The westerly wind blew with about 5 Bft and shifted to northwest during the day. The following day, a high-pressure system south of Iceland extended north-eastwards. In conjunction with a weak low-pressure system over the central North Sea, pressure contrasts increased in the southern area of the Norwegian Sea. The north-easterly wind reached 7 Bft on 25 June and the significant wave height temporarily increased up to 3 metres. The last two days were characterised by a high-pressure ridge, which extended from the mentioned high-pressure system over the Atlantic across the North of the British Isles and the North Sea. The wind blew from northwest to north at a fairly constant 4 Bft.

In the late afternoon of 27 June, *Polarstern* arrived in Bremerhaven under warm and sunny conditions.

3. LTER HAUSGARTEN – IMPACT OF CLIMATE CHANGE ON ARCTIC MARINE ECOSYSTEMS

Christiane Hasemann[1], Melanie Bergmann[1], Michael Busack[1], Jennifer Dannheim[1], Simon Escalle[1], Lennard Frommhold[1], Katharina Gotterbarm[1], Jonas Hagemann[1], Ulrich Hoge[1], Sascha Lehmenhecker[1], Normen Lochthofen[1], Janine Ludszuweit[1], Kirstin Meyer-Kaiser[2], Malte Pallentin[1], Autun Purser[1], Jannik Schnier[1], Kharis Schrage[2], Thomas Soltwedel[1]; Ulrich Hoge[1] (not on board)

[1]DE.AWI
[2]US.WHOI

Grant No. AWI_PS126_01

Objectives and scientific programme

The marine Arctic has played an essential role in the history of our planet over the past 130 million years and contributes considerably to the present functioning of the Earth and its life. The past decades have seen remarkable changes in key arctic variables, including a decrease in sea ice extent and sea ice thickness, changes in temperature and salinity of arctic waters, and associated shifts in nutrient distributions. Since arctic organisms are highly adapted to extreme environmental conditions with strong seasonal forcing, the accelerating rate of recent climate change challenges the resilience of arctic life. The stability of a number of arctic populations and ecosystems is probably not strong enough to withstand the sum of these factors, which might lead to a collapse of subsystems.

Benthos, particularly in deep waters, is a robust ecological indicator for environmental changes, as it is relatively stationary and long-lived, and reflects changes in ecological conditions in the oceans (e.g. organic flux to the seabed) at integrated scales (Gage and Tyler 1991; Piepenburg 2005). To detect and track the impact of large-scale environmental changes in the transition zone between the northern North Atlantic and the central Arctic Ocean, and to determine experimentally the factors controlling deep-sea biodiversity, the Alfred Wegener Institute Helmholtz Center for Polar and Marine Research (AWI) established the deep-sea observatory HAUSGARTEN, which constitutes the first, and until now, only open-ocean long-term observatory in a polar region (Soltwedel et al. 2016).

HAUSGARTEN is located in the eastern Fram Strait and includes 21 permanent sampling sites along a depth transect (250 to 5,500 m) and along a latitudinal transect following the 2,500 m isobath crossing the central HAUSGARTEN station (Fig. 3.1). Multidisciplinary research activities at HAUSGARTEN cover almost all compartments of the marine ecosystem from the pelagic zone to the benthic realm. Regular sampling as well as the deployment of moorings and different stationary and mobile free-falling systems (Bottom-Lander, Benthic Crawler), which act as local observation platforms, have taken place since the observatory was established in 1999. Frequent visual observations with towed photo/video systems allow the assessment of large-scale epifauna distribution patterns as well as their temporal development.

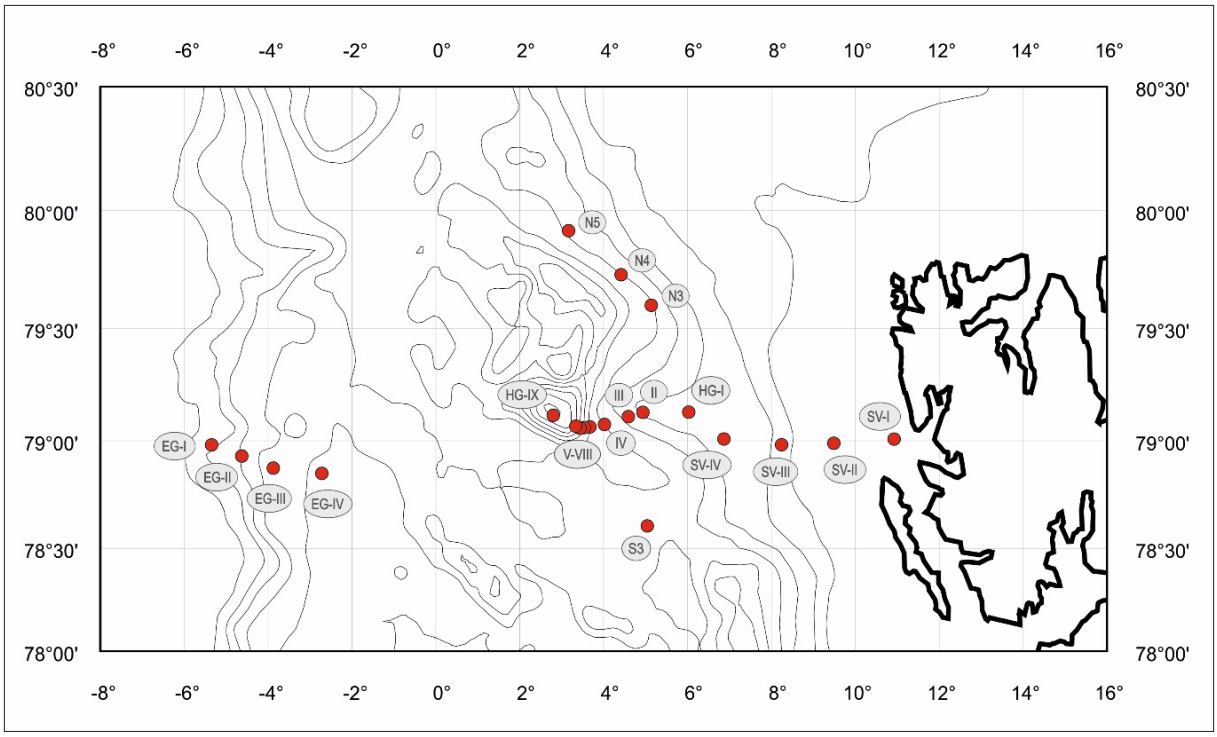

Fig. 3.1: Permanent sampling sites of the LTER Observatory HAUSGARTEN in Fram Strait

Geographical features in the HAUSGARTEN area provide a variety of contrasting marine landscapes and landscape elements (e.g. banks, troughs [marine valleys], ridges and moraines, canyons and pockmarks) that generally shape benthic communities over a variety of different scales (Buhl-Mortensen et al. 2010, 2012). The habitat-diversity (heterogeneity) hypothesis states that an increase in habitat heterogeneity leads to an increase in species diversity, abundance and biomass of all fauna groups (Whittaker et al. 2001; Tews et al. 2004). Improved technologies, particularly the recent deployment of acoustic and side-scan sonar systems at depth by an Autonomous Underwater Vehicle (AUV) and towed camera sleds within the Deep-sea Research Group (Purser et al. 2019) have indicated the high-resolution topographical variability of many deep-sea areas, including HAUSGARTEN (Schulz et al. 2010; Taylor et al. 2016; Purser 2020). So far, the time-series stations maintained across the region do not capture the high degree of local heterogeneity (in terms of physical seafloor terrain variables such as slope, rugosity, aspect, depth). Therefore, during *Polarstern* expedition PS126, dedicated attempts are planned to collect spatial data to capture the role of this heterogeneity in biodiversity and biomass estimation and to complement the investigations on temporal variability of benthos in the HAUSGARTEN area.

Work at sea

Meiobenthos and biogenic sediment compounds

Virtually undisturbed sediment samples were taken using our new video-controlled multiple corer (MUC; Fig. 3.2, Table 3.1). Various biogenic compounds (i.e. chloroplastic pigments, exo-enzyms, particulate proteins, phospholipids) from these sediments were analysed to estimate the input of organic matter to the seafloor, bacterial activities and the total biomass in the sediment. Supplementary samples were taken to determine the abundance and biomass

of sedimentary bacteria as well as meiofauna densities and to study the diversity patterns of nematodes, which are by far the dominant group of metazoan meiofauna organisms in deep-sea sediments.

Sediment-bound chloroplastic pigments (chlorophyll *a* and its degradation products) represent a suitable indicator for the input of phytoplanktonic detritus to the seafloor, representing the major food source for benthic organisms. They can be analysed with high sensitivity by fluorometric methods. To estimate the potential heterotrophic activity of bacteria, we measured cleaving rates of extracellular enzymes using the model-substrate FDA (fluorescein-di-acetate) in incubation experiments. Both parameters, bacterial activity and chloroplastic pigments, were analysed on board. All other sub-samples were stored at –20° C or at room temperature in 4 % formalin for later analyses at the home lab.

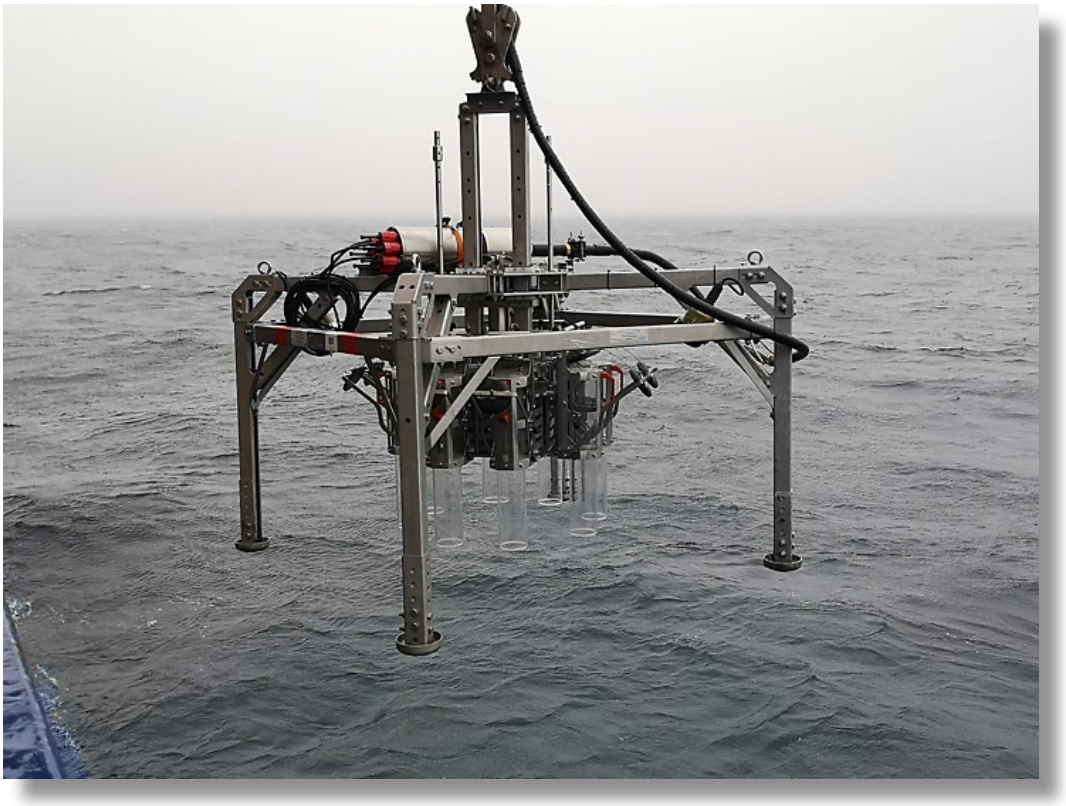

Fig. 3.2: First deployment of the new video-controlled multiple corer (OKTOPUS GmbH) during Polarstern expedition PS126

Macrobenthos und sediment profiling imagery

Macrobenthic samples were obtained by USNEL box corer (0.25 m²), the preferred sampling gear for this size class of benthic organisms in deep waters, as it provides reliably deep and relatively undisturbed sediment samples adequate for macrofauna sampling (Gage and Bett 2005). The samples allow a continuation of the long-term series along depth gradients from the shelf to adjacent deeper areas and a comparison between samples of ice-free zones and stations covered mainly by ice throughout most of the year.

We were able to take a total of 13 box corer samples (18 deployments of which five failed due to uneven seafloor or gear failure, Table 3.1.) at 13 sites to study macrofauna communities in the HAUSGARTEN area. However, at station HG-VII (Fig. 3.1) the box corer did not close properly due to uneven seafloor and was washed out when setting down on deck, thus the sample was sieved but is only useful for analysing presence and absence data.

Tab. 3.1: HAUSGARTEN and East Greenland stations with station ID, date, geographic position and water depth (m) of PS126. Stations were sampled with multiple corer (MUC), sediment profile imaging camera (SPI), box corer (BC) and two deployments of the arcFOCE-Lander for experiments; (f) = box corer failed.

Site	Station ID	Date	Latitude	Longitude	Water Depth [m]	MUC ID	SPI ID	BC ID	Lander ID
Test Site	PS126_1	30.05.2021	78°37.31‘N	006°48.07‘E	1775	1-6			
SV-I	PS126_13	08.06.2021	79°01.85‘N	001°65.26‘E	276	13-5			
SV-II	PS126_12	08.06.2021	78°58.81‘N	009°30.89‘E	230	12-6			
SV-IV	PS126_9	07.06.2021	79°01.33‘N	007°05.08‘E	1300	9-12	9-13	9-14	
HG-I	PS126_8	06.06.2021	79°08.13‘N	006°05.16‘E	1279	8-10	8-11	8-12 (f)	
	PS126_15	08.06.2021	79°08.08‘N	006°03.50‘E	1283			15-1	
HG-II	PS126_6	05.06.2021	79°07.55‘N	004°56.04‘E	1546	6-6	6-7	6-8	
HG-III	PS126_4	04.06.2021	79°06.47‘N	004°36.19‘E	1914	4-4	4-5	4-6	
HG-IV	PS126_3	02.06.2021	79°03.08‘N	004°11.48‘E	2508	3-14	3-15	3-16 (f)	
		03.06.2021				3-24		3-19	
HG-V	PS126_25	19.06.2021	79°03.88‘N	003°39.74‘E	3100	25-3	25-4	25-5	
HG-VI	PS126_28	20.06.2021	79°03.47‘N	003°35.42‘E	3418	28-1	28-2	28-3 (f)	
HG-VII	PS126_24	18.06.2021	79°03.78‘N	003°28.49‘E	3990	24-3		24-4	
HG-IX	PS126_23	18.06.2021	79°08.10‘N	002°48.23‘E	5545	23-10		23-11	
EG-I	PS126_21	16.06.2021	79°00.74‘N	005°37.35‘W	896	21-14	21-15	21-16	
EG-IV	PS126_20	14.06.2021	78°46.27‘N	002°43.11‘W	2617	2-9	20-10	20-11	
S3	PS126_2	31.05.2021	78°36.50‘N	005°04.06‘E	2339	2-13	2-12	2-14	
N3	PS126_17	09.06.2021	79°36.02‘N	005°10.35‘E	2787	17-4	17-5	17-6 (f)	
	PS126_27	20.06.2021	79°35.96‘N	005°07.97‘E	2809			27-3	
N4	PS126_18	10.06.2021	79°43.82‘N	004°29.42‘E	2727	18-9	18-10	18-11 (f)	
N5	PS126_19	12.06.2021	79°56.25‘N	003°00.38‘E	2616	19-7		19-8	
SV-IV	PS126_9	06.06.2021	79°01.80‘N	006°59.78‘E	1303				9-1
NA	PS126_16	21.06.2021	78°50.07‘N	006°40.07‘E	1780				16-1
Sum						19	12	18	2

All other box-corer samples were divided into eight equal subsamples. The upper 12 cm of each subsample and the supernatant seawater (to catch epibenthic animals from the fluffy layer on top of the sediment) were taken for further sample processing. Quantitative and qualitative samples were sifted over a 500 µm mesh size sieve, and sieve residues were preserved in 4 % buffered formalin. In the laboratory at AWI, macrofauna specimens will be determined to the lowest possible taxonomic level, counted and the wet mass per species will be determined. Additional surface sediment samples were derived from each station with 5 cm³ PVC cores. These samples were stored at –20° C until further analysis on (a) median grain size and sorting coefficient and (b) on organic carbon content.

The sediment profile imaging camera (SPI) was deployed the first time in high-latitude deep-sea waters in the HAUSGARTEN area. The SPI takes vertical pictures of the sediment profile down to a depth of 21 cm from the sea bottom surface. Thereby, it determines habitat and ecological changes due to different environmental settings by (a) vertical distribution of sediment layers, i.e. sediment deposition differences, (b) apparent redox potential discontinuity (aRPD), a transition of sediment colour that serves as a relative measure of sediment dissolved oxygen content and oxygen, and (c) benthic successional stages and bioturbation activity as major benthic functions.

We were able to sample 12 sites by the SPI cam with generally 10 pictures at each site. However, at the first site S3 only one picture was taken due to sampling operation difficulties (blind-sided touch down of the gear with erroneous rope tension and winch cable length display), and only seven (HG-IV) and eight (HG-VI) pictures were taken as the SPI cam was not properly triggered at the seafloor.

Megabenthos and seafloor mapping

To assess megafaunal dynamics over time and continue the HAUSGARTEN megafauna time series, we conduct towed camera surveys with an Ocean Floor Observation Bathymetry System, OFOBS (Purser et al. 2018) along the same transect positions every year (Bergmann et al. 2011; Meyer et al. 2013; Taylor et al. 2017; 2018). The bathymetry unit of the system enables 3D-reconstruction of habitat features and seafloor topography using the Agisoft Metashape software application (Purser et al. 2018, 2019). This method is non-invasive and allows us to gain *in-situ* views of the organisms at a large scale.

Five surveys were undertaken at HAUSGARTEN station S3, HG-IV, N3, HG-I, and EG-IV with the OFOBS to continue the megafauna and seafloor litter time series (see Chapter 10; Table 3.2). During the descent and ascent of the system, the camera was set to continue to record so as to take photographs of pelagic biota (see Chapter 11).

In addition to the five scientific dives, six deployments were made with OFOBS to retrieve and/or investigate scientific equipment on the seafloor. For these deployments, a small Remotely Operated Vehicle (ROV) was mounted directly on OFOBS and attached to a hook, which could be manually attached to equipment on the seafloor (see Chapter 8).

The Autonomous Underwater Vehicle (AUV) PAUL was brought onto *Polarstern* to continue the acoustic and image-based mapping of the central HAUSGARTEN area, an activity which had been started with the AUV during PS121 in 2019, and continued with the Ocean Floor Observation and Bathymetry System (OFOBS) during MSM95 in 2020.

During PS126 only two deployments of the AUV were possible, given the substantial and near complete ice coverage encountered across the full working area. During the first dive (PS126_1-2) both image and acoustic data were successfully collected during ~ 4 hrs of seafloor

deployment time. During the second dive (PS126_5-1) only acoustic data was recorded, to map the physical placement of HAUSGARTEN equipment across the central HG-IV site, completing work started during the MSM95 campaign (Purser et al. 2021).

Tab. 3.2: Details of OFOBS casts undertaken at HAUSGARTEN

Station	Cast No.	Date, Time	Action	Latitude (N) dec	Longitude (E) dec	Depth [m]
S3	PS126_2-15	01.06.2021, 00:27	Start	78.616806	5.000178	2363
		01.06.2021, 03:04	End	78.616768	5.160349	2350
HG-IV	PS126_3-21	03.06.2021, 00:16	Start	79.035849	4.171027	2617
		03.06.2021, 04:01	End	79.07263	4.313038	2341
HG-I	PS126_8-13	06.06.2021, 04:11	Start	79.13183	6.262224	1319
		06.06.2021, 06:41	End	79.134081	6.112702	1277
EG-IV	PS126_20-12	14.06.2021 17:40	Start	78.876742	-3.034611	2516
		14.06.2021 20:51	End	78.79573	-3.197399	2469
N3	PS126_27-2	20.06.2021, 01:24	Start	79.569546	5.251566	2660
		20.06.2021, 04:50	End	79.602489	5.153236	2797

Larval biology in the Fram Strait

Very little is known about reproductive biology of Arctic organisms, especially in the deep-sea. Previous research at HAUSGARTEN observatory and in adjacent Svalbard waters has indicated that larval abundances in the water column are very low compared to holoplankton (i.e. pteropods). The prevailing paradigm suggests that species in food-poor environments such as the polar deep seas should have non-pelagic, non-feeding (lecithotrophic) larvae (Thorson 1950), but there are numerous exceptions to this “rule” (Poulin et al. 2002). In fact, it may be more adaptive for species in food-poor environments to have feeding (planktotrophic) larvae because lecithotrophic larvae are too energetically expensive to produce (McClain et al. 2014). Planktotrophic larvae of deep-sea species may migrate to the surface to feed and become entrained in surface currents that carry them long distances (Young et al. 2012). Understanding the reproductive strategies and larval distributions of Arctic deep-sea species is important because as climate change progresses, larvae could be carried out of areas where they can settle, or new species of larvae may be delivered to the high Arctic from sub-Arctic latitudes. Samples were collected using a WTS-LV pump (McLane Research Laboratories, Falmouth, MA, USA) attached to a bottom lander. In ice-covered areas, landers were deployed as moorings and deployed and recovered using a long line. Five lander deployments were conducted at HAUSGARTEN stations and adjacent rocky stations. Larval samples collected during lander deployments are outlined in Table 3.3.

Tab. 3.3: Larvae lander deployments during PS126; N: number of larval specimens collected.

Event number	Station	Device	Latitude	Longitude	Depth [m]	Pump start	Pump end	Volume [L]	N
PS126_1-1	“South reef”	Larvae-Lander I	78°37.221’N	6°48.049’E	1786	6 June 3:00	6 June 15:39	21911	45
PS126_2-1	S3	Larvae-Lander II	78°36.533’N	5°03.942’E	2338	31 May 0:00	31 June 20:04	34593	33

Event number	Station	Device	Latitude	Longitude	Depth [m]	Pump start	Pump end	Volume [L]	N
PS126_3-18	HG-IV	Larvae-Lander II	79°03.810'N	4°09.356'E	2489	2 June 21:00	3 June 17:04	34593	39
PS126_7-1	"Senke"	Larvae-Lander II	79°06.119'N	4°33.271'E	1883	5 June 11:30	6 June 5:45	31586	47
PS126_17-1	N3	Larvae-Lander I	79°35.899'N	5°08.007'E	2809	9 June 21:00	not recovered		

Additional samples were collected opportunistically using a Hand net (20 µm mesh size) in vertical tows at the surface (0 – 20 m) during CTD casts. Biofouling species were collected from moorings and long-term instruments recovered during PS126 (Table 3.4).

Tab. 3.4: Hand net and mooring samples collected opportunistically during PS126; N: number of specimens collected.

Event number	Station	Date	Device	Latitude	Longitude	Water depth [m]	N
PS126_1-4	"South reef"	30 May	Hand net	78°37.308'N	6°48.288'E	1771	6
PS126_3-4	HG-IV	1 Jun	Mooring HG-IV-S-4	79°01.401'N	4°16.154'E	2599	3
PS 126_9-2	SV-IV	6 Jun	Mooring F4-S-4	79°01.803'N	6°59.777'E	1303	8
PS126_9-3	SV-IV	6 Jun	Mooring F4-W-4	79°00.193'N	7°00.837'E	1259	2
PS126_18-8	N4	10 Jun	Mooring FEVI-39	79°43.816'N	4°29.114'E	2718	5
PS126_19-4	N5	12 Jun	Mooring HG-N-S-1	79°56.409'N	3°02.109'E	2600	34
PS126_21-2	EG-I	15 Jun	Long-term lander	79°00.005'N	5°26.361'W	1013	5
PS126_21-3	EG-I	15 Jun	TRAMPER	78°59.767'N	5°26.547'W	1000	6
PS126_21-4	EG-I	15 Jun	Mooring EGC-6	78°59.413'N	5°27.901'W	973	42
PS126_21-5	EG-I	15 Jun	Hand net	78°59.695'N	5°32.177'W	937	11
PS126_23-1	HG-IX	17 Jun	Hand net	79°07.923'N	2°47.645'E	5556	8
PS126_24-1	HG-VII	18 Jun	Hand net	79°03.111'N	3°28.998'E	4023	7
PS126_25-1	HG-V	18 Jun	Hand net	79°03.755'N	3°40.187'E	3112	13
PS126_26-1	HG-IV	19 Jun	NOMAD	79°03.396'N	4°10.570'E	2511	3
PS126_28-1	HG-VI	20 Jun	Hand net	79°03.636'N	3°35.086'E	3437	6

Preliminary (expected) results

Biogenic sediment compounds

Except for one station of the HAUSGARTEN depth transect (HG-VIII), two stations on the East Greenland continental slope (EG-II, EG-III), and a shallow-water site on the Svalbard

shelf (SV-III), we were able to successfully sample all HAUSGARTEN stations. Comparing the concentrations of sediment-bound pigments and potential bacterial activities along the bathymetric transect crossing the Fram Strait, and along the latitudinal transect with stations at different distances to the ice-edge in northern parts of the strait, we found noticeable differences (Fig. 3.3). Irrespectively from their station depths, all sites on the East Greenland continental margin exhibited generally lower pigment values, compared to those stations off Svalbard.

Pigment concentrations and bacterial activities showed a general trend with decreasing values with increasing water depth. However, the deepest station along the HAUSGARTEN depth transect (HG-IX) and the deepest station off Greenland (EG-IV) exhibited conspicuously increased values. Station HG-IX is situated at the Molloy Hole, a deep depression with a maximum depth at 5,600 m water depth. The increase of biogenic sediment compounds at great depth is a feature which has been observed in other deep trenches. The Molloy Hole seems to act as a deposit centre for organic matter, indicating that the Molloy Hole is a natural trap for organic matter at abyssal depths in the Fram Strait. The increased values observed at station EG-IV could probably be explained by its location close to the ice-edge in western parts of the Fram Strait. Generally increased primary production in the Marginal Ice Zone (MIZ) and subsequently enhanced sedimentation of phytodetritial matter, representing a potential food source to benthic organisms, could explain the increased pigment and activity values found at EG-IV. Values along the latitudinal transect showed no clear trend.

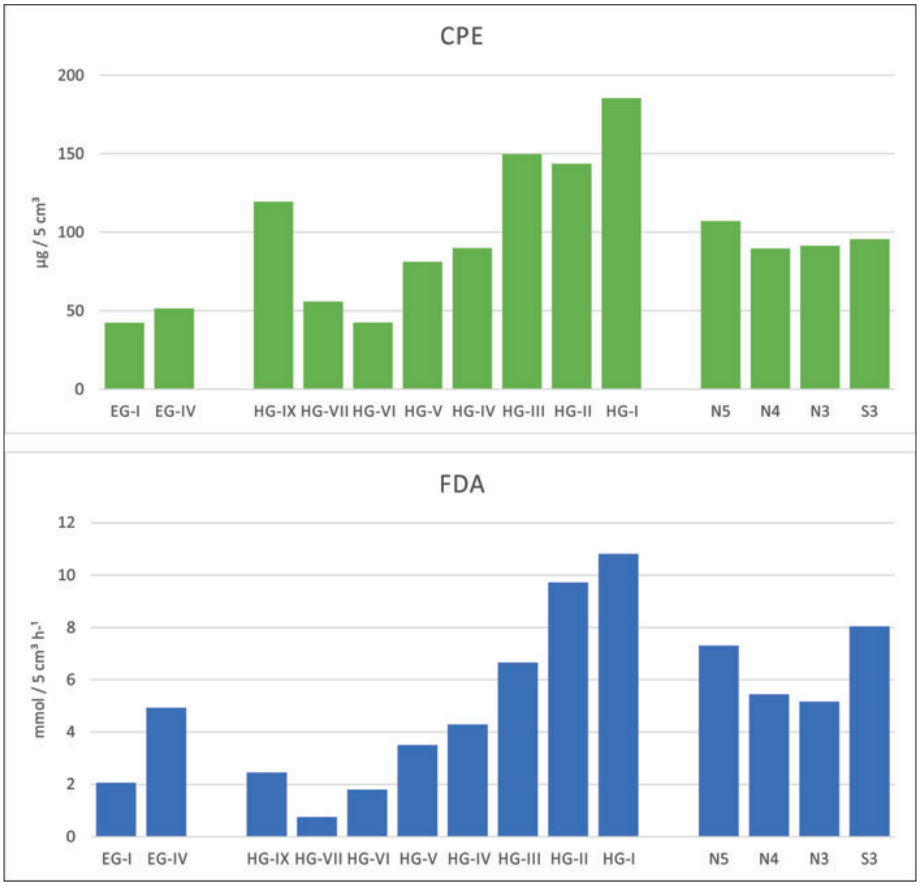

Fig. 3.3: Preliminary results from on-board pigment measurements (top; Concentrations of Chloroplastic Pigment Equivalents, CPE) and bacterial activity assessments (bottom; degradation of the artificial substrate Fluorescein-di-acetate, FDA)

Macrobenthos und sediment profiling imagery

Sediment pictures taken by the SPI camera provide already first insights into differences between sites (Fig. 3.4). The sites SV-IV and HG-I to HG-III showed a distinct layering in sediments which disappeared towards the deeper HAUSGARTEN stations (HG-IV to HG-VI). Along the latitudinal gradient (from south to north: S3 – HG-IV – N3 – N4), sediment layering was rather similar.

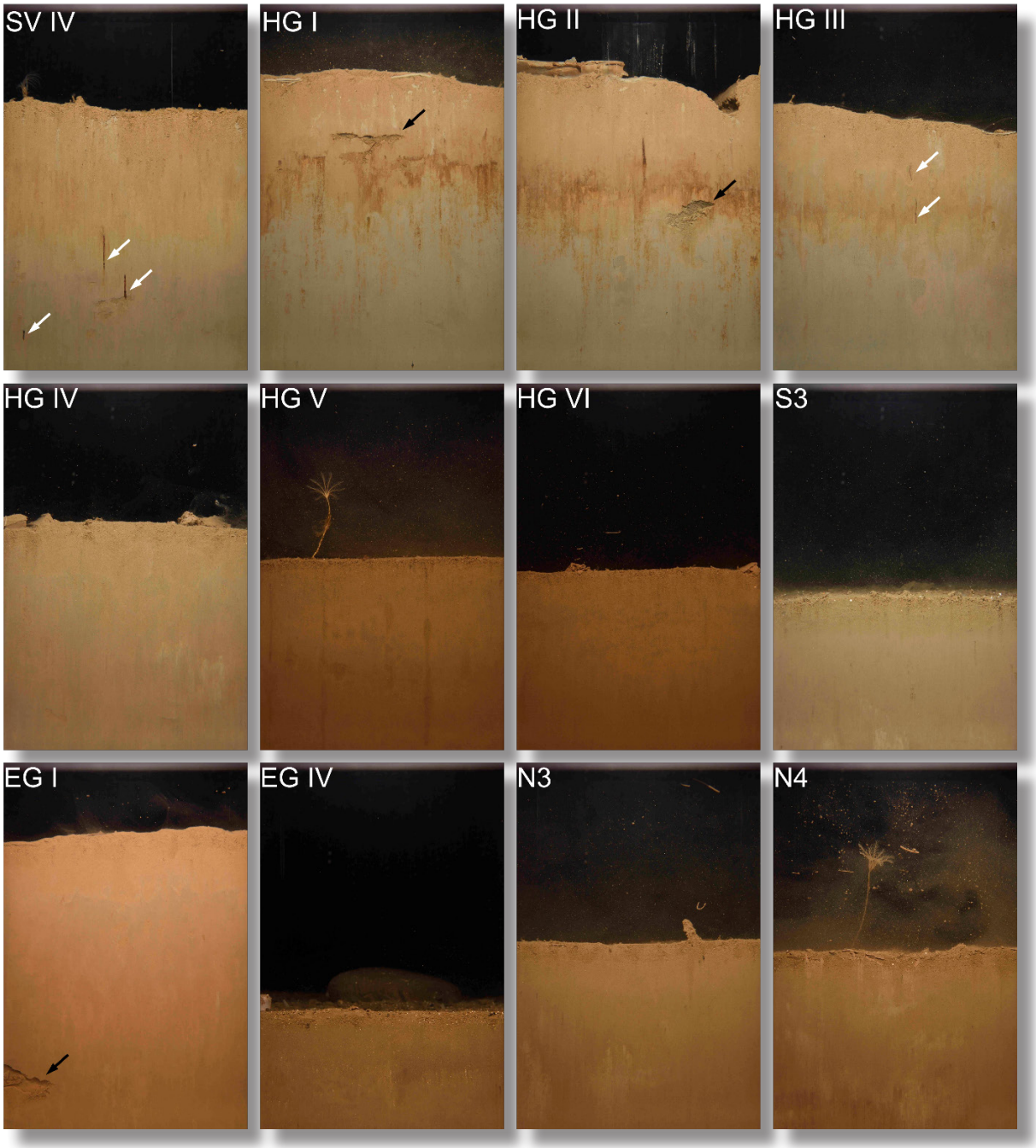

Fig. 3.4: Sediment profile images of selected sites sampled during Polarstern expedition PS126; size of image is 14 x 21 cm. Note the polychaetes in the pictures (white arrows), probably of the family Maldanidae and the burrows (black arrows). Note: HG-V and N4 picture show Bathycrinus spp. at the sediment surface

Further remarkable differences were detected between EG-I and EG-IV. While EG-I exhibited a soft and silty homogenous sediment, the EG-IV consisted of more sandy sediment (and thus low penetration depth of the SPI cam) with lots of Foraminifera, also in deeper sediment layers (small white dots on picture).

We had no idea how informative the SPI pictures would be, as the gear has never been applied in the Arctic deep-sea. Hence, we were surprised about distinct sediment layers and the high bioturbation activity within the sediment by the macrobenthic fauna at shallower sites. Bioturbation activity reached down to 16 cm (see burrows in Fig. 3.4, EG-I) and 14 cm by polychaetes probably of the family Maldanidae (see SV-IV). Even at the sites deeper than 3,000 m (HG-V), clear activity was visible by the vertical colour changes in the sediment. Further in-depth analysis of the pictures will be carried out with software tools in the near future and combined with the diversity data from the box corer samples.

Megabenthos and seafloor mapping

The shallowest station HG-I (1,200 m water depth) was characterised primarily by a host of brittlestars (*Ophiocten hastatum*) and worm tubes with some cerianthid anemones, pycnogonids (*Colossendeis proboscidea*), eelpout fish (*Lycodes squamiventer*) and a few rays (*Amblyraja hyperborea*) (Fig. 3.5). A few features, which resembled pock marks were also observed.

Fig. 3.5: Examples of epibenthic megafauna and pock-mark featurephotographed by OFOBS at HAUSGARTEN station HG-I

The four deeper stations (HG-IV, S3, N3, EG-IV; ca. 2,500 – 2,800 m) had a different species composition with sea cucumbers (*Elpidia heckeri*), sea lilies (*Bathycrinus capenterii*), sponges (*Cladorhiza gelida, Caulophacus arcticus*), different sea anemones, soft corals (*Gersemia fruticosa*) shrimps (*Bythocaris* spp.), and the burrowing amphipod *Neohela lamia*.

At station N3, and to a lesser extent also at HG-IV, traces were observed that may be caused by sponges on stones being dragged along the sediments by strong bottom currents. At EG-IV, numerous algal deposits were seen, which mirrored the occurrence of *Melosira arctica* floating at the sea surface between ice floes. Results of time-series analyses will only be available once the collected images will have been analysed. However, a few selected images and photographed species are shown in Fig. 3.6.

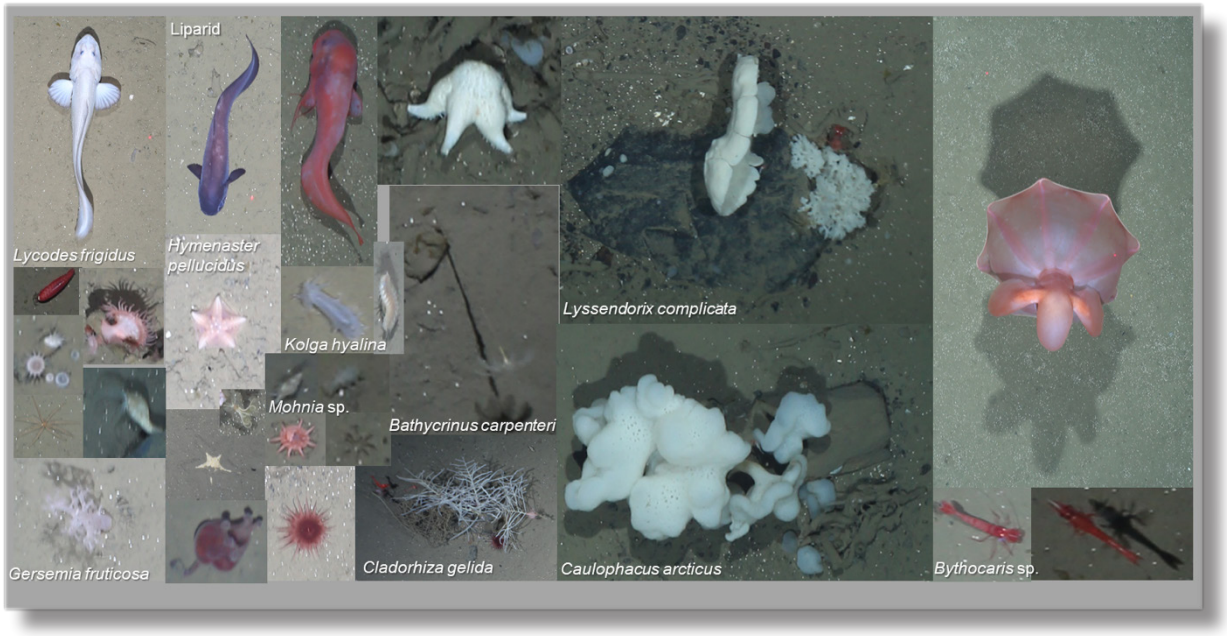

Fig. 3.6: Examples of epibenthic megafauna photographed by OFOBS at HAUSGARTEN station HG-IV, S3, N3, EG-IV)

Dropstones were observed at all of these stations but were particularly abundant at EG-IV. Interestingly, many of these were not colonised by sessile benthic organisms. This could be because of low larval supplies carried by the East Greenland Current, which prevails in this area or because they were dropped only recently. It is conceivable that accelerated glacial melting due to climate change could deliver more (drop-)stones into this area. Indeed, two icebergs were seen during PS126 and further investigated during helicopter visits (see Chapter 10). The cryosphere of one of them had melted exposing the underlying surface of shale gravel and rocks, which resembled the dropstones observed in the area (Fig. 3.7). Further analysis of seafloor photographs will tell if the abundance of hard substrata has increased at EG-IV. This is important as it affects the species composition in otherwise homogenous soft-sediment habitats (Schulz et al. 2010) and thereby biodiversity. This could be a direct link between terrestrial changes due to climate change and deep-sea communities.

Of the non-scientific deployments of OFOBS, three were successful in retrieving stuck equipment, with a further dive identifying that a lander had been pulled from position by an iceberg. The new 'Remora' class ROV developed within AWI's Deep-Sea Ecology and Technology section was used in combination with the OFOBS acoustic systems to locate stranded equipment. The main aim was to recover the Benthic Crawler NOMAD at the central HAUSGARTEN station HG-IV, which had become stuck previously on a rock, and this was carried out successfully.

Fig. 3.7: Mosaic and photographs taken of an iceberg in close vicinity to station EG-IV, whose seafloor harbours many dropstones

At HAUSGARTEN station S3, the Autonomous Underwater Vehicle PAUL successfully collected seafloor images, some of which have already been used to produce 3D models of areas of the seafloor using the Agisoft Metashape software application (Fig. 3.8). Additionally, acoustic data collected concurrently with the image data will be used to map the dropstones in the region (Fig. 3.9). During the forthcoming months the acoustic and image data collected during the cruise will be processed, with assistance from the AWI bathymetry team, to derive high resolution mapping products for the S3 and HG-IV stations. Additionally, features and areas of interest will be used to produce 3D models of the seafloor.

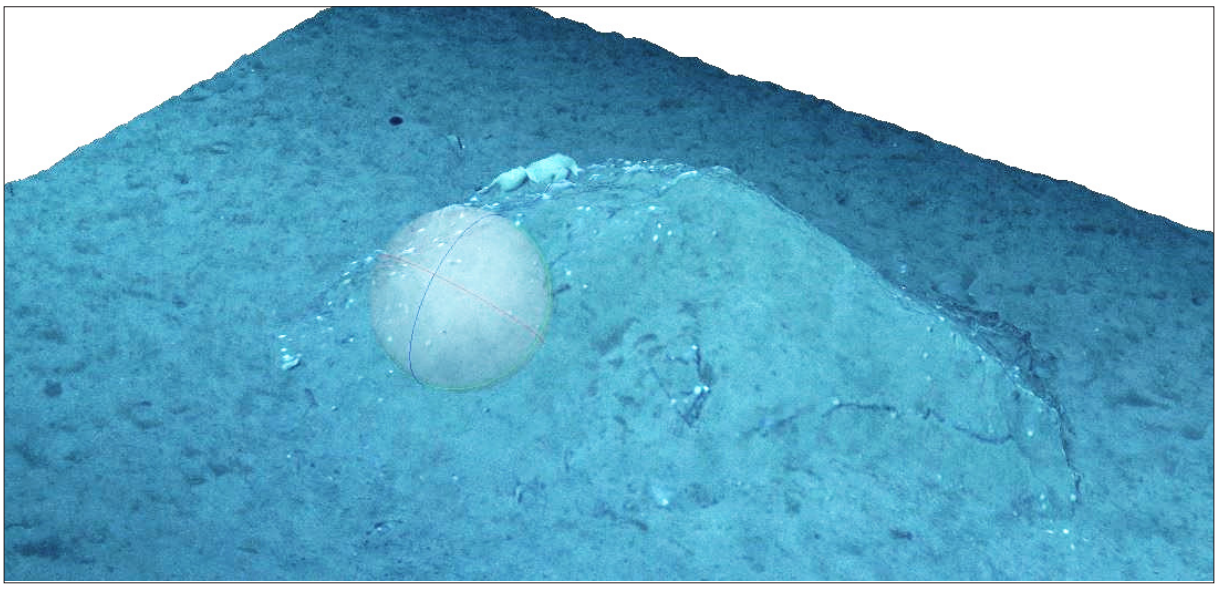

Fig. 3.8: Agisoft Photoscan 3D model of a dropstone from the S3 seafloor generated from AUV PAUL raw image data

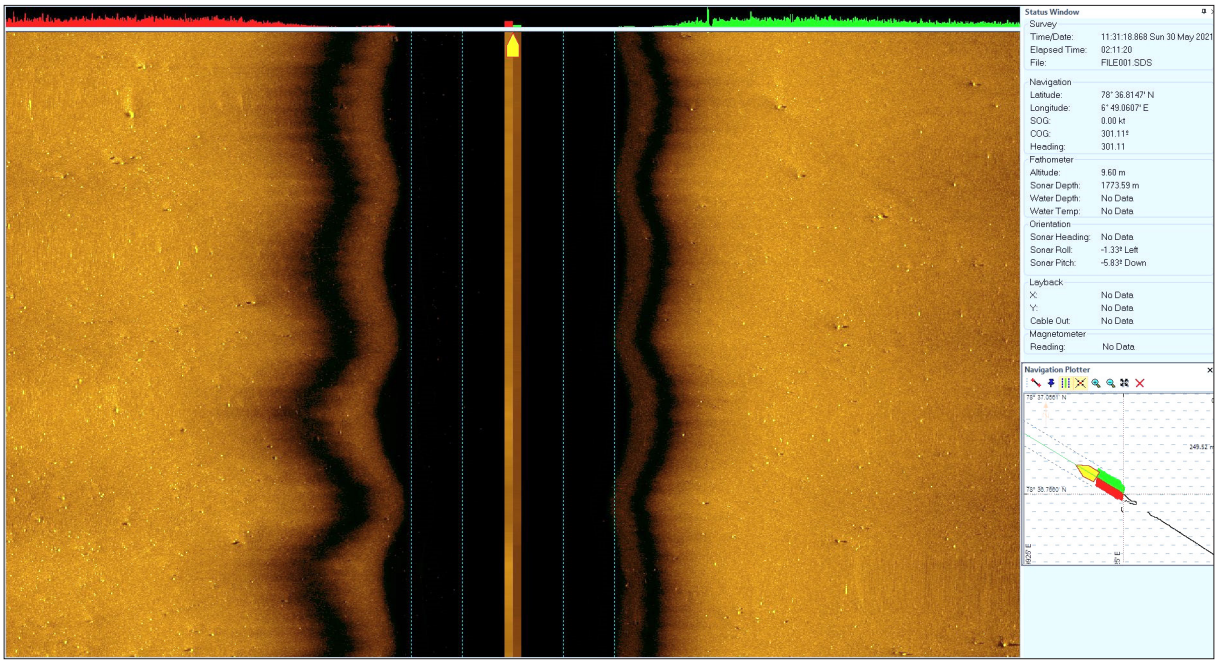

Fig. 3.9: AUV raw sidescan data showing the fairly flat and plain seafloor of the HAUSGARTEN S3 site, with occasional dropstones evident

Larval biology in the Fram Strait

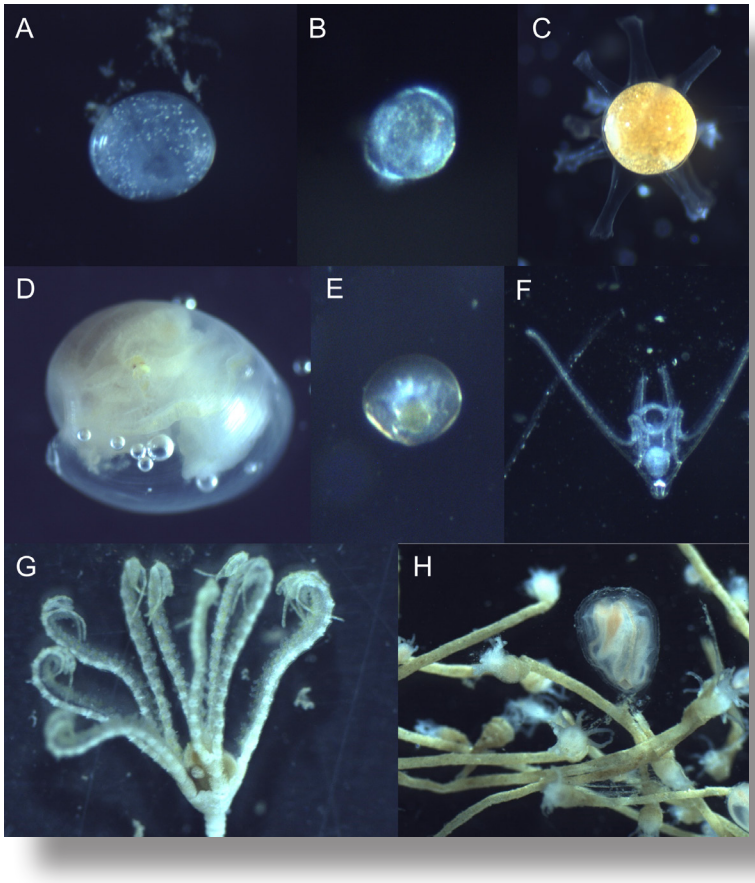

We collected over 300 specimens of larvae and recruits at HAUSGARTEN. These samples provide insights into larval dispersal in the Fram Strait. For example, any species that grows on an oceanographic instrument deployed on a mooring in the middle of the water column must have larvae at that location and depth. The most interesting specimens are shown below (Fig. 3.10). All specimens will be identified to the lowest taxonomic level possible using DNA sequencing after the expedition.

Fig. 3.10: Various types of organismic development stages found during expedition PS126

Sponges (Fig. 3.10 A) were collected with the larval pump at stations S3, HG-IV, and “Senke”. At 540 µm across, these specimens are quite large for larvae. They were observed alone and inside of spherical structures with hexactinellid spicules – potentially juvenile sponges. All known sponge larvae are lecithotrophic (Maldonado 2006). Some species also reproduce via gemmules, which are spore-like asexual structures that disperse, settle, and grow into new sponges. It is possible that the specimens we collected are gemmules. The most common hexactinellid sponge at HAUSGARTEN is *Caulophacus arcticus*, and the spicule spheres we observed bore a resemblance to juvenile sponges collected as part of a long-term recruitment experiment at HG-IV (Meyer-Kaiser et al. 2019).

Trochophore larvae (Fig. 3.10 B) were collected in Hand net samples at the surface at stations EG-I, HG-V, and HG-VII. Several phyla have trochophore larvae, so it is not possible to identify which group this larva belongs to until DNA analysis is conducted. Trochophore specimens were collected far offshore and at the surface, so they are either (1) a shallow coastal species with larvae that disperse far from the coast, or (2) a deep-sea species with larvae that disperse at the surface.

Soft corals (Fig. 3.10 C) with polyps were collected with the larval pump at stations “South reef” and “Senke”. Peach embryos with a similar appearance were collected with the larval pump at stations HG-IV, “Senke,” and “South reef.” There are two species of soft corals at HAUSGARTEN, *Gersemia rubiformis* and *G. fruticosa*. *Gersemia fruticosa* has a planula larva that settles 3 – 70 days after release (Sun et al. 2011). The specimens with polyps that we collected have a very different appearance than *G. fruticosa* planulae, which are elongated and only develop polyps after settlement (Sun et al. 2011). The specimens we collected might belong to *G. rubiformis* or a different species.

Gastropods (Fig. 3.10 D) were collected with the larval pump at station “Senke.” There is only one species of gastropod at HAUSGARTEN, *Mohnia mohnia*. The specimen we collected is very large (2.7 mm across) and could be a juvenile. Analysis of the shell will reveal whether this gastropod is lecithotrophic or planktotrophic during the larval phase.

Bivalve larvae (Fig. 3.10 E) were collected at many stations. The specimen shown here was collected using the Hand net at station HG-V. It strongly resembles specimens collected using a larval trap at 67 m depth on mooring FEVI-37 in 2019 and using the larval pump at station HG-IV during PS126. This bivalve is most likely either a shallow-water species with larvae that disperse far offshore or a deep-sea species with larvae that disperse at the surface.

Pluteus larvae (Fig. 3.10 F) were collected in Hand net tows at stations EG-I, HG-V, and “South reef.” Pluteus larvae develop into echinoids (sea urchins) or ophiuroids (brittle stars). There are several echinoids and ophiuroids at HAUSGARTEN, including *Ophiocten gracilis* and *Pourtalesia jeffreysi*. Juveniles of the upper bathyal brittle star *Ophiura sarsi* have been collected in larval traps on moorings at station N4 (FEVI-39) and the central HAUSGARTEN site (HG-IV-S-3). Genetic identification of the plutei we collected will inform the dispersal patterns of echinoids and ophiuroids at HAUSGARTEN.

Pentacrinoids (Fig. 3.10 G) were collected from shallow (47 – 67 m) instruments and floats on the mooring EGC-6. These specimens do not resemble the eurybathic feather star *Poliometra prolixa* and may belong to its shallow-water counterpart *Heliometra glacialis*. Because the pentacrinoids were found on instruments in the middle of the water column and far from the seafloor (~1,000 m at station EG-I), it can be inferred that the larvae disperse far away from their parents and are carried in the East Greenland Current.

Hydroids were collected from multiple moorings, the long-term lander, and benthic crawlers TRAMPER and NOMAD. For three species, *Bouillonia cornucopia*, *Stegopoma plicatile*, and an unidentified stolonal athecate hydroid (Fig. 3.10 H), reproductive structures were observed. The latter two species bore gonozooids and released medusae in lab dishes during PS126. Reproduction via medusae is logical for these species that have broad distributions and opportunistically colonize moorings in the Fram Strait.

Data management

Many of the samples will be processed and further analysed at AWI within approximately one year after the cruise. We plan that the full data set will be available at latest about 2-3 years after the cruise. Faunal and environmental data as well as all acoustic and image data collected by the AUV and the towed camera systems during PS126 will be archived, published and disseminated according to international standards by the World Data Center PANGAEA Data Publisher for Earth & Environmental Science (https://www.pangaea.de) within two years after the end of the cruise at the latest. The CC-BY license will be applied after publication.

In addition, all macrobenthic data will also be deposited in CRITTERBASE at AWI, seafloor still images will be uploaded to the online image database BIIGLE to enable access by other parties, and DNA sequences of larvae and recruits collected during PS126 will be archived in GenBank. Interested researchers, particularly taxonomists, can request access to images and specimens by contacting K. Meyer-Kaiser (kmeyer@whoi.edu).

In all publications, based on this cruise, the **Grant No. AWI_PS126_01** will be quoted and the following *Polarstern* article will be cited: Alfred-Wegener-Institut Helmholtz-Zentrum für Polar- und Meeresforschung (2017) Polar Research and Supply Vessel POLARSTERN Operated by the Alfred-Wegener-Institute. Journal of large-scale research facilities, 3, A119. http://dx.doi.org/10.17815/jlsrf-3-163.

References

Bergmann M, Soltwedel T, Klages M (2011) The interannual variability of megafaunal assemblages in the Arctic deep sea: Preliminary results from the HAUSGARTEN observatory (79°N). Deep-Sea Research I, 58, 711-723.

Buhl-Mortensen L, Buhl-Mortensen P, Dolan MFJ, Dannheim J, Bellec V, Holte B (2012) Habitat complexity and bottom fauna composition at different scales on the continental shelf and slope of northern Norway. Hydrobiologia, 685(1), 191-219.

Buhl-Mortensen L, Vanreusel A, Gooday AJ, Levin LA, Priede IG, Buhl-Mortensen P, Gheerardyn H, King NJ, Raes M (2010) Biological structures as a source of habitat heterogeneity and biodiversity on the deep ocean margins. Marine Ecology – an Evolutionary Perspective, 31(1), 21-50.

Gage JD, Tyler PA (1991) Deep-sea biology: a natural history of organisms at the deep-sea floor. London: Cambridge University Press.

Maldonado M (2006) The ecology of the sponge larva. Canadian journal of zoology, 84, 175-194.

McClain CR, Filler R, Auld JR (2014) Does energy availability predict gastropod reproductive strategies? Proceedings of the Royal Society B, 281, 20140400.

Meyer K, Bergmann M, Soltwedel T (2013) Interannual variation in the epibenthic megafauna at the shallowest station of the HAUSGARTEN observatory (79°N, 6°E). Biogeosciences, 10, 3479-3492.

Meyer-Kaiser K, Bergmann M, Soltwedel T, Klages M (2019) Recruitment of Arctic deep-sea invertebrates: results from a long-term hard-substrate colonization experiment at the Long-Term Ecological Research observatory HAUSGARTEN. Limnology and oceanography, 64, 1924-1938.

Piepenburg D (2005) Recent research on Arctic benthos: common notions need to be revised. Polar Biology, 28(10), 733-755

Poulin E, Palma AT, Féral J-P (2002) Evolutionary versus ecological success in Antarctic benthic invertebrates. Trends in ecology and evolution, 17, 218-222.

Purser A, Marcon Y, Dreutter S, Hoge U, Sablotny B, Hehemann L, Lemburg J, Dorschel B, Biebow H, Boetius A (2018) OFOBS – Ocean Floor Observation and Bathymetry System: A new towed camera/sonar system for deep sea exploration and survey. IEEE Journal of Oceanic Engineering, doi: 10.1109/JOE.2018.2794095.

Purser A, Herr H, Dreutter S, Dorschel B, Glud R, Hehemann L, Jamieson A, Linley T, Stewart H, Wenzhöfer F (2019) Depression chains in seafloor of contrasting morphology, Atacama Trench margin. A comment on Marsh el al. (2018). Royal Society Open Science, 6, 182053.

Purser A, Hoge U, Busack M, Hagemann J, Lehmenhecker S, Dauer E, Korfman N, Boehringer L, Merten V, Priest T, Dreutter S, Warnke F, Hehemann L (2021) Arctic Seafloor Integrity, Cruise No. MSM95 – (GPF 19-2_05), 09.09.2020 – 07.10.2020, Emden (Germany) – Emden (Germany). doi: 10.48433/cr_msm95.

Schulz M, Bergmann M, von Juterzenka K, Soltwedel T (2010) Colonisation of hard substrata along a channel system in the deep Greenland Sea. Polar Biology, 33, 1359-1369.

Soltwedel T, Bauerfeind E, Bergmann M, Bracher A, Budaeva N, Busch K, Cherkasheva A, Fahl K, Grzelak K, Hasemann C, Jacob M, Kraft A, Lalande C, Metfies K, Nöthig E-M, Meyer K, Quéric N-V, Schewe I, Wlodarska-Kowalczuk M, Klages M (2016) Natural variability or anthropogenically – induced variation? Insights from 15 years of multidisciplinary observations at the arctic marine LTER site HAUSGARTEN. Ecological Indicators, 65, 89-102.

Sun Z, Hamel J-F, Mercier A (2011) Planulation, larval biology, and early growth of the deep-sea soft corals *Gersemia fruticosa* and *Duva florida* (Octocorallia: Alcyonacea). Invertebrate Biology, 130, 91-99.

Taylor J, Krumpen T, Soltwedel T, Gutt J, Bergmann M (2016) Regional- and local-scale variations in benthic megafaunal composition at the Arctic deep-sea observatory HAUSGARTEN. Deep-Sea Research Part I: Oceanographic Research Papers, 108, 58-72.

Taylor J, Krumpen T, Soltwedel T, Gutt J, Bergmann M (2017) Dynamic benthic megafaunal communities: Assessing temporal variations in structure, composition and diversity at the Arctic deep-sea observatory HAUSGARTEN between 2004 and 2015. Deep Sea Research I, 122, 81-94.

Taylor J, Staufenbiel B, Soltwedel T, Bergmann M (2018) Temporal trends in the biomass of three epibenthic invertebrates from the deep-sea observatory HAUSGARTEN (Fram Strait, Arctic Ocean). Marine Ecology Progress Series, 602, 15-29.

Tews J, Brose U, Grimm V, Tielbörger K, Wichmann MC, Schwager M, Jeltsch F (2004) Animal species diversity driven by habitat heterogeneity/diversity: the importance of keystone structures. Journal of Biogeography, 31(1), 79-92.

Thorson G (1950) Reproductive and larval ecology of marine bottom invertebrates. Biological reviews of the Cambridge Philosophical Society, 25, 1-45.

Whittaker RJ, Willis KJ, Field R (2001) Scale and species richness: towards a general, hierarchical theory of species diversity. Journal of Biogeography, 28(4), 453-470.

Young CM, He R, Emlet RB, Li Y, Qian H, Arellano SM, Van Gaest A, Bennett KC, Wolf M, Smart TI, Rice ME (2012) Dispersal of deep-sea larvae from the intra-american seas: simulations of trajectories using ocean models. Integrative and comparative biology, 52, 483-496.

4. PEBCAO – PLANKTON ECOLOGY AND BIOGEOCHEMISTRY IN A CHANGING ARCTIC OCEAN

Katja Metfies[1], Sandra Golde[2], Christian Hohe[1], Anabel von Jackowski[2], Dong-gyun Kim[1], Tanja Klüver[2], Nadine Knüppel[1], Alexandra Kraberg[1], Anja Nicolaus[1], Tobias Strickmann[1], JosefineWeiss[1], Hongyan Xi[1]; Astrid Bracher[1], Eva-Maria Nöthig[1], Barbara Niehoff[1], Ilka Peeken[1], Anja Engel[2] (not on board)

[1]DE.AWI
[2]DE.GEOMAR

Grant-No. AWI_PS126_02

Outline

The Arctic Ocean has gained increasing attention in recent decades due to the drastic decrease in sea ice and increase in temperature, which is approximately twice as fast as the global average. It is also expected that the chemical equilibrium and the elemental cycling in the surface ocean changes due to ocean acidification. Only long-term observations can unravel the effects of such changes on the Plankton Ecology and Biology in the Arctic Ocean; investigations are carried out in the working group of the same title, which bears the acronym PEBCAO (Fig. 4.1).

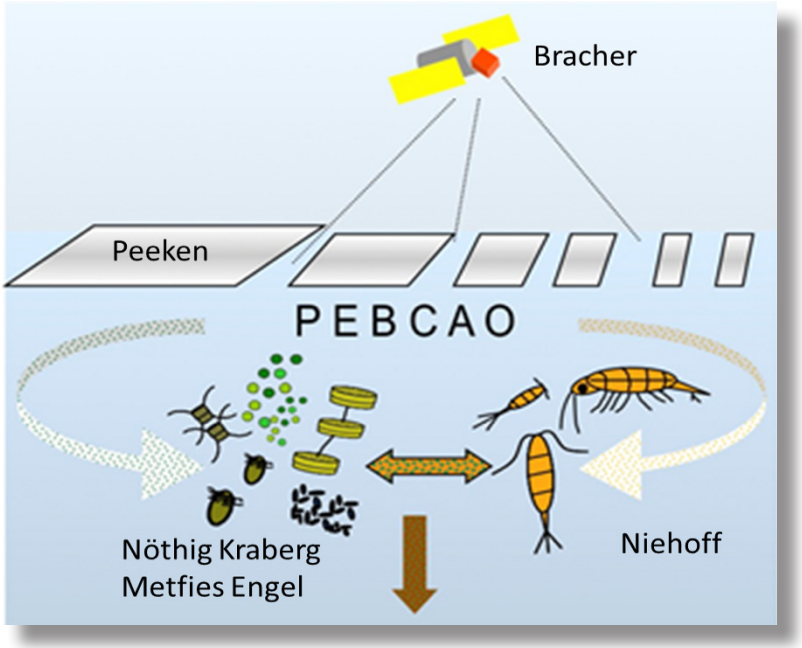

Fig. 4.1: Schematic overview illustrating the scientific contributions of the participating groups to the PEBCAO approach

The PEBCAO group began its studies on plankton ecology in the Fram Strait (~79° N) in 1991 and intensified its efforts in 2009. Since then, we have combined classical bulk measurements of biogeochemical parameters, microscopy, optical methods, satellite observations, and molecular genetic approaches in a holistic approach. By doing so, we have compiled comprehensive information on annual variability in phyto- and zooplankton composition, primary production, and bacterial activity.

Our long term-observations so far have already revealed important patterns of spatio-temporal distributional patterns and changes in plankton diversity. Our results clearly indicate, for instance, that chlorophyll *a* (Chl *a*) values increase in summer in the eastern but not in the western Fram Strait (Nöthig et al. 2015, 2020). This is in accordance with the increasing contributions of *Phaeocystis pouchetii* and nanoflagellates to the summer phytoplankton community. The concentration of dissolved organic carbon (DOC) was relatively stable over the last two decades, but we observed a slight decrease in the particulate organic carbon (POC) during the summer months (Engel et al. 2019). This could suggest that the phytoplankton composition affected the POC. We also observed that *Themisto compressa*, an invading amphipod species, increased in abundance (Kraft et al. 2013; Schröter et al. 2019). All of this suggests that the ecosystem in Fram Strait is undergoing profound changes likely induced by climate conditions, which warrants sustained observation.

As of 2014, the PEBCAO group is a member of the FRAM (Frontiers in Arctic Monitoring) Ocean Observatory Team and provides baseline information on plankton ecology, biogeochemical parameters, and microbial (prokaryotic and eukaryotic) biodiversity. We are also involved in the development of automatic platforms and sampling technology for long-term monitoring in the Arctic Ocean with a main focus on the LTER observatory HAUSGARTEN.

Objectives

The overarching objectives of PEBCAO are (1) to improve our mechanistic understanding of biogeochemical and microbiological feedback processes in the Arctic Ocean, (2) to document ongoing and long-term changes in the biotic and abiotic environment, and (3) to assess the potential future consequences of these changes. In particular, we aim to identify climate-induced changes in the biodiversity of Arctic pelagic ecosystems and, concomitantly, in carbon cycling and sequestering. These objectives are addressed using a range of approaches:

Primary production is expected to increase in the changing Arctic Ocean, however, it is currently unclear whether this will lead to increased export of particulate organic carbon or whether primary production will remain at the surface, fuelling growth of zooplankton and heterotrophic bacteria. Heterotrophic bacteria play a vital role in global biogeochemical cycles. To fully assess bacterial activity, we measure bacterial production and use three techniques (including Winkler titration, optodes and *in-vivo* INT [Iodo-Nitro-Tetrazolium] reduction method) to measure bacterial respiration in the Fram Strait. By linking compound dynamics with rate measurements and community structure, we will gain further insights into the flow of carbon through the Arctic food web. To address the effects of global change on microbial biogeochemistry in the Arctic Ocean, we will also continue to monitor concentrations of organic carbon, nitrogen, and phosphorus, as well as specific compounds like amino acids, carbohydrates, and gel particles. To assess cell abundances and community composition, we will sample for microscopic counts and flow cytometry (< 50 µm), to determine phytoplankton, bacteria, and viral abundances. In addition, we perform rate measurements of phytoplankton primary and heterotrophic bacterial production. Phytoplankton primary production was distinguished into particulate primary production (carbon remaining in the cells) and dissolved primary production (organic carbon subsequently released by cells).

We expect that the small algae at the base of the food web gain importance in mediating element and matter turnover as well as energy fluxes in Arctic pelagic systems. In order to detect changes, also in this smallest fraction of the plankton, traditional microscopy and flow cytometry is complemented by molecular methods that are independent of cell-size and morphological features. The assessment of the biodiversity and biogeography of Arctic prokaryotic and eukaryotic microbes is based on the analysis of ribosomal genes with high-throughput sequencing technology. Many zooplankton species are affected by the changes at the base of the food web as they rely on phytoplankton as a food source.

During PS126, for the first time, we included protistan parasites in our research programme. These are severely understudied in the marine realm although they are likely to affect the population dynamics of phytoplankton (including bloom timing and magnitude) and zooplankton. We therefore conducted a baseline study of the diversity of different parasite groups and their association with potential hosts. This investigation will also form the basis for future biogeographic studies. The analyses in the laboratories will combine different microscopy techniques (LM, SEM, CFLM) as well as obtaining molecular data, the latter facilitating observation of parasitism even at times where easily discernible parasite life-cycle stages are absent.

The zooplankton community composition may also shift due to the increasing inflow of warmer Atlantic water into the Fram Strait. Most of zooplankton species are related to specific water masses. For examples, while the boreal zooplankton *Calanus finmarchicus* is transported with the North Atlantic current, its sibling species *C. glacialis* inhabits Arctic water masses. Rising water temperatures and altered hydrographical conditions could therefore result in a shift in the zooplankton species composition in the Fram Strait and the Arctic Ocean. Altered zooplankton trophic interactions and community compositions will have consequences for the carbon sequestration and flux. Most of our knowledge on zooplankton species composition and distribution has been derived from traditional multiple net samplers, which integrate depth intervals of up to several hundred meters. Nowadays, optical systems, such as the zooplankton recorder LOKI (Lightframe On-sight Key species Investigation), continuously take pictures of the organisms during vertical casts from 1,000 m to the surface. Linked to each picture, hydrographical parameters are being recorded, i.e. salinity, temperature, oxygen concentration, and fluorescence. This allows us to exactly identify distribution patterns in relation to environmental conditions. To detect the impacts of climate change on pelagic ecosystems in the Arctic, we used this approach to study the zooplankton community composition and depth distribution in Fram Strait during PS126 and we will compare the results with those gained on previous cruises to the same area.

Ocean colour remote sensing allows for estimating the overall phytoplankton biomass (indicated by Chl *a* concentration), distinctive major groups (abbreviated as phytoplankton functional types, PFT) and coloured dissolved organic matter (CDOM) at global and high temporal (daily) scales not met by our discrete sampling during the expedition. However, at high latitudes, ocean colour satellite data has sparse coverage due to the presence of sea ice, clouds and low sun elevation. To complement remote sensing data, underway spectrophotometry and hyperspectral radiometry enables to obtain attenuation and absorption data which can be further processed to Chl *a* and marker pigment concentrations, PFT Chl *a* and CDOM (Liu et al. 2018, 2019; Bracher et al. 2020) at high sampling resolution for the surface waters crossed during the entire cruise and for the underwater light profile at the CTD stations. However, the derivation of these final biogeochemical products requires the verification with direct analysis of these parameters on regularly sampled discrete water in order to quantify the potential and limitations in terms of uncertainties of these optically derived biogeochemical parameters. In conjunction with satellite data (e.g. products from Losa et al. 2017; Oelker et al. 2020; Xi et al. 2020) these discrete and continuously sampled data sets are of high value to upscale

biogeochemical or phytoplankton quantities at higher resolution and better coverage. In addition, these data serve for validating ocean colour products from the Sentinel-3 OLCI and the Sentinel-5P TROPOMI sensors. The group of A. Bracher is part of the Sentinel-3 Validation Team and the PI of the ESA study Sentinel-5P Ocean Colour. Overall the cruise data provide a fundamental contribution for further development of hyper- and multispectral ocean colour satellite retrievals focusing on fluorescence and absorption signals.

In summary during PS126 the following topics were covered:

- Monitoring plankton species composition and biomass distribution
- Determining autotrophic and heterotrophic microbial activities
- Monitoring biogeochemical parameters
- Investigating selected phyto- and zooplankton (including their parasites)
- Determining the composition of organic matter and gel particles
- Investigating amount and composition of CDOM and their interplay with phytoplankton
- Characterisation of the underwater light field and its interplay with optical constituents, such as phytoplankton and CDOM abundance and composition.

Work at sea

Measurements and sample collections for a large variety of parameters were accomplished by the PEBCAO-group at 19 stations of the LTER observatory HAUSGARTEN during PS126, including the frontal zone separating the warm and cold-water masses originating from the West Spitsbergen Current and the East Greenland Current. Measurements and sampling comprised CTD/Rosette Water Sampler casts, underway sampling with the automated filtration device AUTOFIM, net hauls as well as the deployment of RAMSES and the LOKI system.

Biogeochemistry (AG Engel)

We collected seawater samples from 5 to 12 depths by a CTD/Rosette Water Sampler (Fig. 4.2) in the Fram Strait area to determine the impact of microbial processes on the cycling of organic matter. Samples were taken for dissolved biogeochemical parameters, such as dissolved organic carbon / total dissolved nitrogen (DOC/TDN) and dissolved organic phosphorus (DOP), which were filtered over 0.45 µm GMF syringe filters and stored at 4° C and –20° C, respectively. Dissolved amino acids (DAA) and carbohydrates (DCHO) were filtered over 0.45 µm Acrodisc filters into combusted glass vials and stored at –20° C. Similarly, seawater was filtered for total amino acids (TAA) and total carbohydrates (TCHO), which will allow for the determination of the particulate fraction. Concentrations will be determined by the use of high-performance liquid chromatography (HPLC) and high-performance anion-exchange chromatography (HPAEC) coupled with pulsed amperometric detection (PAD) at GEOMAR, Kiel, Germany.

Additionally, we sampled for chromophoric (CDOM) and fluorescent dissolved organic matter (FDOM). CDOM refers to DOM that absorbs light over a broad spectrum from UV to visible wavelengths, while FDOM is a part of CDOM that may fluoresce due to its aromatic nature. CDOM and FDOM are used to infer DOM quality and will be analysed by a spectrophotometer at GEOMAR, Kiel, Germany.

We sampled seawater of the upper three depths by CTD/Rosette Water Sampler within the Fram Strait to explore the sources of surfactants. The sources of surfactants will be measured by phase-sensitive alternating voltammetry (Cosović and Vojvodić 1998). To our knowledge, this will be the first dataset for surfactants in the Arctic Ocean.

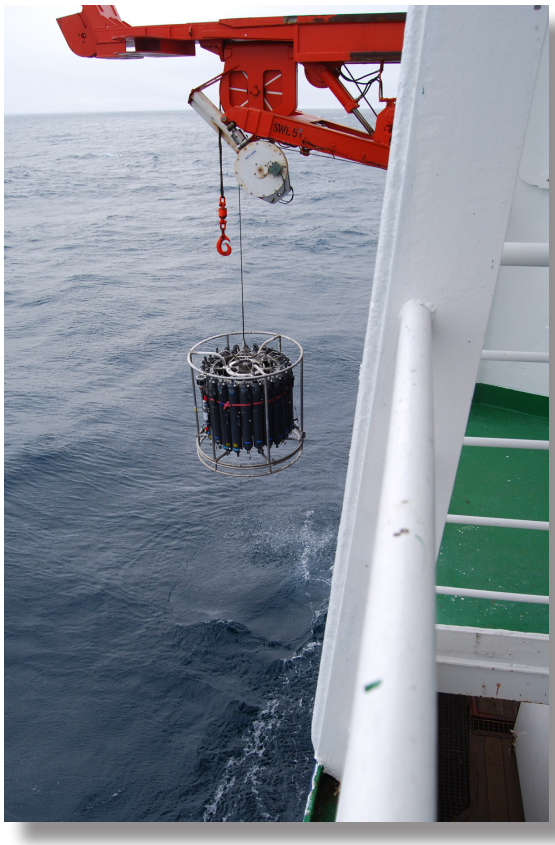

Fig. 4.2: Deployment of the CTD / Rosette Water Sampler

Samples for transparent exopolymer particles (TEP) and Coomassie stainable particles (CSP) were taken and stored at –20° C until analysis by photometry and microscopy back at GEOMAR, Kiel, Germany (Engel 2009).

Furthermore, we sampled for community abundance, activity and respiration. The samples for bacterial (BA) and phytoplankton (PA; < 50 µm) abundance were fixed and frozen at – 80° C for further analysis by flow-cytometry at GEOMAR, Kiel, Germany. The *in-situ* phytoplankton primary production (PhytoPP) was assessed using a FastOcean APD Profiling System (Chelsea Technologies, UK). Moreover, primary production (PP) rates determined onboard using a radioactive isotope approach with 14-C sodium bicarbonate and bacterial biomass production (BBP) rates were determined using 3-H leucine. Community respiration was measured by Winkler titrations (Krey et al. 1980, Grasshoff et al. 1999), optodes, and *in-vivo* INT reduction method (García-Martín et al. 2019).

Table 4.1 provides an overview of which stations were sampled for the different parameters.

Tab. 4.1: Sampling for bacteria and biogeochemistry; DOM: dissolved organic matter (includes: dissolved organic carbon, total dissolved nitrogen, dissolved organic phosphorus, dissolved and total amino acids, dissolved and total carbohydrates, coloured and fluorescent organic matter); TEP: transparent exopolymer particles; CSP: Coomassie stainable particles; BA: bacterial cell numbers; PA: phytoplankton cell numbers; PhytoPP The *in-situ* assessment of phytoplankton primary production; PP: Primary Production 14-C; BBP: Bacterial Biomass Production 3-H; O2: Oxygen Respiration (includes: Winkler titration, optodes); INT: *in-vivo* INT reduction method.

Station ID	DOM	Surfactants	TEP/CSP	BA/PA	PhytoPP	PP	BBP	O_2	INT
HG-I	x	x	x	x			x		
HG-II	x	x	x	x			x	x	x
HG-III	x	x	x	x		x	x		
HG-IV	x	x	x	x			x		
HG-V	x	x	x	x		x	x	x	
HG-VI	x	x	x	x			x	x	
HG-VII	x	x	x	x			x		
HG-IX	x	x	x	x	x	x	x	x	
N3	x	x	x	x		x	x		
N4	x	x	x	x			x	x	

Station ID	DOM	Surfactants	TEP/CSP	BA/PA	PhytoPP	PP	BBP	O_2	INT
N5	x	x	x	x	x	x	x		x
EG-I	x	x	x	x		x	x	x	
EG-IV	x	x	x	x		x	x	x	
SV-I	x	x	x	x	x	x	x	x	x
SV-II	x	x	x	x			x		
SV-III	x	x	x	x			x		
SV-IV	x	x	x	x	x	x	x	x	
S3	x	x	x	x		x	x		
0°	x	x	x	x		x	x	x	
Test station					x			x	x

Protistian and Microbial Plankton (AGs Nöthig, Kraberg, Metfies)

Seawater samples were taken at 5 to 12 depths by a CTD/Rosette Water Sampler in the HAUSGARTEN area and aliquots were filtered for analysing biogeochemical parameters such as chlorophyll *a* (unfractionated, and fractionated), particulate organic carbon and nitrogen (POC and PN), and biogenic silica (PbSi), respectively. At mooring stations filtrations for seston (TPM, total particulate matter) were carried out. Furthermore, unfiltered water samples were fixed with formalin (final concentration 0.5 – 1.0 %) for later quantitative assessment of the phytoplankton community by inverted microscopy. At all stations, apart from SV-II and HG-VI, vertical tows with a Hand net (20 µm mesh size) were carried out. These samples were initially examined onboard for a preliminary biodiversity assessment and then fixed with formalin (1 %) for later, more detailed analysis in the laboratory. The net hauls were also screened for the presence of protistan parasites which were taken into culture where possible.

Additional samples were collected from five depths via the CTD/Rosette Water Sampler from the top 100 m of surface waters for molecular analyses in order to assess microbial community compositions by 16S/18S meta-barcoding. Samples for 18S meta-barcoding analyses were fractionated by three filtrations on 10 µm, 3 µm and 0.2 µm filters, while samples for prokaryotic community analyses were filtered directly on 0.2 µm filters. One additional archive sample was collected from every depth by filtration on 0.2 µm to provide a sample for future analyses methods.

To address spatial variability of microbial plankton communities we complemented sampling for molecular analyses using the CTD/Rosette Water Sampler with sampling via the underway sampling system AUTOFIM, permanently installed on board *Polarstern*. We used the device to collect samples on a transect from Fram Strait to Bremerhaven with a resolution of 3 h (~33 nm) on a 0.4 µm filter. Sea ice cores were collected at three different stations for molecular characterization of microbial sea ice communities and Chl *a* biomass (Fig. 4.3). All samples were preserved, refrigerated or frozen at –20° C or –80° C for storage until analyses in the laboratory at AWI, Bremerhaven.

Table 4.2 provides an overview which stations were sampled for the different parameters.

Fig. 4.3: Sampling of sea ice cores for molecular characterization of microbial sea ice communities

Tab. 4.2: Sampling for molecular analyses and other parameters; DNA Euk and Prok: DNA of eukaryotes and prokaryotes; POC/N/bSI: particulate organic carbon, nitrogen and biogenic silica; TPM, seston = total particulate matter

Station ID	DNA Euk and Prok	Archive Filter	POC/N, PbSi shallow	POC, PON, PbSi, TPM deep	Hand net 20 µm	Utermöhl counting
HG-I	X	X	X		X	X
HG-II	X	X	X			X
HG-III	X	X	X			X
HG-IV	X	X	X	X	X	X
HG-V	X	X	X			X
HG-VI	X	X	X			X
HG-VII	X	X	X			X
HG-IX	X	X	X			X
N5	X	X	X			X
N4	X	X	X	X		X
N3	X	X	X		X	X
EG-I	X	X	X		X	X
EG-IV	X	X	X	X	X	X

Station ID	DNA Euk and Prok	Archive Filter	POC/N, PbSi shallow	POC, PON, PbSi, TPM deep	Hand net 20 µm	Utermöhl counting
SV-IV	X	X	X			X
SV-III	X	X	X			X
SV-II	X	X	X			X
SV-I	X	X	X			X
S3	X	X	X	X	X	X
F4	X	X	X			X
0°	X	X	X			X

Zooplankton (AG Niehoff)

The meso-zooplankton community composition and depth distribution were investigated at six HAUSGARTEN stations and one station in the East Greenland Current (Table 4.3). To analyse the large-scale zooplankton distribution in the upper 1,500 m of the water column, we used a Multi net equipped with five nets of 150 µm mesh size. The net was towed vertically (S3, HG-IV, HG-I, HG-IX, N5, EG-I) to sample five depths layers (1,500 - 1,000 - 500 - 200 - 50 - 0 m). At EG-I, the bottom depth was shallower than 1,500 m, and here the depth intervals were adjusted, yielding a higher resolution of the upper water. All samples were immediately preserved in 4 % formalin buffered with hexamethylenetetramine. In the laboratories at AWI, these samples will be analysed to determine zooplankton species composition and abundance.

An additional Multi net cast was taken at HG-II to collect and deep-freeze individual zooplankton organisms for carbon and nitrogen measurements as well as for lipid content and fatty acid composition analysis. These samples were deep-frozen at –20° C (carbon and nitrogen content) and at –80° C (lipid analysis) and will also be later analysed in the laboratory.

To analyse the vertical distribution of zooplankton species in the upper 1,000 m of the water column with high spatial resolution, the optical system LOKI (Lightframe On-sight Key species Investigation; Fig. 4.4) was deployed at seven stations (S3, HG-IV, HG-II, HG-I, HG-IX, N5, EG-I). LOKI was equipped with a 150 µm plankton net and took images of zooplankton organisms and particles at a rate of 18 frames per second while being towed vertically through the water column. Simultaneously, depth, temperature, oxygen content and fluorescence were recorded to relate the zooplankton abundance to the environmental conditions. Unfortunately, at S3 station, a technical issue occurred, so that no proper pictures were recorded during the cast.

Tab. 4.3: List of stations where LOKI and Multi net were deployed.

ID	Station	LOKI	Multi net
S3	PS126_2	X	X
HG-IV	PS126_3	X	X
HG-II	PS126_6	X	X
HG-I	PS126_8	X	X
N5	PS126_19	X	X
EG-I	PS126_21	X	X
HG-IX	PS126_23	X	X

Fig. 4.4: Deployment of the LOKI (Lightframe On-sight Key species Investigation)

Phytoplankton pigments, particulate matter absorption (PAB) and coloured dissolved organic matter (CDOM) (AG Bracher)

At the main HAUSGARTEN/FRAM stations we deployed our optical Profiler (profiling system to measure the optical properties vertically) integrated with an *in-situ* spectrophotometer (AC-S; WETlabs), TRIOS RAMSES sensors (for light downwelling irradiance: Ed, and upwelling radiance: Lu), a pressure sensor, a datalogger and battery (Fig. 4.5 left). They were operated during CTD stations out of the shade. The frame was lowered to maximal 150 m with a continuous speed of 0.1 m/s or during daylight with additionally stops at 2, 5, 8, 10, 15, 20, 25 and 30 m to allow a better collection of radiometric data. On the monkey deck another RAMSES Ed sensor for irradiance in the air was also mounted and measured during the stations. The Apparent Optical Properties of water (AOPs) (mostly light attenuation through the water column) were estimated based on downwelling and upwelling irradiance measurements in the surface water profile (down to the 0.1 % light depth) from the radiometers calibrated for the incident sunlight with measurements of a radiometer on deck and directly from the radiance and irradiance above water radiometry. The AC-S measured the inherent optical properties (IOPs: total attenuation, scattering and absorption) in the water profile. Table 4.4 gives an overview of the bio-optical parameters assessed during PS126 stations.

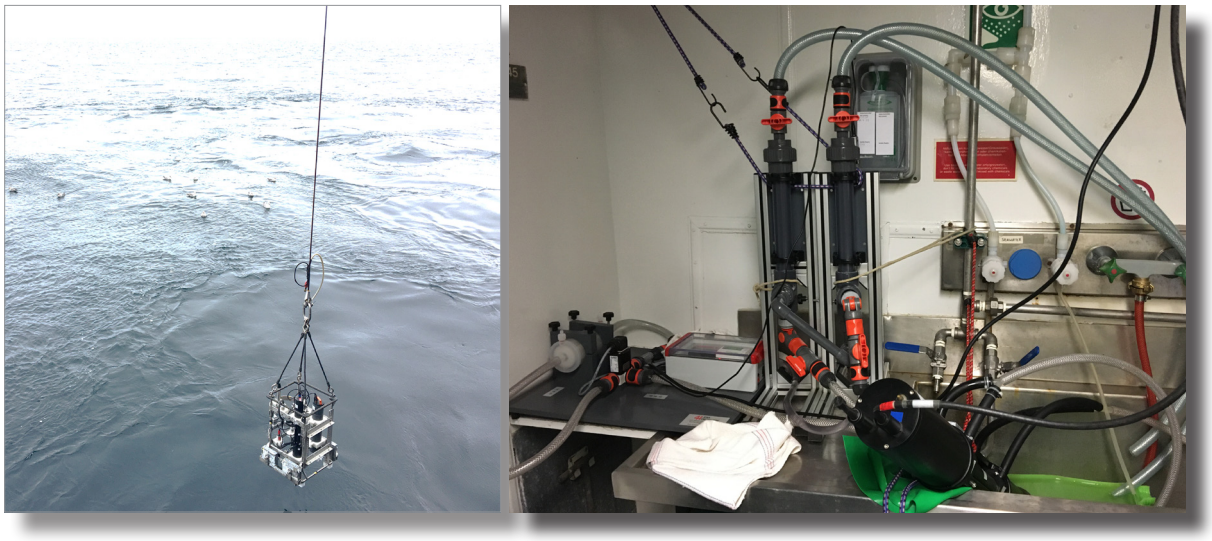

Fig. 4.5: Underwater light field measurements with TRIOS RAMSES radiometers detecting the hyperspectral up- and downwelling radiation and WETLABS AC-s (including pressure sensor, data logger and battery) measuring extinction and absorption within the surface water profile (left); Continuous measurements of the extinction and absorption of light in Arctic surface waters using a WETLABS AC-s mounted to the Polarstern surface seawater pump system. From those measurements directly, the absorption and scattering of particles and CDOM is determined for the whole spectrum in the visible resolved with about 3 nm resolution. This data then can be decomposed by various specific algorithms to determine the particle size distribution and the various phytoplankton pigment composition (right)

In addition, we also sampled Arctic seawater with the CTD/Rosette Water Sampler at the main HAUSGARTEN/FRAM stations at 4 to 6 depths from surface to 100 m for further filtration in the laboratory to have HPLC samples and measure the filtered pads to obtain the absorption spectra of total particulates, phytoplankton and CDOM (Tab. 4.5).

Tab. 4.4: Bio-optical parameters sampled at PS126 stations; HPLC: Phytoplankton pigments by High Pressure Liquid Chromatography; CDOM: Coloured Dissolved Organic Matter absorption by LWCC; PAB: Particulate and phytoplankton absorption; RAMSES: hyperspectral upwelling and downwelling radiation in the water; ACS: hyperspectral total absorption and attenuation. *: only surface water sample was taken.

ID	CTD station No.	Light station No.	HPLC	PAB	CDOM	ACS-profile	RAMSES
HG-I	PS126_8-1	PS126_8-2	x	x	x	x	x
HG-II	PS126_6-1	PS126_6-2	x	x	x	x	x
HG-III	PS126_4-1	PS126_4-2	x	x	x		x
HG-IV	PS126_3-3	PS126_3-2	x	x	x	x	x
HG-V	PS126_25-2	PS126_25-1	x	x	x	x	x
HG-VI	PS126_28-7	PS126_28-5	x	x	x	x	x
HG-VII	PS126_24-2	PS126_24-1	x	x	x	x	x
HG-IX	PS126_23-2	PS126_23-1	x	x	x	x	x

ID	CTD station No.	Light station No.	HPLC	PAB	CDOM	ACS-profile	RAMSES
S3	PS126_2-11	PS126_2-10	x	x	x	x	x
N3	PS126_17-3	PS126_17-2	x	x	x	x	x
N4	PS126_18-2	PS126_18-1	x	x	x	x	x
N5	PS126_19-6	PS126_19-5	x	x	x	x	x
SV-I	PS126_13-1	PS126_13-3	x	x	x	x	
SV-II	PS126_12-1	PS126_12-5	x	x	x	x	x
SV-III	PS126_11-2	PS126_11-1	x	x	x	x	x
SV-IV	PS126_9-6	PS126_9-5	x	x	x	x	x
EG-I	PS126_21-7	PS126_21-5	x	x	x	x	x
EG-IV	PS126_20-1	PS126_20-6	x	x	x	x	x
0°	PS126_22-2	PS126_22-1	x	x	x	x	
Test	UW47, UW48	PS126_1-7	x*	x*	x*	x	x

Tab. 4.5: List of date, time, sample depth of Phytooptics discrete water samples at CTD Stations during PS126

ID	Station	UTC Date	Time (at max depth)	Sampled Depth [m]
HG-I	PS126_8-1	2021-06-05	11:05:04	10, 25, 35, 50, 100
HG-II	PS126_6-1	2021-06-04	17:51:49	10, 17, 25, 50, 75, 100
HG-III	PS126_4-1	2021-06-03	20:11:41	10, 15, 25, 50, 100
HG-IV	PS126_3-3	2021-06-01	12:06:50	10, 15, 30, 50
HG-V	PS126_25-1	2021-06-18	18:34:45	3, 10, 25, 50, 100
HG-VI	PS126_28-5	2021-06-21	01:53:28	5, 20, 35, 50, 100
HG-VII	PS126_24-1	2021-06-18	09:57:17	3, 12, 25, 50, 100
HG-IX	PS126_23-1	2021-06-17	09:56:42	10, 20, 35, 50, 100
S3	PS126_2-11	2021-05-31	14:33:27	10, 14, 40, 80, 100
0°	PS126_22-1	2021-06-17	03:02:11	5, 12, 20, 50, 100
N3	PS126_17-2	2021-06-09	17:10:05	5, 20, 35, 50, 100
N4	PS126_18-1	2021-06-10	03:34:48	5, 20, 35, 50, 100
N5	PS126_19-5	2021-06-12	08:40:13	10, 14, 25, 50, 100
SV-I	PS126_13-3	2021-06-08	05:10:37	10, 25, 35, 50, 100
SV-II	PS126_12-5	2021-06-08	00:27:45	10, 25, 40, 50, 100

ID	Station	UTC Date	Time (at max depth)	Sampled Depth [m]
SV-III	PS126_11-1	2021-06-07	18:53:03	10, 17, 30, 50, 100
SV-IV	PS126_9-5	2021-06-06	16:53:47	10, 25, 35, 50, 100
EG-I	PS126_21-5	2021-06-15	10:37:24	10, 20, 35, 50, 100
EG-IV	PS126_20-6	2021-06-13	19:18:43	5, 14, 30, 50, 75, 100

Laboratory work on board:

- Continuous optical measurements

Inherent optical properties (IOPs) were analysed with a hyperspectral spectrophotometer. For the continuous underway surface sampling, we used an AC-S in flow-through mode to obtain total and particulate matter attenuation and absorption of surface water. The instrument was mounted to a seawater supply taking surface ocean water (Fig. 4.5, right). A flow control with a time-programmed filter was mounted to the AC-S to allow alternating measurements of the total and the CDOM inherent optical properties of the seawater. A flow control and debubbler system ensured that water flowed through the instrument without air bubbles.

- Discrete surface seawater sampling (underway surface sampling)

Surface water was sampled from the seawater pump on *Polarstern* with an interval of 3 hours to have a full coverage of the surface water samples along the whole cruise track (Table 4.6). Water samples from both, underway and CTD stations, were filtered in the laboratory to have the following samples and measurement: (1) HPLC phytoplankton pigment samples (pore size 0.7 µm filtered pads were immediately stored onboard in the –80° C freezer); (2) particle and phytoplankton absorption spectra (ap, ad, and aph) were obtained by measuring a second set of filtered pads for each sample; and (3) CDOM absorption spectra were obtained by measuring the filtered water samples with 0.2 µm pore size filters.

Tab. 4.6: List of Phytooptics discrete water sample analysis of phytoplankton pigments (analysed at AWI with HPLC), determination of CDOM (analysed with LWCC on board), particulate and phytoplankton absorption (analysed with QFT-ICAM on board) at underway stations (sampled from seawater supply pumped from 9 m depth) at given date, time, latitude and longitude during PS126.

Sample ID	Date UTC	Time UTC Pumping Start	Time UTC Pumping End	Latitude (dec)	Longitude (dec)
1	2021-05-24	17:01:40	17:03:46	54.5117303	7.2069343
2	2021-05-24	20:00:30	20:03:48	54.9746382	6.8016224
3	2021-05-24	22:57:00	23:00:45	55.4390881	6.4522095
4	2021-05-25	02:00:00	02:04:00	55.9304696	6.1302474
5	2021-05-25	05:00:00	05:04:05	56.4278059	5.8451195
6	2021-05-25	08:00:00	08:04:05	56.9099866	5.539875
7	2021-05-25	10:56:15	11:00:00	57.3754464	5.1729371
8	2021-05-25	14:00:00	14:04:04	57.873245	4.7748451
9	2021-05-25	17:00:00	17:04:00	58.3564427	4.3833946

Sample ID	Date UTC	Time UTC Pumping Start	Time UTC Pumping End	Latitude (dec)	Longitude (dec)
10	2021-05-25	19:57:40	20:00:40	58.8379245	3.9877786
11	2021-05-25	22:58:04	23:02:00	59.3456767	3.7384747
12	2021-05-26	02:01:15	02:04:50	59.8690481	3.5244355
13	2021-05-26	05:00:00	05:04:00	60.3705725	3.316052
14	2021-05-26	08:00:00	08:04:00	60.8574066	3.1107608
15	2021-05-26	11:00:00	11:04:00	61.3096553	3.108386
16	2021-05-26	14:00:00	14:01:25	61.7439316	3.1142664
17	2021-05-26	17:11:20	17:14:20	62.1875834	3.132857
18	2021-05-26	20:02:40	20:06:20	62.6148273	3.1662502
19	2021-05-26	23:00:00	23:04:00	63.0682001	3.2030518
20	2021-05-27	1:59:20	2:03:00	63.5111547	3.2389904
21	2021-05-27	5:00:00	5:03:10	64.0056628	3.2802435
22	2021-05-27	8:00:00	8:03:10	64.6241554	3.3326408
23	2021-05-27	11:00:00	11:03:00	65.3003024	3.3913171
24	2021-05-27	14:00:00	14:01:15	65.8938101	3.4439626
25	2021-05-27	17:23:00	17:25:15	66.5688147	3.4992475
26	2021-05-27	20:00:15	20:01:50	67.0923203	3.547338
27	2021-05-27	22:52:00	22:53:20	67.6638556	3.6048037
28	2021-05-28	1:57:30	1:59:00	68.2771187	3.6659778
29	2021-05-28	5:00:00	5:01:30	68.884651	3.7284805
30	2021-05-28	8:00:00	8:01:45	69.4797788	3.7948054
31	2021-05-28	11:00:00	11:01:45	70.0772612	3.8633425
32	2021-05-28	14:19:00	14:20:45	70.742354	3.9416062
33	2021-05-28	17:00:00	17:01:30	71.2916134	4.0080843
34	2021-05-28	20:00:00	20:01:50	71.8909856	4.0836391
35	2021-05-28	22:52:10	22:54:20	72.4653772	4.1526968
36	2021-05-29	1:58:00	2:00:35	73.089274	4.2264796
37	2021-05-29	5:00:00	5:04:00	73.6987626	4.3006753
38	2021-05-29	8:00:00	8:02:45	74.2943484	4.3761037
39	2021-05-29	11:00:00	11:03:25	74.9038392	4.4732464
40	2021-05-29	14:00:00	14:03:45	75.4856181	4.7980895
41	2021-05-29	17:00:00	17:03:30	76.0809299	5.1440837
42	2021-05-29	20:00:00	20:05:00	76.6749903	5.5042202
43	2021-05-29	22:52:00	22:55:00	77.2603216	5.8750948
44	2021-05-30	1:59:00	2:02:00	77.8613569	6.2627234
45	2021-05-30	5:00:00	5:03:00	78.4344868	6.6710849
46	2021-05-30	8:00:00	8:03:05	78.6206981	6.7952564
47	2021-05-30	11:00:00	11:03:00	78.6216343	6.8005186
48	2021-05-30	20:00:00	20:04:00	78.6085206	5.0683256
49	2021-05-31	5:00:00	5:03:15	78.6096078	5.0685447
50	2021-05-31	22:59:00	23:00:50	78.6207838	4.9684327
51	2021-06-01	05:00:00	05:03:30	78.6886546	4.993498

Sample ID	Date UTC	Time UTC Pumping Start	Time UTC Pumping End	Latitude (dec)	Longitude (dec)
52	2021-06-01	08:00:00	08:03:25	79.0747534	4.3693413
53	2021-06-01	17:00:15	17:03:00	78.9897236	4.3755943
54	2021-06-01	20:01:20	20:06:00	79.0647442	4.1836023
55	2021-06-02	05:01:30	05:04:50	79.0662581	4.1733439
56	2021-06-02	17:00:00	17:03:00	79.0477484	4.1409189
57	2021-06-03	05:01:00	05:05:00	79.0583124	4.2858634
58	2021-06-03	17:00:00	17:02:35	79.0628961	4.1548631
59	2021-06-04	05:01:00	05:03:30	79.0674289	4.1578956
60	2021-06-04	17:00:00	17:03:00	79.0843018	4.6897504
61	2021-06-05	05:19:00	05:24:15	79.1051819	4.552996
62	2021-06-05	08:00:00	08:06:00	79.1019934	4.5545696
63	2021-06-05	20:00:00	20:03:00	79.2006887	5.9066309
64	2021-06-06	05:00:00	05:02:35	79.1322868	6.2186272
65	2021-06-06	08:00:00	08:02:30	79.0859001	6.5187719
66	2021-06-06	11:03:00	11:06:15	79.026521	6.9158493
67	2021-06-06	14:00:00	14:02:20	79.016309	7.0409063
68	2021-06-06	23:00:45	23:03:45	79.0143267	7.0778986
69	2021-06-07	05:01:00	05:03:00	78.9167029	6.9980195
70	2021-06-07	08:00:00	08:02:30	78.6297404	6.7867721
71	2021-06-07	11:15:25	11:20:00	79.0371633	6.9916442
72	2021-06-07	14:00:00	14:02:00	79.0319715	6.9762614
73	2021-06-07	17:07:15	17:09:50	79.0127125	7.5715334
74	2021-06-08	08:00:04	08:02:55	79.0215862	10.7491467
75	2021-06-08	10:59:00	11:01:10	79.0002799	8.0168036
76	2021-06-08	17:03:00	17:07:00	79.0119436	6.9627291
77	2021-06-08	20:35:28	20:37:50	79.0802329	6.5126887
78	2021-06-08	23:55:00	23:57:30	79.0373218	6.2613598
79	2021-06-09	07:11:21	07:14:15	79.0725497	4.2260661
80	2021-06-09	08:01:30	08:04:15	79.1018639	4.553522
81	2021-06-09	11:00:00	11:02:45	79.2410949	4.7438068
82	2021-06-09	14:00:00	14:02:50	79.528096	5.089959
83	2021-06-10	11:07:30	11:15:40	79.7064594	4.2701742
84	2021-06-10	17:09:00	17:10:45	79.7327599	4.4948687
85	2021-06-11	02:24:50	02:26:10	79.6486711	4.8919509
86	2021-06-11	05:00:00	05:03:05	79.6005573	5.1568434
87	2021-06-11	08:00:00	08:02:30	79.7408454	4.4819919
88	2021-06-11	14:08:00	14:09:50	79.6026517	5.1244796
89	2021-06-11	22:58:00	23:00:00	79.8164196	3.9204244
90	2021-06-12	05:07:30	05:12:15	79.9450774	3.0073936
91	2021-06-12	11:27:45	11:30:00	79.931862	2.9875629
92	2021-06-12	16:58:20	17:00:05	79.7582996	2.1605439
93	2021-06-12	19:59:10	20:01:00	79.5447768	1.0009496

Sample ID	Date UTC	Time UTC Pumping Start	Time UTC Pumping End	Latitude (dec)	Longitude (dec)
94	2021-06-12	22:58:50	23:00:35	79.3753256	-0.024701
95	2021-06-13	02:00:00	02:01:25	79.195518	-0.8256862
96	2021-06-13	05:00:00	05:01:40	78.9818686	-1.9246569
97	2021-06-13	14:31:45	14:33:30	78.8089865	-2.7035118
98	2021-06-14	00:52:00	00:55:00	78.6334846	-2.8357823
99	2021-06-14	07:58:30	08:00:50	78.7589353	-2.8238391
100	2021-06-14	14:05:30	14:11:30	78.7841556	-2.8882333
101	2021-06-14	16:59:00	17:02:00	78.8985931	-3.0008832
102	2021-06-14	19:58:30	20:00:00	78.8194385	-3.1618805
103	2021-06-14	23:00:25	23:04:30	78.8057516	-3.6641673
104	2021-06-15	01:38:20	01:41:40	78.8840386	-4.9815089
105	2021-06-15	05:05:15	05:07:45	79.000307	-5.4552577
106	2021-06-15	19:58:20	20:01:40	78.9582224	-5.4281799
107	2021-06-16	04:58:40	05:01:15	78.9936922	-5.3081472
108	2021-06-16	11:03:00	11:05:45	78.8581307	-4.4785092
109	2021-06-16	14:00:40	14:02:40	78.797839	-3.337986
110	2021-06-16	16:58:40	17:01:35	78.7917284	-2.8638153
111	2021-06-16	23:05:50	23:08:10	78.8377253	-1.5644801
112	2021-06-17	07:27:00	07:29:00	79.0600598	1.6333281
113	2021-06-18	04:52:20	04:56:00	79.1337268	2.8545354
114	2021-06-18	08:22:00	08:25:30	79.108377	3.0281592
115	2021-06-19	05:01:50	05:04:45	79.0717722	4.1809505
116	2021-06-19	14:00:45	14:03:50	79.2867879	4.5766917
117	2021-06-19	17:00:30	17:03:45	79.5995799	5.1500258
118	2021-06-20	04:59:40	05:03:00	79.6014032	5.1522557
119	2021-06-20	08:54:25	08:57:20	79.4945975	5.013207
120	2021-06-20	11:02:25	11:05:35	79.2596872	4.7367196
121	2021-06-20	14:07:25	14:10:50	79.0839013	4.1359168
122	2021-06-20	17:02:35	17:05:50	79.0595926	3.601198
123	2021-06-21	04:59:30	05:03:15	79.0755927	3.9437991
124	2021-06-21	08:03:40	08:07:05	79.1020441	4.5578313
125	2021-06-21	19:34:00	19:38:20	78.9829865	5.500473
126	2021-06-21	22:46:50	22:50:30	78.6710669	6.5662013
127	2021-06-22	02:00:30	02:04:00	78.0542372	6.2821928
128	2021-06-22	05:14:20	05:17:50	77.4414348	6.0136986
129	2021-06-22	08:03:40	08:05:00	76.9028956	5.7877903
130	2021-06-22	11:02:20	11:04:30	76.3290687	5.5569735
131	2021-06-22	13:59:40	14:03:00	75.7727574	5.3426489
132	2021-06-22	17:01:00	17:04:10	75.1840407	5.1239566
133	2021-06-22	19:57:20	20:01:20	74.6334799	4.9276304
134	2021-06-22	22:51:20	22:55:20	74.0845831	4.7379083
135	2021-06-23	02:01:10	02:05:35	73.4855074	4.5388289

Sample ID	Date UTC	Time UTC Pumping Start	Time UTC Pumping End	Latitude (dec)	Longitude (dec)
136	2021-06-23	05:23:50	05:27:40	72.8459325	4.333331
137	2021-06-23	08:24:30	08:30:40	72.2744394	4.1560091
138	2021-06-23	11:00:10	11:05:35	71.7742824	4.0683002
139	2021-06-23	14:00:00	14:05:25	71.2055355	3.9971984
140	2021-06-23	17:01:00	17:04:30	70.6426415	3.92902
141	2021-06-23	20:02:40	20:06:00	70.1022445	3.5528704
142	2021-06-23	22:59:35	23:02:20	69.5498054	3.5264274
143	2021-06-24	02:01:35	02:05:20	68.9879294	3.7396167
144	2021-06-24	05:03:25	05:06:45	68.415899	3.680293
145	2021-06-24	07:58:35	08:01:45	67.8708066	3.6253279
146	2021-06-24	10:52:00	10:54:36	67.3079366	3.5700774
147	2021-06-24	14:04:30	14:07:30	66.6433519	3.5117133
148	2021-06-24	16:59:40	17:03:25	66.1004601	3.4569656
149	2021-06-24	20:01:45	20:04:45	65.5435281	3.4080545
150	2021-06-24	22:59:00	23:03:00	64.9708571	3.3581437
151	2021-06-25	02:00:15	02:04:40	64.3991816	3.3104262
152	2021-06-25	05:04:45	05:07:45	63.8163536	3.2622562
153	2021-06-25	08:01:10	08:06:20	63.2469025	3.216013
154	2021-06-25	10:58:20	11:00:30	62.6985056	3.1719331
155	2021-06-25	14:00:00	14:02:50	62.1504656	3.1509023
156	2021-06-25	16:59:30	17:02:20	61.5952546	3.1123916

Exchange of moored autonomous sampling devices for biological and biogeochemical parameter (Knüppel, Metfies, Nicolaus)

The PEBCAO-group accomplished the preparation and post-deployment processing of sediment traps, long-term lander and automated water samplers (PPS and RAS) deployed on moorings at the stations HG-IV, F4, N4. Overall, we recovered 9 sediment traps, 2 benthic lander traps, 6 RAS and 2 PPS (Fig. 4.6; Table 4.7).

Fig. 4.6 (left): Recovery of PPS (upper device) and RAS (lower device)

Tab. 4.7: Deployments and recoveries of sediment traps, lander-traps, PPS and RAS.

Station	Latitude	Longitude	Device-Name	Depth [m]	Deployment period
Recovery Sediment traps					
HG-N4	79°44.348'N	004°30.356'E	FEVI-39-upper	223	10.09.2019 – 01.07.2021
HG-N4	79°44.348'N	004°30.356'E	FEVI-39-lower	2461	10.09.2019 – 01.07.2021
HG-IV	78°59.996'N	004°19.92'E	FEVI-40-upper	200	10.09.2019 – 01.07.2021
HG-IV	78°59.996'N	004°19.92'E	FEVI-40-middle	1227	10.09.2019 – 01.07.2021
HG-IV	78°59.996'N	004°19.92'E	FEVI-40-lower	2345	10.09.2019 – 01.07.2021
EG-4	78°59.746'N	005°23.78'W	EGC-6-1st year	449	10.09.2019 – 16.09.2020
EG-4	78°59.746'N	005°23.78'W	EGC-6-2nd year	522	16.09.2020 – 16.09.2021
F4S	79°00.706'N	006°57.81'E	F4S-4 upper	197	10.09.2019 – 01.07.2021
F4S	79°00.706'N	006°57.81'E	F4S-4 lower	606	10.09.2019 – 01.07.2021
Deployment Sediment traps					
HG-IV	79°00.012'N	004°20.049'E	Fevi-42-upper		15.06.2021 – 30.06.2022
HG-IV	79°00.012'N	004°20.049'E	Fevi-42-middle		15.06.2021 – 30.06.2022
HG-IV	79°00.012'N	004°20.049'E	Fevi-42-lower		15.06.2021 – 30.06.2022
EG-4	78°59.395'N	005°19.826'W	EGC-7		17.06 –2021 – 30.06.2022
F4S	79°00.732'N	006°57.833'E	F4S-5 (2021) upper		15.06.2021 – 30.06.2022
F4S	79°00.732'N	006°57.833'E	F4S-5 (2021) lower		15.06.2021 – 30.06.2022
Recovery Long-Term Lander					
	79°04.150'N	004°10.099'E		2460	10.09.2019 – 01.10.2020
	79°00.026'N	005°29.683'W		1000	10.09.2019 – 01.10.2020
Deployment Long-Term Lander					
	79°02.733'N	004°10.466'E		2564	30.06.2021 – 30.06.2022
Recovery Remote Access Sampler (RAS)					
HG-N4	79°44.348'N	004°30.356'E	RAS13464-02	23	11.09.2019 – 21.09.2020

Station	Latitude	Longitude	Device-Name	Depth [m]	Deployment period
F4S	79°00.706'N	006°57.810'E	RAS14128-04	21	09.11.2019 – 19.11.2020
F4S	79°00.706'N	006°57.810'E	RAS14128-08	249	11.09.2019 – 21.09.2020
EG1	78°59.746'N	005°23.780'W	RAS14128-06	67	11.09.2019 – 21.09.2020
EG1	78°59.746'N	005°23.780'W	RAS14333-02	236	11.09.2019 – 21.09.2020
Deployment Remote Access Sampler (RAS)					
F4S	79°00.706'N	006°57.810'E	RAS13380-01	21	14.06.2021 – 25.06.2022
F4S	79°00.706'N	006°57.810'E	RAS14128-09	245	14.06.2021 – 25.06.2022
EG1	78°59.746'N	005°23.780'W	RAS13464-01	39	22.06.2021 – 03.07.2022
EG1	78°59.746'N	005°23.780'W	RAS14128-07	233	22.06.2021 – 03.07.2022
Recovery PPS					
HG-N4	79°44.348'N	004°30.356'E	PPS14333-01	25	11.09.2019 – 13.09.2020
F4S	79°00.706'N	006°57.810'E	PPS14128-03	23	11.09.2019 – 13.09.2019

Preliminary (expected) results

Biogeochemistry (AG Engel)

Preliminary results on bacterial biomass production and oxygen based on Winkler titrations (Fig. 4.7) suggest higher bacterial production at stations around 5° E, 79° N.

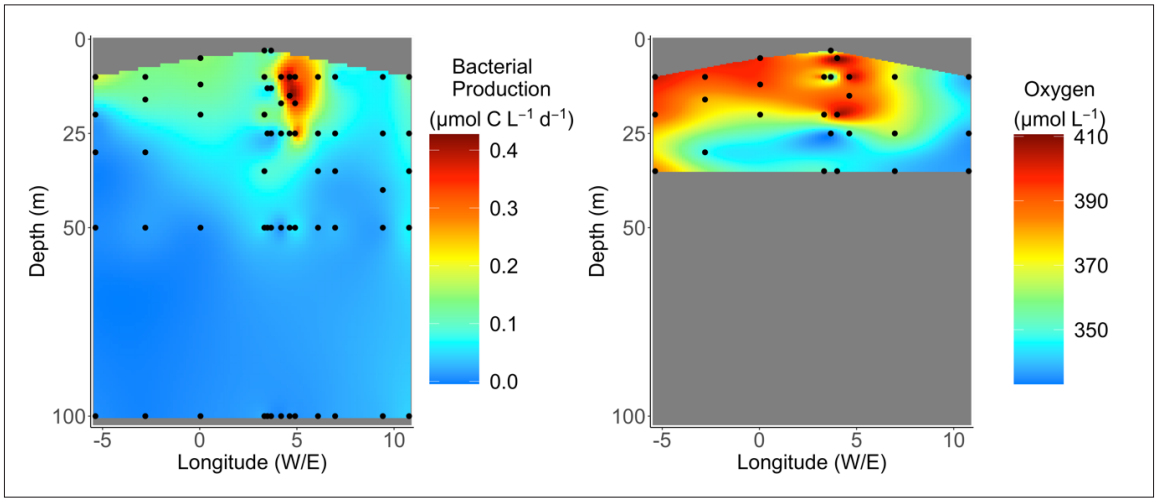

Fig. 4.7: Bacterial biomass production as units carbon demand and oxygen concentration in the upper 100 m of a west-east transect across Fram Strait

Protistian and Microbial Plankton (AGs Nöthig, Kraberg, Metfies)

Quantitative analyses of phytoplankton community composition by microscopy will be carried out in the laboratory at AWI Bremerhaven. However, preliminary results from semi-quantitative assessments of net samples (with a controlled sampling effort) indicate that the phytoplankton community in the sampling area was largely controlled by *Phaeocystis pouchetii* blooms with the exception of stations EG-I and EG-IV (Fig. 4.8). These stations were characterized by a more species rich diatom assemblage and absence or low abundance respectively of *P. pouchetii*.

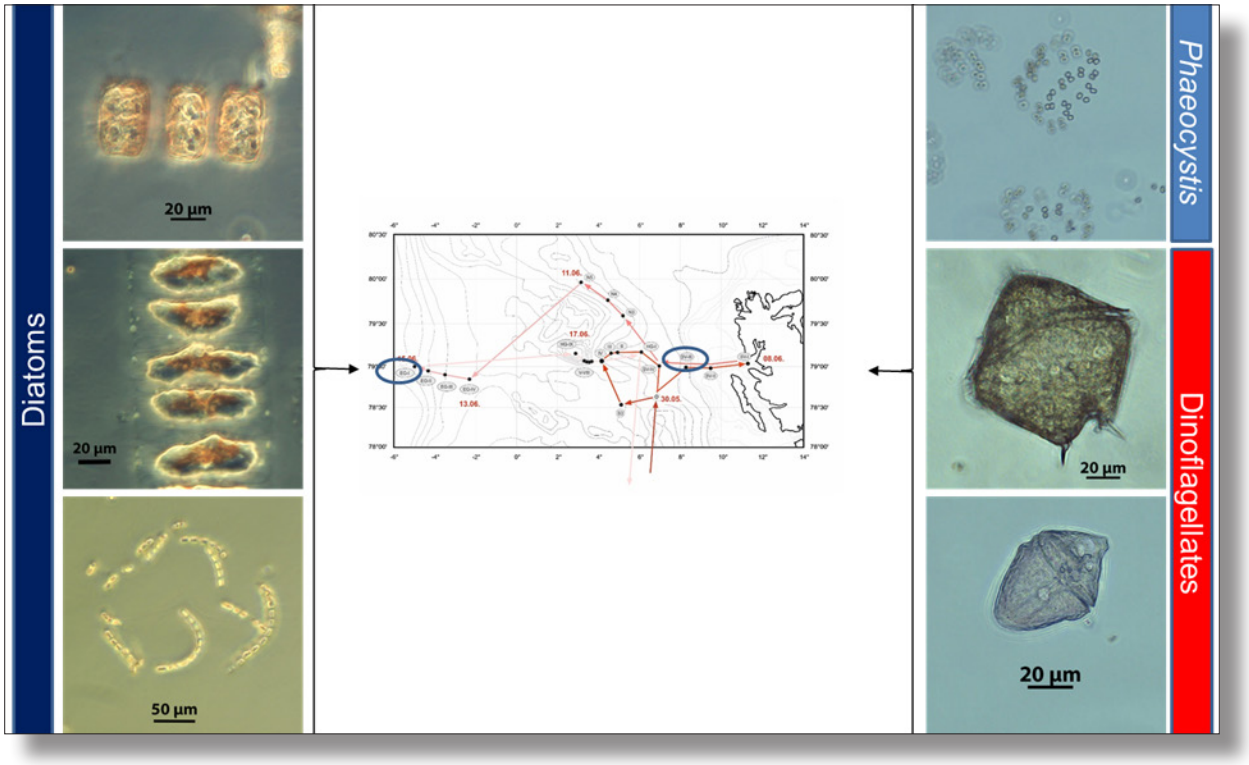

Fig. 4.8: Examples of phytoplankton collected at different locations in the HAUSGARTEN: Left panel top to bottom: Thalassiosira spp., Entomoneis spp., Chaetoceros socialis; right panel top to bottom: Phaeoocystis, Protoperidinium pallidum, Gymnodinium spp.

This is also reflected in the nMDS analyses were EG sites are clearly separated from the rest of the sites (Fig. 4.9). The latter formed a big cluster at a similarity level of 30 %. Within this cluster a second large cluster formed at a similarity of 40 % which comprised the Svalbard and N3 and five stations which had a larger richness of dinoflagellate species.

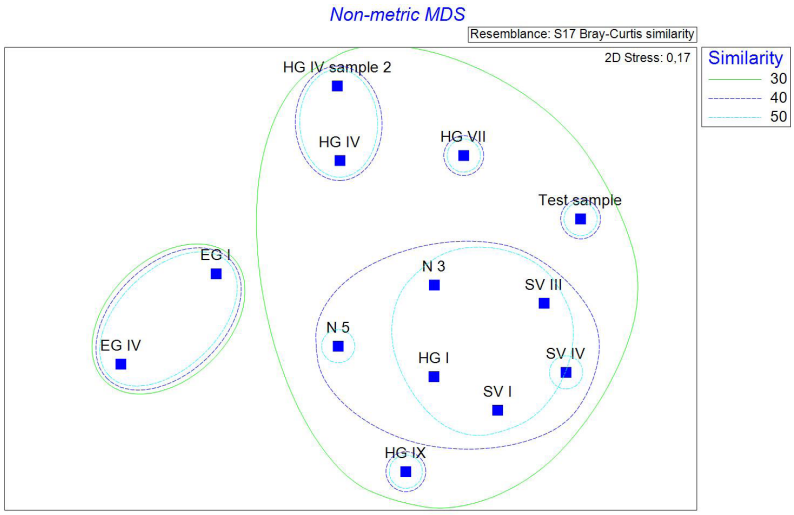

Fig. 4.9: nMDS plot based on the preliminary results of the analysis of Hand net samples

Zooplankton (AG Niehoff)

First insights in the wealth of images obtained from the LOKI system revealed the presence of Amphipoda, Hydrozoa, Polychaeta, Ostracoda, Sinphonophora, Chaetognatha and copepods in the observation area (Fig. 4.10). Copepods, however, clearly dominated the zooplankton community at all stations. We will analyse the samples and image data collected during PS126 in the laboratories at AWI under the stereomicroscope and using semi-automatic image analyses methods, respectively. This will yield detailed information on biodiversity and distribution of the zooplankton community in relation to environmental conditions (depth, temperature, salinity, chlorophyll *a* concentration) and the data will continue our time series on zooplankton biomass and abundance started in 2011.

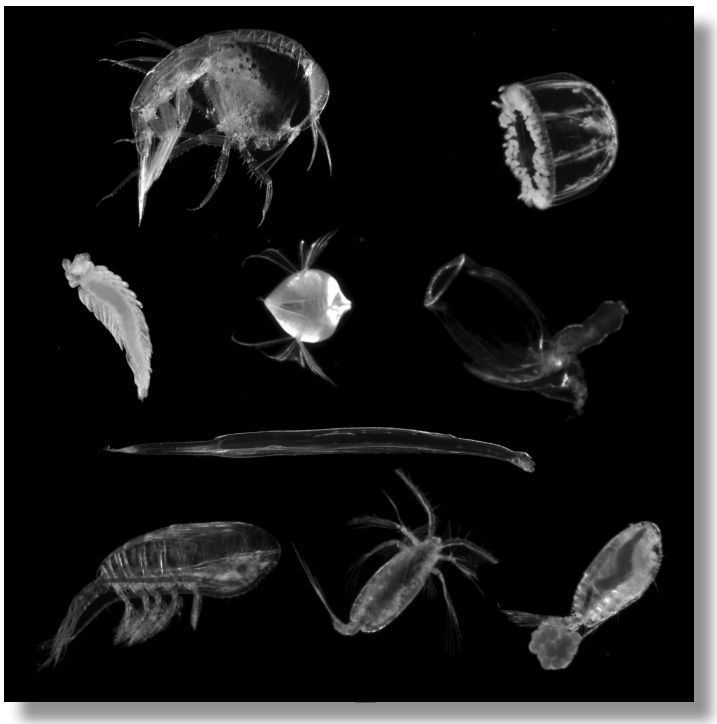

Fig. 4.10: Zooplankton in the Fram Strait: Images from the optical system LOKI (Lightframe On-sight Key species Investigations)

Upper row: Amphipoda, Hydrozoa; second row: Polychaeta, Ostracoda, Siphonophora; third row: Chaetognatha; lower row: Copepoda

Phytoplankton pigments, particulate matter absorption (PAB) and coloured dissolved organic matter (CDOM) (AG Bracher)

The continuously measured optical data are used via using semi-analytical techniques to determine the spectrally resolved underwater light attenuation and the concentration of optical constituents, such as Chl *a* concentration, CDOM absorption and particle backscattering, but also for validating satellite ocean colour retrievals following formerly established procedures for HAUSGARTEN/FRAM cruises PS93.2, PS99, and PS107 (see Liu et al. 2018; Liu et al. 2019). We expect this new data set for our long-term measurements to elucidate further changes in the Fram Strait pelagic environment due to Global Change and/or other environmental shifts.

So far, we have obtained the following measurements/data:

- Underway flow-through measurements:
  31-days non-stop particulate absorption/attenuation measurements from AC-S
- Discrete samples:
  a. HPLC pigments, 96 samples from CTDs, 156 samples from underway sampling (will be analysed at AWI)
  b. Phytoplankton absorption, 96 samples from CTDs, 156 samples from underway
  c. CDOM (coloured dissolved organic matter) absorption: 95 samples from CTDs, 156 samples from underway
- Station work from RAMSES+ACS profiler (20 stations):
  a. 16 valid RAMSES light profiles (4 invalid due to bad weather or instrumental issues)
  b. 20 valid ACS profiles for the particulate absorption from surface to maximum 150 m

On board we were able to already analyse the RAMSES, LWCC and QFT-ICAM data. We have obtained some first results on the Chl *a* concentration (Fig. 4.11 and Fig. 4.12, left) for the underway surface water and the CTD samples. Results show that for most of the HAUSGARTEN stations the highest Chl *a* concentrations were found in the first 20 m and then decreased with the depth. HAUSGARTEN stations HG-I to HG-IX showed the highest biomass compared to the other stations. The underway Chl *a* showed that along the cruise track we have encountered a few phytoplankton blooming areas around 65° N, central Fram Strait and also between 77–78° N. In addition, we show the results of underway CDOM absorption at 440 nm which is a good indicator of DOM in the Arctic Ocean (Fig. 4.12, right). It shows that the CDOM concentrations were abundant in the North Sea and then decreased when the latitude is above 66° N. In the eastern Fram Strait the CDOM was at low to moderate level but was high in the west Fram Strait where the Arctic current dominates, indicating that Arctic waters contain more DOM compared to north Atlantic waters. These results are comparable to the historical data collected in the same season, and can be used to investigate seasonality and time series change in optical properties, CDOM, and phytoplankton composition structure by combining the data from previous cruises to Fram Strait.

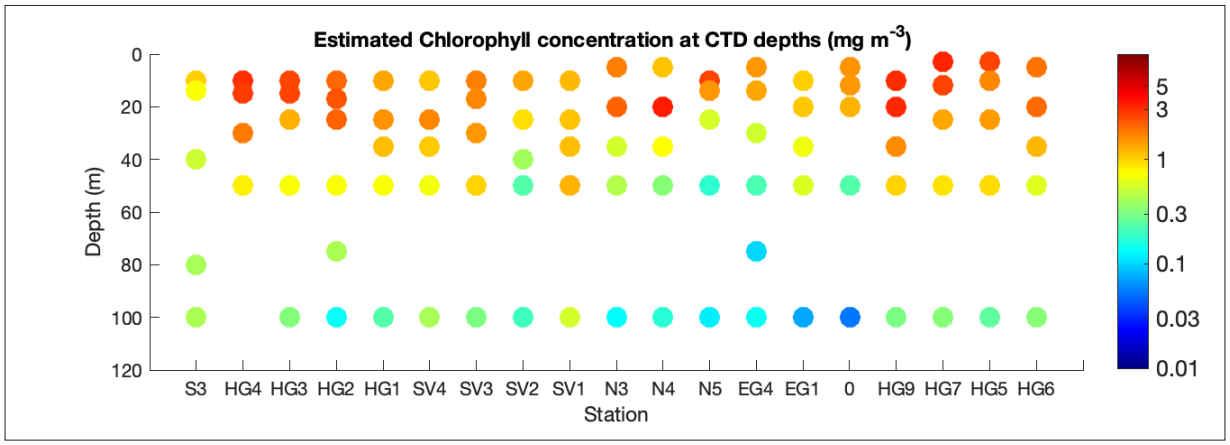

Fig. 4.11: Chl a concentrations at CTD depths estimated using the absorption peak line height method (Roesler and Barnard 2013, Liu et al. 2018) from the QFT-ICAM measured particulate absorption spectra

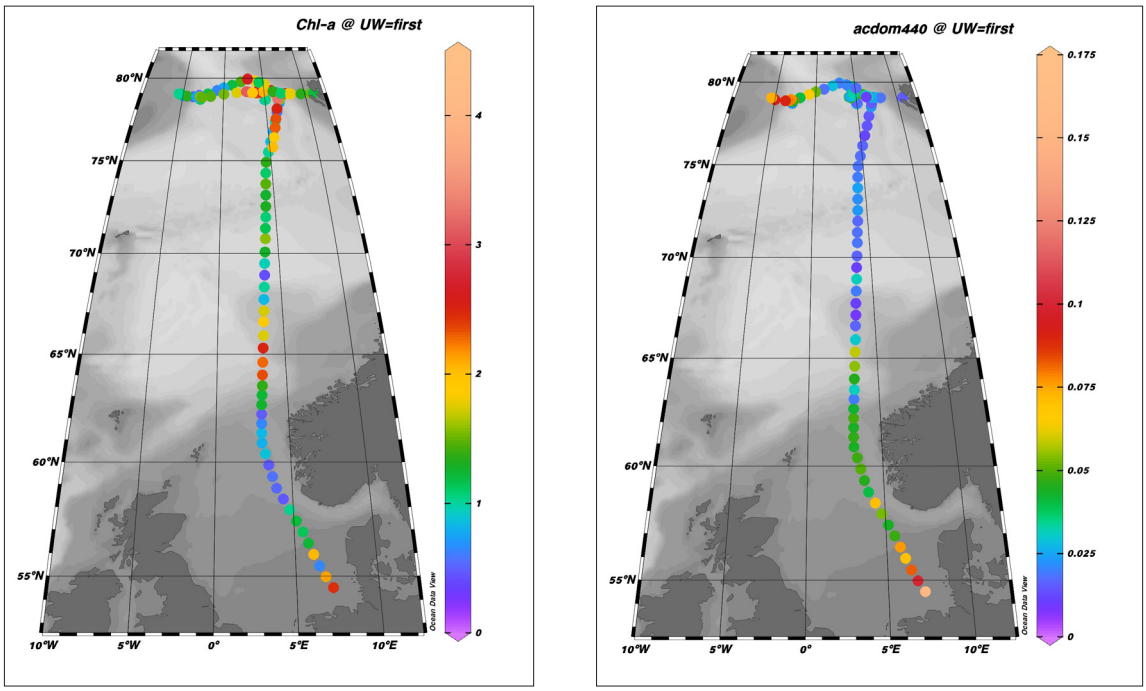

Fig. 4.12: Left: Surface Chl a concentrations (mg m^{-3}) from PS126 underway sampling estimated using the absorption peak line height method (Roesler and Barnard 2013; Liu et al. 2018) from the QFT-ICAM measured particulate absorption spectra. Right: Uncalibrated surface CDOM concentration acdom(440) (m^{-1}) from PS126 underway sampling

Data management

Many of the samples (e.g. sediment trap data, molecular analyses, pigment analyses and optical measurements) will be processed and further analysed at AWI within approximately one year after the cruise. We plan that the full data set will be available at latest about 2 – 3 years after the cruise. Data will be made available to the public via PANGAEA (https://www.pangaea.de) in accordance with current institute data policies. AC-S data are foreseen to be uploaded to the FRAM data portal as raw data immediately after the cruise and as calibrated data set after carefully executing quality controls and calibrations with discrete water sample measurements.

In all publications, based on this cruise, the **Grant No. AWI_PS126_02** will be quoted and the following *Polarstern* article will be cited: Alfred-Wegener-Institut Helmholtz-Zentrum für Polar- und Meeresforschung. (2017). Polar Research and Supply Vessel POLARSTERN Operated by the Alfred-Wegener-Institute. Journal of large-scale research facilities, 3, A119. http://dx.doi.org/10.17815/jlsrf-3-163.

References

Bracher A, Xi H, Dinter T, Mangin A, Strass VH, von Appen WJ, Wiegmann S (2020) High resolution water column phytoplankton composition across the Atlantic Ocean from ship-towed vertical undulating radiometry. Frontiers in Marine Science, 7, 235.

Cosović B, Vojvodić V (1998) Voltammetric Analysis of Surface Active Substances in Natural Seawater. Electroanalysis 10(6), pp. 429-434.

Engel A (2009) Determination of marine gel particles. In Practical guidelines for the analysis of seawater (ed O Wurl), pp. 125-143. Clermont, FL: CRC Press.

Engel A, Piontek J, Metfies K, Endres S, Sprong P, Peeken I, Gäbler-Schwarz S, Nöthig EM (2017) Inter-annual variability of transparent exopolymer particles in the Arctic Ocean reveals high sensitivity to ecosystem changes. Scientific Reports, 7(4129), 1-9.

Engel A, Bracher A, Dinter T, Endres S, Grosse J, Metfies K, Peeken I, Piontek J, Salter I, Nöthig E-M (2019) Inter-annual variability of organic carbon concentrations across the Fram Strait (Arctic Ocean) during summer 2009 -2017. Frontiers in Marine Science 6, 187.

García-Martín E, Aranguren-Gassis M, Karl DM, Martínez-García S, Robinson C, Serret P, Teira E (2019) Validation of the *in vivo* Iodo-Nitro-Tetrazolium (INT) Salt Reduction Method as a Proxy for Plankton Respiration. Frontiers in Marine Science 6, 220.

Kraft A, Bauerfeind E, Nöthig E M, Klages M, Beszczynska-Möller A and Bathmann U (2013): Amphipods in sediment traps of the eastern Fram Strait with focus on the life-history of the lysianassoid *Cyclocaris guilelmi*, Deep-Sea Research Part I-Oceanographic Research Papers, 73, pp. 62-72. doi: 10.1016/j.dsr.2012.11.012

Liu Y, Roettgers R, Ramírez-Pérez M, Dinter T, Steinmetz F, Noethig EM, Hellmann S, Wiegmann S, Bracher A (2018) Underway spectrophotometry in the Fram Strait (European Arctic Ocean): a highly resolved chlorophyll *a* data source for complementing satellite ocean color. Optics Express, 26(14), A678-A698.

Liu Y, Boss E, Chase AP, Xi H, Zhang X, Röttgers R, Pan Y, Bracher A (2019) Retrieval of phytoplankton pigments from underway spectrophotometry in the Fram Strait. Remote Sensing, 11, 318.

Losa S, Soppa MA, Dinter T, Wolanin A, Brewin RJW, Bricaud A, Oelker J, Peeken I, Gentili B, Rozanov VV, Bracher A (2017) Synergistic exploitation of hyper- and multispectral precursor Sentinel measurements to determine Phytoplankton Functional Types at best spatial and temporal resolution (SynSenPFT). Frontiers in Marine Science, 4, 203.

Metfies K, Bauerfeind E, Wolf C, Sprong P, Frickenhaus S, Kaleschke L, Nicolaus A, Nöthig EM (2017) Protist Communities in Moored Long-Term Sediment Traps (Fram Strait, Arctic) – Preservation with Mercury Chloride Allows for PCR-Based Molecular Genetic Analyses. Frontiers in Marine Sciences. doi: 10.3389/fmars.2017.00301.

Nöthig E-M, Bracher A, Engel A, Metfies K, Niehoff B, Peeken I et al. (2015). Summertime plankton ecology in Fram Strait – a compilation of long- and short-term observations. Polar Research, 34. doi: 10.3402/polar.v34.23349.

Nöthig E-M, Ramondenc S, Haas A, Hehemann L, Walter A, Bracher A et al. (2020). Summertime chlorophyll *a* and particulate organic carbon standing stocks in surface waters of the Fram Strait and the Arctic Ocean (1991–2015). Frontiers in Marine Sciences, 350. doi: 10.3389/fmars.2020.00350.

Oelker J, Losa SN, Richter A, Bracher A (*submitted*) TROPOMI-retrieved underwater light attenuation in three spectral regions: ultraviolet to blue. Frontiers in Marine Science.

Roesler S, Barnard AH (2013) Optical proxy for phytoplankton biomass in the absence of photophysiology: Rethinking the absorption line height. Methods in Oceanography, 7, 79-94.

Schröter F, Havermans C, Kraft A, Knueppel N, Beszczynska-Möller A, Bauerfeind E and Nöthig E M (2019) Pelagic amphipods in the eastern Fram Strait with continuing presence of *Themisto compressa* based on sediment trap time series. Front. Mar. Sci., 6 (311). doi: 10.3389/fmars.2019.00311.

Xi H, Losa SN, Mangin A, Soppa MA, Garnesson P, Demaria J, Liu Y, Fanton d'Andon O, Bracher A (2020) Global retrieval of phytoplankton functional types based on empirical orthogonal functions using CMEMS GlobColour merged products and further extension to OLCI data. Remote Sensing of Environment, 240, 111704.

Xi H, Losa SN, Mangin A, Garnesson P, Bretagnon M, Demaria J, Soppa MA, Fanton d'Andon O, Bracher A (2021) Global chlorophyll *a* concentrations of phytoplankton functional types with detailed uncertainty assessment using multisensor ocean color and sea surface temperature satellite products. Journal of Geophysical Research: Oceans, 126, e2020JC017127.

5. SEAPUMP – THE ROLE OF SETTLING AGGREGATES IN THE BIOLOGICAL PUMP

Christian Konrad[1,2]; [1]DE.WI
Morten Iversen[1,2] (not on board) [2]DE.MARUM

Grant No. AWI_PS126_03

Objectives

In-situ long-term monitoring of abundance, size-distribution, sinking velocity of settling aggregates with the BioOptical Platform *BOP*

During the *Polarstern* cruise PS121 we deployed the BioOptical Platform (BOP) on the FEVI-40 mooring at HAUSGARTEN station HG-IV. We developed the BOP system to be able to follow aggregate dynamics at high temporal resolution at different seasons throughout a whole year. BOP uses an *in-situ* camera system to determine daily size-distribution, abundance and size-specific sinking velocities of settling particles at one particular depth throughout one year (during the FEVI-40 deployment it was at approx. 565 m water depth). This is done by having a settling cylinder where particles sink through. At the bottom part of the settling cylinder we have attached a perpendicular camera system that records image sequences daily. At the bottom of the settling cylinder, we attached two rotation tables with 40 collection cups so that each cup could be placed under the settling column for a pre-determined collection period (Fig. 5.1). The cups are filled with a viscous gel, which preserves the size and three-dimensional structures of particles sinking into the gel. This makes it possible to identify and quantify different particle types as well as their compositions.

Fig. 5.1: The BOP system deployed during PS121 and recovered during PS126 with the glass settling column and camera system (left image) and the rotation table with collection cups (right image)

The BOP system is based on a modified sediment trap (KUM GmbH) where the collection funnel was replaced by a glass cylinder to avoid that the settling particles were sliding/rolling down the sides of the funnel, which may alter their physical structure. The glass cylinder has an inner diameter of 35 mm and functions as a settling cylinder that excludes ocean currents while the particles settling through it (Fig. 5.1). The camera system placed at the lower part of the settling cylinder consisted of an industrial camera (Basler), a fixed focal length lens (Edmund Optics) and a single board computer including an SSD hard disc and custom-made power and time management circuitry. The images were illuminated by a custom made visible light source providing backlight. The whole camera system was powered by a Li-Ion battery (24 V, 1670 Wh, SubCTech GmbH) (Fig. 5.1).

Vertical profiles with the In-situ Camera

The *In-situ* Camera (ISC) consisted of an industrial camera with removed infrared filter (from Basler) with backend electronics for timing, image acquisition and storage of data and a fixed focal length lens (16 mm Edmund Optics). Furthermore, a DSPL battery (24 V, 38 Ah) was used to power the system (Fig. 5.2).

A single-board computer served both as the operating system for the infrared camera and to acquire images from the camera and send them to an SSD hard drive where they were stored. The illumination was provided by a custom-made light source that consisted of infrared LEDs which were placed in an array in front of the camera. The infrared illumination was chosen so as not to disturb the zooplankton that might feed on the settling particles. With this geometrical arrangement of the camera and the light source, we obtained shadow images of particles through the water column. We captured two images per second and lowered the ISC with 0.3 meters per second (lowest possible speed of winch).

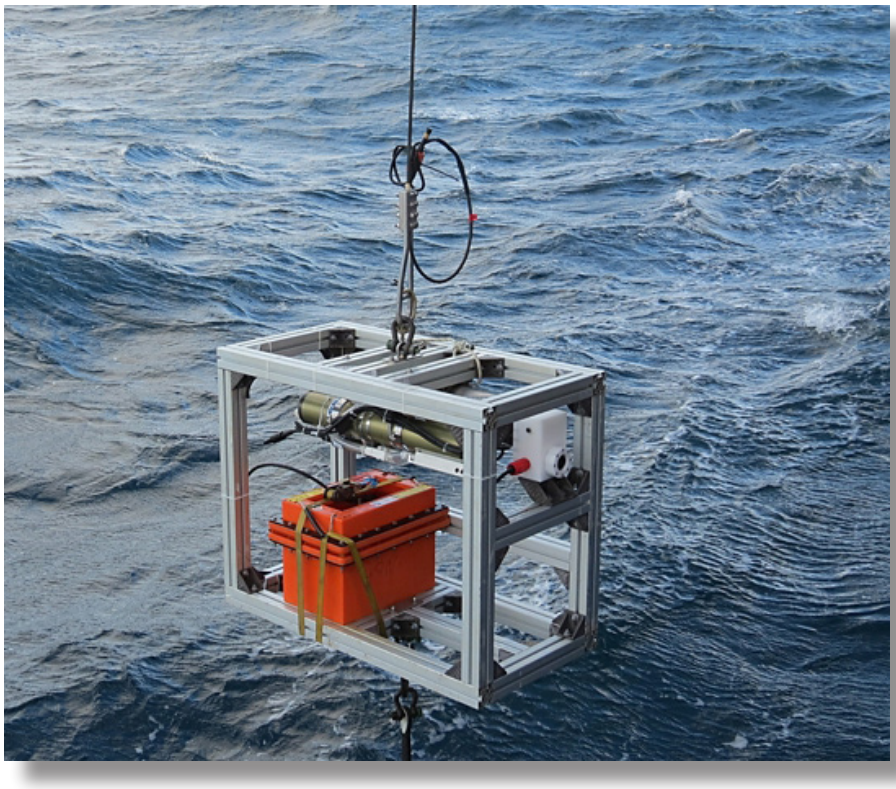

Fig. 5.2: Deployment of the In-situ Camera (ISC), consisting of an industrial camera and lens with electronics, an infrared light source, the DSPL battery and a Seabird SBE19 CTD

Particle camera on the SWIPS winch system

The SWIPS particle camera was designed to be a part of the SWIPS winch system (Fig. 5.3) in the FRAM mooring arrays. The SWIPS camera system performs vertical profiles of particle size-distribution and abundances during SWIPS profiler casts.

The SWIPS camera consists of an industrial camera (from Basler) with backend electronics for power distribution, image acquisition, image analysis, communication to the SWIPS profiler and storage of data. A fixed focal length lens (25 mm Edmund Optics) and a custom designed flash are the main optical components, which define the optical properties of the system. These components used with the given optical arrangement result in a pixel size of approx. 16 µm and a volume of approx. 33 x 33 x 43 mm (~49 ml).

Once a cast is initiated by the winch system, the SWIPS camera is powered up and acts as a slave of the SWIPS profiler. Using different commands, the SWIPS profiler requests a new image (every 1 m during upcast) and processed image and particle data as well as system requests. Parallel to image acquisition, the SWIPS camera performs image analysis for particle detection and particle property determination. Further processes are responsible for housekeeping and logging of system information. The raw- and processed-data is saved on the SWIPS camera, but the most essential profile information is also sent via serial interface to the SWIPS profiler (and after the cast from profiler to the winch electronics). This is a safety feature in case of profiler loss.

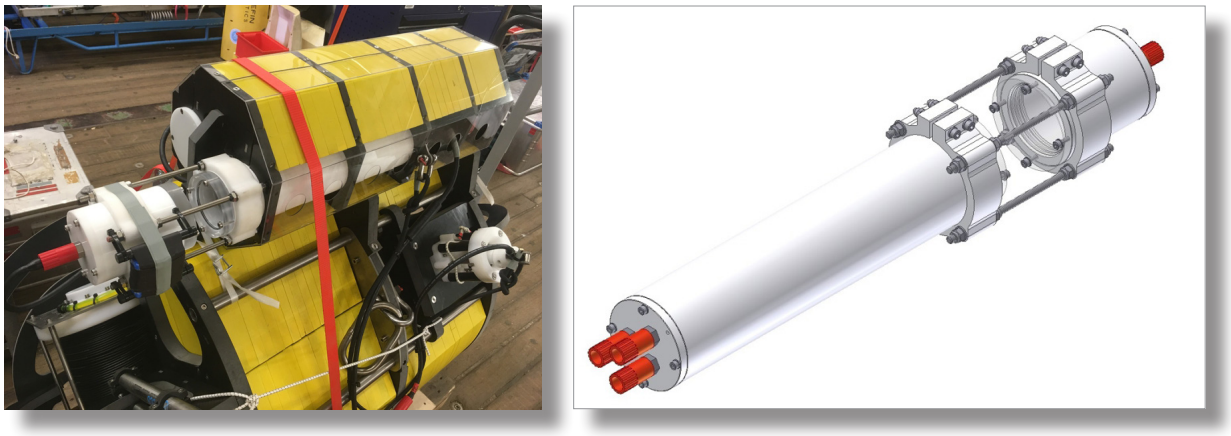

Fig. 5.3: SWIPS camera mounted on the profiler of the SWIPS winch system (left image) and a sketch of the SWIPS camera (right image)

Work at sea

Recovery of the BOP at FEVI-40, HG-IV (deployed during PS121)

During this cruise (PS126), we recovered the BOP system at the FEVI-40 mooring at station HG-IV on 1 June 2021. The cups had all rotated through their programmed position and contained material. From this we could confirm that the BOP system was able to capture settling particles at all seasons.

The camera system had captured 10 min of images every second day from 1 September 2019 until 27 June 2020, which resulted in 151 days of image sequences. Due to the planned deployment period of two years, the camera capture duration as well as the interval had to be adjusted to a deployment setting of one year.

Deployment of the BOP system at F4-W3 (deployed during PS126)

We deployed a new version of the BOP system, which was equipped with two rotating tables and capable of collecting sinking particles in 40 gel-cups. The camera system was similar to that described above. We deployed the BOP system on the F4-W3 mooring at station PS126_14-03 on 8 June 2021 at 79° 00.704'N and 07° 02.089'E. Please see further information about the mooring under the mooring cruise report (see Chapter 9). We timed the cup openings according to the deep ocean sediment traps on the same mooring, but ensured that we would have several gel cups with only three days of opening period at each collection period of the deep ocean sediment traps. This was to ensure that no particles would fall on top of each other, which would prevent image analysis of the particles collected in the gel traps. We programmed the camera for measurements of particle type, size-distribution, abundance, and sinking velocities so that it switched on every 24 hours at 00:00 (UTC) and captured one image every four seconds for 28 minutes.

Deployments of the In-situ Camera

We made 10 vertical profiles with the *In-situ* Camera. The camera frame was equipped with a Seabird SBE19 CTD. The parallel measurements with the CTD allowed correlation of depth and images. During the whole cruise both instruments were used in standalone mode and data was then afterwards correlated with Python-scripts. Table 5.1 gives an overview of all measured profiles.

Tab. 5.1: List of stations where the *In-situ* Camera (ISC) was deployed in the profiling mode.

Station No.	ID	Profile No.	Date	Start Time	Water depth [m]	Profiling depth [m]
PS126_2-3	S3	1	30.05.2021	23:02:30	2338	500
PS126_3-6	HG-IV	2	01.06.2021	19:32:02	2462	500
PS126_6-5	HG-II	3	04.06.2021	22:33:20	1558	500
PS126_8-3	HG-I	4	05.06.2021	12:28:20	1278	500
PS126_9-11	SV-IV	5	06.06.2021	23:18:27	1298	500
PS126_13-4	SV-I	6	08.06.2021	05:46:50	273	250
PS126_18-12	N4	7	11.06.2021	07:44:27	2616	500
PS126_21-13	EG-I	8	15.06.2021	21:59:50	883	500
PS126_23-9	HG-IX	9	17.06.2021	23:12:52	5460	500
PS126_28-6	HG-VI	10	21.06.2021	02:39:41	3444	500

Recovery of the SWIPS camera at HG-IV-W3 (deployed during PS121)

The recovery of the SWIPS winch system with the particle camera was successful after the two years of deployment. After retrieving the data, the SWIPS particle camera system had performed 116 profiles with an interval of 11.6 hours (instead of the intended interval of 48 hours), resulting in a measurement period from 30 August 2019 to 30 October 2019. The higher sample interval consumed more power from the SWIPS winch, the profiling stopped at the above-mentioned date and we did not obtain profiles for the full two-year deployment.

Deployment of the SWIPS camera at SV-IV, F4-W3 (deployed during PS126)

After maintenance of the SWIPS particle camera, the system was reintegrated into a SWIPS winch system and deployed as part of the SWIPS winch system at station SV-IV in mooring F4-W3. The system was programmed with an interval of 96 hours.

Preliminary (expected) results

Processing of image sequences of the BOP system and the *In-situ* Camera is a time-consuming process and will be performed in the home laboratories at AWI-Bremerhaven and MARUM after the cruise. Samples in the collection cups will also be analysed after the cruise. Thus, preliminary particles profiles from the ISC were processed already during the cruise. Fig. 5.4 shows example profiles of particle abundance data at selected HAUSGARTEN stations.

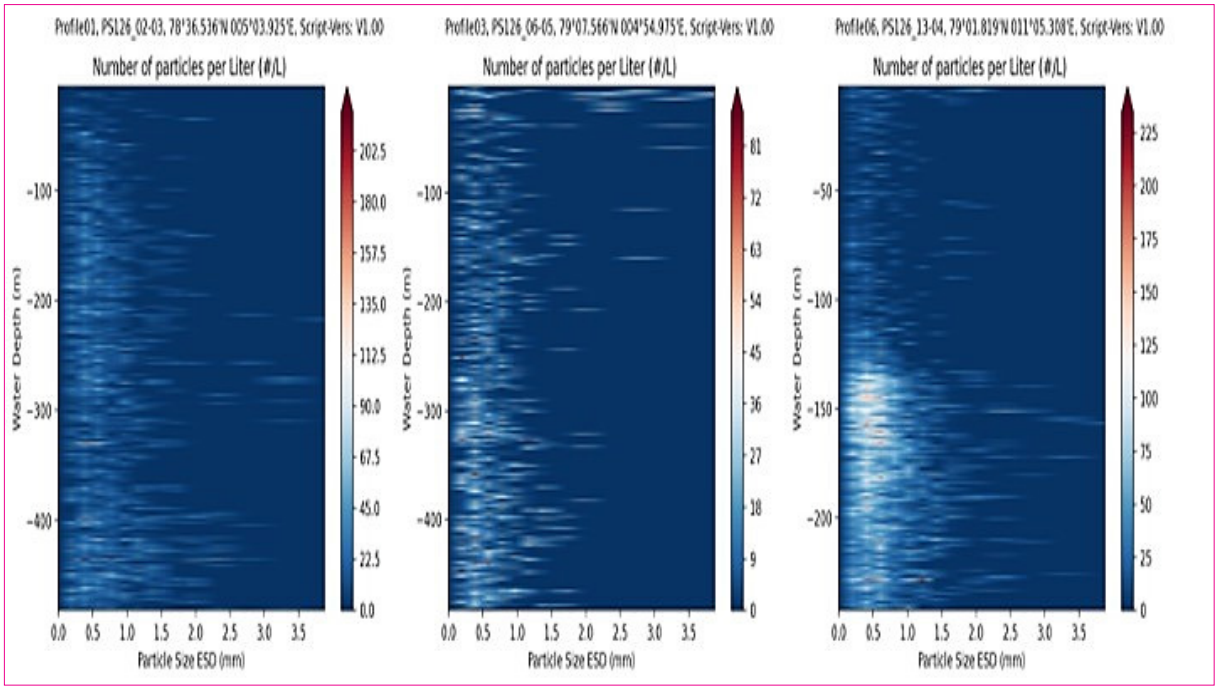

Fig. 5.4: Example ISC particle profiles at different HAUSGARTEN stations

The particle profile plot in Fig. 5.5 is the first time series particle profile of SWIPS camera in the Fram Strait and shows a clear decrease in particle abundance in the period from end of August 2019 to end of October 2019.

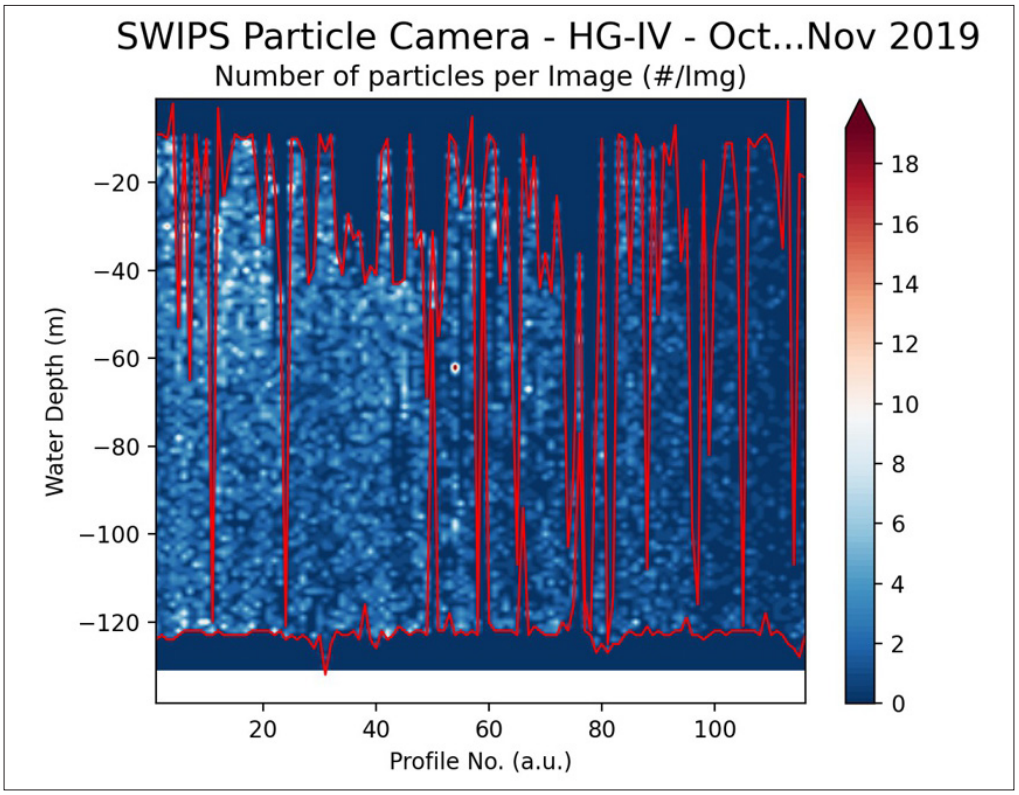

Fig. 5.5: Preliminary SWIPS camera profiles during the period from 30 August 2019 to 30 October 2019; the red lines mark the starting and ending depth of the individual profiles. Due to communication failures between the SWIPS winch and the SWIPS camera profiler, not all profiles could be performed from the maximum depth at approximately 125 m to the shallow depth of 10 m.

Data management

Analysis of BOP, SWIPS and ISC data is quite time consuming and will therefore be done in the home laboratories at AWI-Bremerhaven and MARUM. All data will be published in the World Data Center PANGAEA Data Publisher for Earth & Environmental Science (https://www.pangaea.de).

In all publications, based on this cruise, the **Grant No. AWI_PS126_03** will be quoted and the following *Polarstern* article will be cited: Alfred-Wegener-Institut Helmholtz-Zentrum für Polar- und Meeresforschung. (2017). Polar Research and Supply Vessel POLARSTERN Operated by the Alfred-Wegener-Institute. Journal of large-scale research facilities, 3, A119. http://dx.doi.org/10.17815/jlsrf-3-163.

6. EFFECTS OF RISING TEMPERATURES AND NITROGEN LIMITATION ON ARCTIC UNICELLULAR PLANKTON COMMUNITY STRUCTURE

Antonia Uthoff[1], Uwe John[1] [1]DE.AWI

Grant-No. AWI_PS126_04

Objectives

Unicellular plankton communities play a fundamental role within marine ecosystems by providing organic matter to oceanic food webs and by fostering major biogeochemical cycles (Katz et al. 2004). Currently, they are facing drastic alterations of their abiotic environment due to Climate Change (Doney et al. 2012), especially in the Arctic (Miller et al. 2010). For Arctic marine microbes, two highly important aspects of Climate Change are rising temperatures and a decrease in nitrogen supply via increased stratification. Instead of acting independently, their effects on species' performance seem to interact strongly (Gerhard et al. 2019; Marañón et al. 2018; Thomas et al. 2017). Furthermore, they influence the various groups within the communities differently and thus shape the outcome of competition, facilitation, herbivory and parasitism (Bestion et al. 2018; Boyd et al. 2018; Branco et al. 2020). Although the resulting structural composition of unicellular plankton communities affects processes relevant for Climate Change itself, e.g. the biological carbon pump (Guidi et al. 2009; Lafond et al. 2020), little is known about the mechanisms governing community assembly.

Most studies investigating the effect of multiple drivers on microplankton communities focus on culture experiments with single strains or populations (Boyd et al. 2018). Bearing in mind the multitude of interactions within complex plankton communities, the outcome of single species experiments might not reflect the actual situation in the field (Celiker and Gore 2014; Turcotte et al. 2012). In fact, the presence of another species in an experimental setting seems to alter their reactions to abiotic change (Hall et al. 2018) and some authors stress that even two-species interactions are poor predictors for whole community responses (McClean et al. 2019). Furthermore, relatively small changes within some functional groups could have large knock-on effects on other groups (Camarena-Gómez et al. 2018). This does not underestimate the detailed physiological insights gained from experiments with only one species, but underlines the importance of additional experiments with natural assemblages including several species and groups. Of particular interest is the question, which members of a multispecies community will prevail the prospective changes in abiotic conditions. Identifying the characteristics of these so-called "winner species" is an essential part of assessing future microplankton community resilience and functioning (Hoffmann and Sgró 2011).

Therefore, the aim of our work during expedition PS126 is to generate experimental data which helps to understand the interactive effects of rising temperatures and nitrogen limitation on the structural composition of Arctic microplankton communities. Our main objective is to determine principles that govern the assemblage of these communities with a focus on the role of taxonomy and functional traits as well as the characteristics of successful community members.

Work at sea

To set up the experiments, 150 L of water were sampled at Chl_{max} (15 m depth) via the CTD/Rosette Water Sampler at two stations: the central HAUSGARTEN station HG-IV (E1) and the western station EG-IV (E2). To serve as dilution water and fresh medium we pumped simultaneously 600 L of sterile-filtrated seawater through the internal Teflon-system into tanks. The water from Chl_{max} was filtered through a 150 µm nylon mesh to exclude mesozooplankton and arranged in two sets of a two-point dilution micro-grazing experiment (see Landry and Hassett 1982) on plankton wheels in light-controlled boxes (30 µmol m^{-2} s^{-1} photons for E1, 100 µmol m^{-2} s^{-1} photons for E2, Figs. 6.1 and 6.2).

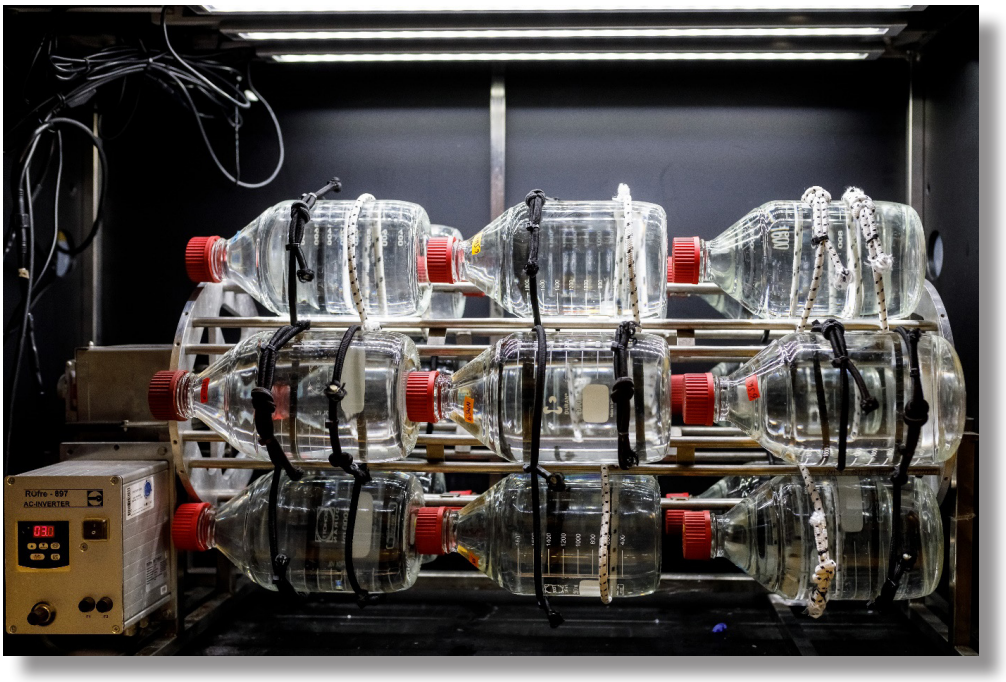

Fig. 6.1: Treatment bottles attached to a rotating plankton wheel in a light-controlled box; photo: Mario Hoppmann

Experiments were run at three different temperatures (2° C, 6° C, 9° C) in cooling containers on board and after 24 hours, all relevant parameters were taken for the first set. The second set continued for another 72 hours (E1) and 96 hours (E2) before it was harvested. Within E1, the second set of bottles at each temperature was transferred into another experimental period including two nitrogen levels (N-replete and N-limited) with three replicates per treatment combination (Fig. 6.2). *In-vivo* chlorophyll *a,* pH and flow cytometric counts were monitored daily to determine when enough biomass for minimum detection limits had been reached keeping concentrations low to avoid nitrogen limitation in all treatments. During the harvests, parts of the samples were preserved with either hexamine buffered formaldehyde and glutardialdehyde for flow cytometric analyses, Lugol's solution for microscopy or sterile-filtration for total alkalinity and nutrient measurements. Other parts were concentrated via gentle vacuum filtration (< 200 mbar) on either pre-combusted Gf/f filters (for chlorophyll and POC/PON measurements) or polycarbonate filters (0.8 µm nominal pore size) and added to warm lysis buffer (for DNA and RNA analyses). Preserved samples were stored at 4° C, –20° C or –80° C for further processing in the home laboratory of the Alfred Wegener Institute.

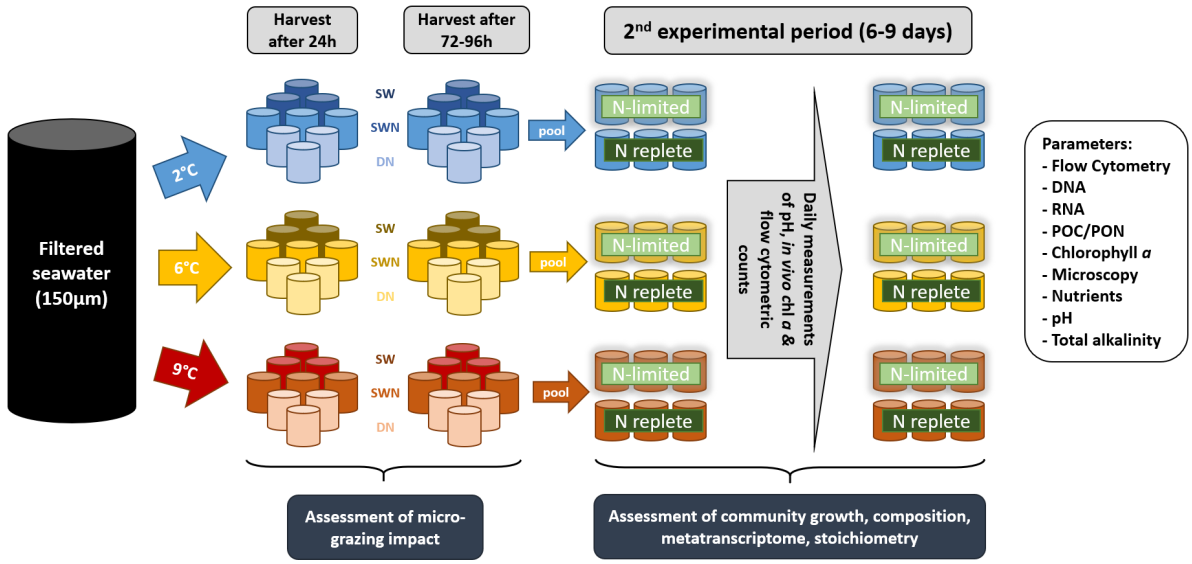

Fig. 6.2: Experimental design of on-board experiments; different shades represent different treatments.

Preliminary (expected) results

The micro-grazing assessment of both experiments (E1 and E2) was successful as we observed positive growth in the first 24 hours through *in-vivo* chlorophyll measurements in all bottles. However, experiments differed strongly in their growth patterns after the initial sampling. Communities in E1 stayed stable for a while before they formed a bloom with aggregated colonies after six days (most probably *Phaeocystis pouchettii*). In contrast, we observed negative growth among all treatments in E2, which stabilized only at 2° C after five days – all other communities crashed. These discrepancies could be due to the differing water masses from which the experiments were started. The central HAUSGARTEN station HG-IV was located in the West Spitsbergen Current, which transports “warmer” Atlantic water northwards, whereas EG-IV was most probably composed of Arctic water masses coming from the Arctic ocean with the East Greenland current. For cold-adapted, rather stenotherm, species from the Arctic, our treatment temperatures could have been too high while the warmer-adapted species from the Atlantic could have coped better with them. Another hypothesis is that the communities sampled from the two stations differed in their bloom stage, the first one being at the start of the bloom and the second one being at the end. Finally, we observed a slight increase in pico-phytoplankton at the end of the second experimental phase of E2. This might indicate that the community shifted towards smaller species (most likely a *Micromonas sp.* population), which would explain an initial drop in chlorophyll. The proposed explanations will be investigated in more detail when all samples have been processed.

Further analyses regarding the carbonate system, community composition, transcriptomic responses, biomass and nutrients will also be performed after sample processing. We expect the outcome of our experiments to contribute to the general understanding of microplankton community assembly and how it is influenced by rising temperatures and nitrogen limitation. The relative importance of functional traits and taxonomic identity as well as characteristics of prevailing species should be identified. Differences within and among treatments could shed light on alternative stable states and the resilience of specific sets of species in a community. Furthermore, the generated data could help to improve future microzooplankton

grazing experiments by assessing the impact of temperature and different nutrient levels on phytoplankton community composition within grazing experiments. Finally, the results will be compared to similar experiments which will be performed in the North Sea to gain an insight into differences and similarities in responses among Arctic and temperate communities. We hope that the output of our experiments will be highly relevant to the new Helmholtz Research Programme "Changing Earth – Sustaining our Future", Subtopic 6.2 (Adaptation of marine life: from genes to ecosystems) and partly Subtopic 6.1 (Future ecosystem functionality).

Sample and data management

Experimental data will be archived, published and disseminated according to international standards by the World Data Center PANGAEA Data Publisher for Earth & Environmental Science (https://www.pangaea.de) within two years after the end of the cruise at the latest. By default, the CC-BY license will be applied.

Molecular data (DNA and RNA data) will be archived, published and disseminated within one of the repositories of the International Nucleotide Sequence Data Collaboration (INSDC, www.insdc.org) comprising of EMBL-EBI/ENA, GenBank and DDBJ).

Any other data will be submitted to an appropriate long-term archive that provides unique and stable identifiers for the datasets and allows open online access to the data.

In all publications, based on this cruise, the **Grant No. AWI_PS126_04** will be quoted and the following *Polarstern* article will be cited: Alfred-Wegener-Institut Helmholtz-Zentrum für Polar- und Meeresforschung. (2017). Polar Research and Supply Vessel POLARSTERN Operated by the Alfred-Wegener-Institute. Journal of large-scale research facilities, 3, A119. http://dx.doi.org/10.17815/jlsrf-3-163.

References

Bestion E, García-Carreras B, Schaum CE, et al. (2018) Metabolic traits predict the effects of warming on phytoplankton competition. Ecology Letters, 21, 655-664.

Boyd PW, Collins S, Dupont S, et al. (2018) Experimental strategies to assess the biological ramifications of multiple drivers of global ocean change - A review. Global Change Biology, 24, 2239-2261.

Branco P, Egas M, Hall SR, et al. (2020) Why Do Phytoplankton Evolve Large Size in Response to Grazing? The American Naturalist, 195, E20-E37.

Camarena-Gómez MT, Lipsewers T, Piiparinen J, et al. (2018) Shifts in phytoplankton community structure modify bacterial production, abundance and community composition. Aquatic Microbial Ecology, 81, 149-170.

Celiker H, Gore J (2014) Clustering in community structure across replicate ecosystems following a long-term bacterial evolution experiment. Nature Communications, 5, 4643.

Doney SC, Ruckelshaus M, Emmett Duffy J, et al. (2012) Climate change impacts on marine ecosystems. Annual Review of Marine Science, 4, 11-37.

Gerhard M, Koussoropolis AM, Hillebrand H, et al. (2019) Phytoplankton community responses to temperature fluctuations under different nutrient concentrations and stoichiometry. Ecology, 100, e02834.

Guidi L, Stemmann L, Jackson GA, et al. (2009) Effects of phytoplankton community on production, size and export of large aggregates: A world-ocean analysis. Limnology and Oceanography, 54, 1951-1963.

Hall JPJ, Harrison E, Brockhurst MA (2018) Competitive species interactions constrain abiotic adaptation in a bacterial soil community. Evolution Letters, 2, 580-589.

Hoffmann AA, Sgró CM (2011) Climate change and evolutionary adaptation. Nature, 470, 479-485.

Katz ME, Finkel ZV, Grzebyk D, et al. (2004) Evolutionary trajectories and biogeochemical impacts of marine eukaryotic phytoplankton. Annual Review of Ecology, Evolution, and Systematics, 35, 523-556.

Lafond A, Leblanc K, Legras J, et al. (2020) The structure of diatom communities constrains biogeochemical properties in surface waters of the Southern Ocean (Kerguelen Plateau). Journal of Marine Systems, 212, 103458.

Landry MR, Hassett RP (1982) Estimating the grazing impact of marine micro-zooplankton. Marine Biology, 67, 283-288.

Marañón E, Lorenzo MP, Cermeño P, et al. (2018) Nutrient limitation suppresses the temperature dependence of phytoplankton metabolic rates. ISME Journal, 12, 1836-1845.

McClean D, Friman V-P, Finn A, et al. (2019) Coping with multiple enemies: pairwise interactions do not predict evolutionary change in complex multitrophic communities. Oikos, 128, 1588-1599.

Miller GH, Alley RB, Brigham-Grette J, et al. (2010) Arctic amplification: Can the past constrain the future? Quaternary Science Reviews, 29, 1779-1790.

Thomas MK, Aranguren-Gassis M, Kremer CT, et al. (2017) Temperature–nutrient interactions exacerbate sensitivity to warming in phytoplankton. Global Change Biology, 23, 3269-3280.

Turcotte MM, Corrin MSC, Johnson MTJ (2012) Adaptive evolution in ecological communities. PLoS Biology, 10(5), e100133.

7. TEMPORAL VARIABILITY OF NUTRIENT AND CARBON TRANSPORTS INTO AND OUT OF THE ARCTIC OCEAN

Daniel Scholz[1], Klara Köhler[1], Normen Lochthofen[1], Rebecca McPherson[1], Mario Hoppmann[1]; Sinhué Torres-Valdés[1], Wilken-Jon von Appen[1] (not on board)

[1]DE.AWI

Grant-No. AWI_PS126_05

Rationale and Objectives

Current gaps in knowledge concerning nutrient and carbon biogeochemical cycles at the pan-Arctic scale stem from the lack of information needed to constrain their budgets. Available computations (MacGilchrist et al. 2014; Torres-Valdés et al. 2013, 2016) indicate the Arctic Ocean (AO) is a net exporter of phosphate, dissolved organic phosphorus, silicate, dissolved organic nitrogen and dissolved inorganic carbon (DIC). Net nitrate transports are balanced despite large losses due to denitrification. Silicate export derives largely from riverine inputs, suggesting alterations in river loads might have an impact on exports too, potentially modifying the stoichiometric abundance of nutrients. These computations are based mostly on summer time observations across the main gateways (i.e. Fram Strait, the Barents Sea Opening, Bering Strait and Davis Strait), which hinders our complete understanding given data to resolve temporal variability over seasonal and longer time scales are rather scarce. Because of this, there are still unknowns regarding sources and sinks of these biogeochemically relevant variables. Under ongoing and predicted climate change, identifying and quantifying sinks and sources becomes relevant to: (a) generate baseline measurements against which future change can be evaluated, (b) assess the impact of climate change on biogeochemical processes (e.g. primary production, organic carbon export, remineralisation), (c) understand the complex interaction between biogeochemical and physical processes, and how such interactions affect the transport of nutrients downstream and the capacity of the AO to function as a sink of atmospheric CO_2, and to (d) determine whether long-term trends occur and what is their origin.

To address the points listed above, we began the deployment of FRAM sensors and remote access samplers, targeting core (~250 m) and surface waters of the West Spitsbergen Current and the East Greenland Current since 2018, with the current deployment being the third. With these data we will be able to assess the role of transports across the Fram Strait, one of the main Arctic gateways, relative to the wider Arctic Ocean nutrient and carbon budgets.

The deployments of RAS are done in collaboration with Katja Metfies (AWI) and Matthias Wietz (AWI/MPIMM), who study phytoplankton and bacterial genetics, respectively.

Work at sea

Sensors and remote access samplers

We prepared and deployed sensors and remote access samplers (RAS) in the following moorings: EGC-7 at 55 and 249 m depth in the East Greenland Current, and F4S-5 at 21 and 245 m in the West Spitsbergen Current. Each package consists of a RAS with a SUNA nitrate, SAMI pH, SAMI pCO_2 and a Microcat CTD-O_2 sensor attached (Fig. 7.1). With additional Wetlabs PAR and Eco-triplet sensors in close-to-surface deployments.

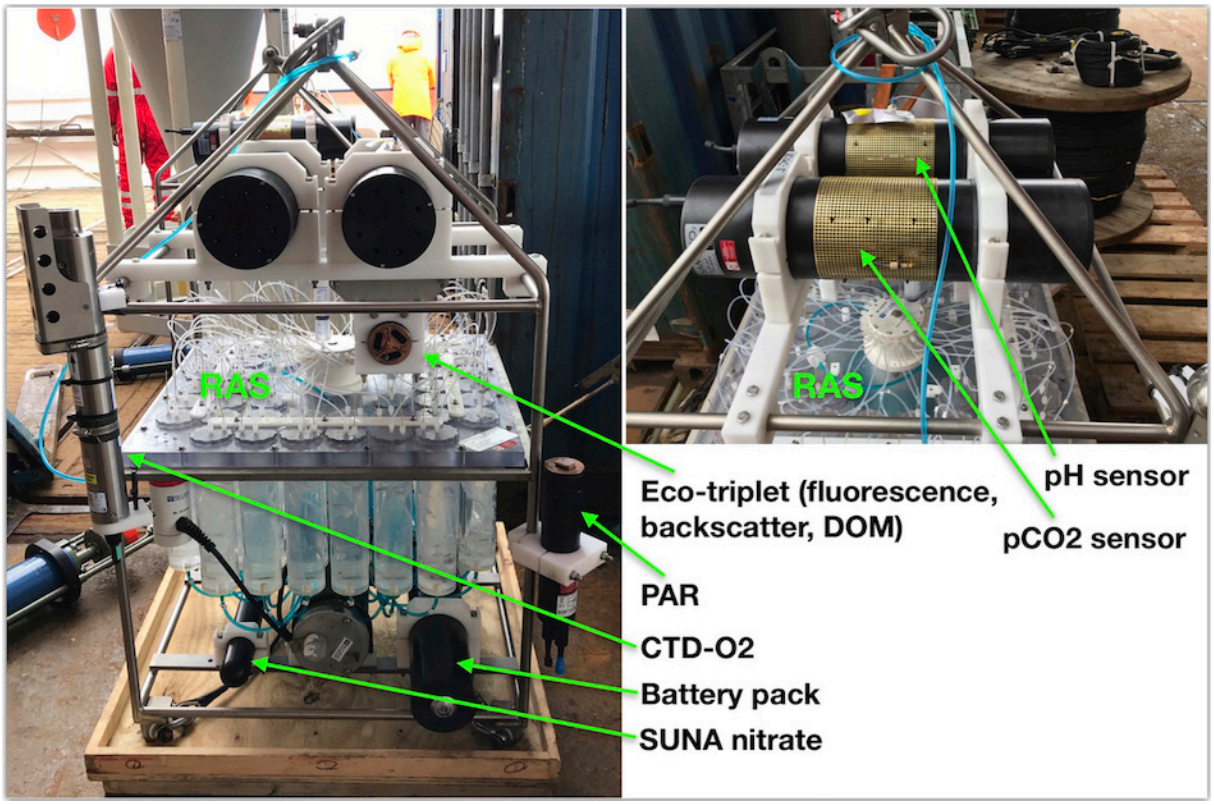

Fig. 7.1: Sensor package: remote access sampler (RAS) with sensors attached to its frame; for illustration, this image shows one of the packages attached to mooring EGC-5, deployed during PS114 in 2018

We successfully recovered the sensor packages deployed on the same mooring locations during PS121. All sensors recorded data. Both pH sensors installed in the moorings in the West Spitsbergen Current recorded data but were affected by a clocked sample tube after about three months into the deployment, which resulted in irregular data and needs further investigation back at the AWI. Furthermore, the SUNA nitrate sensor deployed at 239 m depth in the East Greenland Current shows erroneous data between 28.09.2020 and 21.03.2021. A preliminary data analysis shows reasonable results for all other sensors, which measured throughout the entire two-year deployment period except for the pH and pCO_2 whose sampling schedule was setup for one year only. Additionally, we recovered an ISUS nitrate sensor along with a PAR and eco-triplet sensor at the HG-IV-S-4 mooring. The ISUS sensor was flooded and no data was retrieved.

RAS samples were subsampled for nutrients and will be shipped to AWI for analysis. The RAS at the EGC-6 mooring at 67 m consistently collected about one third of the defined sample volume. In total we lost 6 of 240 samples due to broken sample bags (2.4 %).

Additionally, a SUNA nitrate sensor was used to generate high resolution profiles in 23 CTD casts shallower than 2,000 m. The CTD's temperature and salinity data are used to process the nitrate data following Sakamoto et al. (2009). The nitrate data of the CTD's Niskin bottle subsamples will be used to further improve the SUNA data quality.

Sample collection

In total, 223 seawater samples (19 stations) were collected from CTD casts for the later analysis of dissolved inorganic and total dissolved nutrients back in the laboratory at the AWI. The samples were collected in 125 mL HDPE Bottles and stored at –20° C.

Due to the reduction of team capacity during PS126, we did not collect samples for carbonate system variables.

Table 7.1 summarizes the stations and depths at which we took seawater samples during the *Polarstern* expedition PS126.

Preliminary (expected) results

Water samples have to be analysed at AWI and the sensor data needs further processing. Both datasets will be compiled after quality control measures have been applied. We expect the analysis of samples collected during PS126 to take place within the next year.

Data management

Our aim is to compile data from the different devices in a single file once individual data sets have been retrieved, quality controlled and analysed. Environmental data will be archived, published and disseminated according to international standards by the World Data Center PANGAEA Data Publisher for Earth & Environmental Science (https://www.pangaea.de) within two years after the end of the cruise at the latest. By default, the CC-BY license will be applied.

In all publications, based on this cruise, the **Grant No. AWI_PS126_05** will be quoted and the following *Polarstern* article will be cited: Alfred-Wegener-Institut Helmholtz-Zentrum für Polar- und Meeresforschung. (2017). Polar Research and Supply Vessel POLARSTERN Operated by the Alfred Wegener Institute. Journal of large-scale research facilities, 3, A119. http://dx.doi.org/10.17815/jlsrf-3-163.

References

MacGilchrist GA, Naveira-Garabato AC, Tsubouchi T, Bacon S, Torres-Valdés S, Azetsu-Scott K (2014) The Arctic Ocean carbon sink. Deep Sea Research I, 86, 39-55. doi: 10.1016/j.dsr.2014.01.002.

Torres-Valdés S, Tsubouchi T, Bacon S, Naveira-Garabato AC, Sanders R, McLaughlin FA, Petrie B, Kattner G, Azetsu-Scott K, Whitledge TE (2013) Export of nutrients from the Arctic Ocean. Journal of Geophysical Research: Oceans, 118(4), 1625-1644. doi: 10.1002/jgrc.20063.

Torres-Valdés S, Tsubouchi T, Davey E, Yashayaev I, Bacon S (2016) Relevance of dissolved organic nutrients for the Arctic Ocean nutrient budget. Geophysical Research Letters, 43(12), 6418-6426.

Sakamoto, CM, Johnson, KS, Coletti, LJ (2009) Improved Algorithm for the Computation of Nitrate Concentrations in Seawater using an in situ Ultraviolet Spectrophotometer. Limnology and Oceanography: Methods, 7, 132-143.

Tab. 7.1: Overview for the seawater samples for later nutrient analysis with information about the Station ID, station name and the depths, at which the samples were taken. Additional to the listed CTD casts, the SUNA nitrate sensor was used at the CTD casts 1 and 20 (PS126_1-5 and PS126_20-6), from which no seawater samples for nutrient analysis were taken.

	CTD cast	2	3	4	6	7	8	9	10	11	12	13	14
	Station ID	PS126 _2-2	PS126 _2-11	PS126 _3-1	PS126 _3-13	PS126 _4-1	PS126 _6-1	PS126 _8-1	PS126 _8-9	PS126 _9-5	PS126 _11-1	PS126 _12-5	PS126 _13-3
	Station	S3	S3	HG-IV	HG-IV	HG-III	HG-II	HG-I	HG-I	SV-IV	SV-III	SV-II	SV-I
	SUNA		x		x	x	x	x	x	x	x	x	x
Depth [m]	5												
	10		x		x	x	x		x	x	x	x	x
	15		x		x (17 m)	x	x (17 m)			x (17 m)	x (17 m)		
	20												
	25				x	x	x		x			x	x
	30										x		
	35								x	x			x
	40		x									x	
	50				x	x	x		x	x	x	x	x
	75								x				
	100		x		x	x	x		x	x	x	x	x
	150		x		x	x				x	x	x	x
	200	x	x		x	x	x				x	x	
	250			x		x		x	x	x	x		x
	400												
	500	x		x				x					
	750	x		x				x					
	850									x			
	1000	x		x				x					
	1200												
	1300	x		x									
	1600			x									
	2000	x		x									
	2250	x											
	3000												
	above bottom	x 2276 m		x 2222 m				x 1238 m		x 1262 m			

▶ *Fortsetzung Tab.7.1*

	CTD cast	15	16	17	18	19	21	22	23	24	25	26	27	28	29
	Station ID	PS126	PS126	PS126	PS126	PS126	PS126	PS126	PS126	PS126	PS126	PS126	PS126	PS126	PS126
		_17-2	_18-1	_18-7	_19-5	_20-2	_20-8	_21-5	_21-12	_22-1	_23-1	_23-8	_24-1	_25-1	_28-5
	Station	N3	N4	N4	N5	EG-IV	EG-IV	EG-I	EG-I	0°	HG-IX	HG-IX	HG-VII	HG-V	HG-VI
	SUNA	x	x		x		x	x	x	x	x		x	x	x
Depth [m]	5	x	x							x			x (3 m)	x (3 m)	x
	10				x		x		x	x (12 m)	x		x (12 m)	x	
	15				x (14 m)		x (16 m)								
	20	x	x						x	x	x				x
	25				x								x	x	
	30						x		x						
	35	x	x								x				x
	40														
	50	x	x		x		x		x	x	x		x	x	x
	75														
	100	x	x		x		x		x	x	x		x	x	x
	150		x		x		x		x	x	x		x	x	x
	200		x		x		x		x	x	x	x	x	x	x
	250	x		x	x	x		x			x		x	x	x
	400							x				x			
	500			x	x	x		x		x	x		x	x	x
	750			x				x							
	850														
	1000			x		x						x			
	1200											x			
	1300			x		x									
	1600			x		x									
	2000			x		x						x			
	2250														
	3000											x			
	above bottom			x		x		x				x			
				2853 m		2500 m		900 m				5546 m			

8. BENTHIC FLUXES

Frank Wenzhöfer[1], Simon Escalle[1], [1]DE.AWI
Axel Nordhausen[2], Elena Schiller[1]; [2]DE.MPIMM
Michael Hofbauer[1], Volker Asendorf[2]
(not on board)

Grant-No. AWI_PS126_06

Objectives

Benthic communities are strictly dependent on carbon supply through the water column, which is determined by temporal and spatial variations in the vertical export flux from the euphotic zone but also lateral supply from shelf areas. Most organic carbon is recycled in the pelagic, but a significant fraction of the organic material ultimately reaches the seafloor, where it is either re-mineralized or retained in the sediment record. One of the central questions is to what extent sea ice cover controls primary production and subsequent export of carbon to the seafloor on a seasonal and interannual scale. Benthic oxygen fluxes provide the best and integrated measurement of the metabolic activity of surface sediments. They quantify benthic carbon mineralization rates and thus can be used to evaluate the efficiency of the biological pump. In order to link long-term variations in surface and sea-ice productivity and consequently in export flux to the seafloor, detailed investigation of the temporal variations in benthic oxygen consumption rates would be very valuable. Yearly measurements with benthic lander provide information on the interannual variations. Benthic crawler, capable to perform weekly oxygen gradient measurements for a 12-month period, provide information on the seasonal variations. In addition, long-term lander systems equipped with sediment traps and cameras for time-lapse imaging of the seafloor record the supply of organic material throughout the year.

Work at sea

Benthic fluxes

Seafloor carbon mineralization was studied at *in-situ* sites with varying sea ice conditions (HG-IV, N4, and EG-IV) using a benthic lander system (Hoffmann et al. 2018). The benthic O_2 uptake is a commonly used measure for the benthic mineralization rate. We measured benthic oxygen consumption rates at different spatial and temporal scales.

The Flux Lander was equipped with two different profiling instruments to investigate the oxygen penetration and distribution as well as the benthic oxygen uptake of Arctic deep-sea sediments: (1) electrode-microprofiler, for high-resolution pore water profiles (O_2, resistivity) across the sediment-water interface, and (2) a deep optode-profiler, to measure the entire oxygen penetration depth. Clark-type oxygen micro-electrodes were incrementally (100 µm steps) inserted into the sediment to investigate the upper horizon (ca. 10 cm). The individual sensors were custom-made from glass with typical tip-diameters in the range of 25 to 50 µm. Up to nine oxygen electrodes were attached to a 150 mm diameter titanium housing that contained electronics for signal amplification and processing. To account for the deep oxygen

penetration, the recently developed fibre-optical microprofiler was deployed in parallel. It uses two sets of four fibre-optical sensors (230 micrometre tip diameter, Pyroscience, DE) that are embedded in hypodermic needles mounted to solid shafts made from carbon-reinforced plastic. This allows to record longer profiles, that are better suited for low-respiration environments and deep oxygen penetration sites. These sensors allowed to take 30 cm long profiles with a step resolution of 250 µm.

During PS126, the Flux Lander was deployed at three sites (HG-IV, N-4, and EG-IV; Table 8.1). Unfortunately, due to strong surface currents and sea ice drifts, we were not able to recover the lander at EG-IV. Additional we recovered two long-term lander systems (equipped with sediment traps, current meters and seafloor cameras) at both sites (Table 8.1). Sediment trap samples provide an estimate on the amount of settling organic matter at the seafloor. Data are compared with benthic oxygen consumption rates. Due to technical problems only the Long-Term lander at HG-IV, equipped with sediment trap, current meter system and time-lapse camera, could be re-deployed (Table 8.1).

Tab. 8.1: Benthic flux lander and crawler deployments

Station	ID	Device	Date	Latitude	Longitude	Depth [m]	Comment
PS126_3-17	HG-IV	Flux Lander	02.06.21	79°03.898‘N	004°11.068‘E	2459	
PS126_3-22	HG-IV	Long-Term Lander HG-IV	03.06.21	79°04.150‘N	004°10.099‘E	2463	Recovery
PS126_5-2	HG-IV	NOMAD	04.06.21	79°04.215‘N	004°11.014‘E	2447	Rescue with OFOBS mini-ROV
PS126_18-6	N4	Flux Lander	11.06.21	79°42.705‘N	004°14.586‘E	2918	
PS126_20-1	EG-IV	Flux Lander	13.06.21	78°47.410‘N	002°50.923‘W	2593	
PS126_21-2	EG-I	Long -Term Lander EG-I	15.06.21	79°00.005‘N	005°26.361‘W	1013	Recovery
PS126_21-3	EG-I	TRAMPER	15.06.21	78°59.767‘N	005°26.547‘W	1000	
PS126_26-1	HG-IV	NOMAD	19.06.21	79°04.334‘N	004°10.826‘E	2444	Rescue with OFOBS mini-ROV
PS126_26-2	HG-IV	Long-Term Lander HG-IV	19.06.21	79°02.750‘N	004°10.466‘E	2564	Deployment

Seasonal variations

At two contrasting sites – HG-IV (West Spitzbergen) and EG-I (East Greenland) – benthic crawler systems (TRAMPER and NOMAD) were recovered after their 24-month mission (both were deployed in 2019 during *Polarstern* cruise PS121) (Tab. 8.1). Both crawler systems were pre-programmed to perform >100 measurements along an approximately 1.5 km transect. TRAMPER (Wenzhöfer et al. 2016) deployed at EG-I uses oxygen optodes to measure vertical concentration profiles across the sediment-water interface (one set of profiles each week). Unfortunately, TRAMPER (Fig. 8.1) had some problems with its battery and the mission stopped already shortly after the deployment. Thus, not data were recorded.

Fig. 8.1: TRAMPER recovery in drifting ice floes

NOMAD, additionally equipped with benthic chambers and a seafloor imaging and scanning camera system (Lemburg et al. 2018), was deployed at HG-IV. NOMAD took images of the seafloor combined with a laser scan. From this information we are able to reconstruct the sediment surface at high resolution. When seafloor images and topography scans are overlaid, we will be able to identify hot spots of intensified organic matter accumulation. These two seafloor observations were performed during the 10 m long transect at the beginning of each measuring cycle. At the end of this transect, concentration profiles of oxygen were measured across the sediment water interface. From these profiles diffusive oxygen fluxes can be obtained. Chamber incubations, performed at the same time, provide the total oxygen demand of the seafloor. Both measurements provide information on the oxygen consumption related to carbon mineralization. These cycles were repeated every week for a period of 24-month. Already during *Maria S. Merian* expedition MSM95 in 2020, we know from OFOBS dives that NOMAD was stopped by a drop stone. However, attempts to rescue the crawler failed at that time. During PS126, we were now able to rescue NOMAD using OFOBS in combination with

a miniROV attached to it (Fig. 8.2). A first inspection of the sensor systems revealed that NOMAD had worked for almost one year. All data – oxygen profiles, chamber incubations, high-resolution images and seafloor topography scans – will be analysed back home.

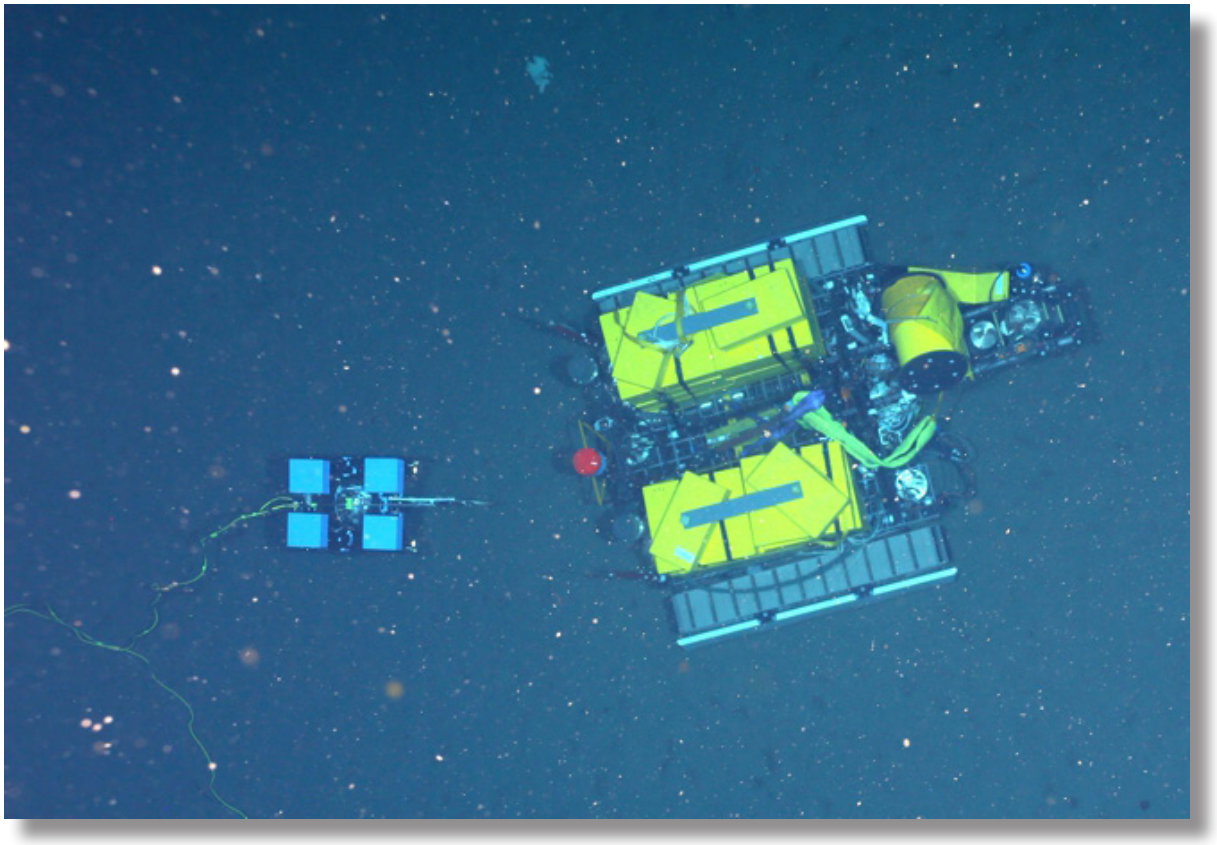

Fig. 8.2: NOMAD rescue using OFOBS and the miniROV

Due to the technical problems with both crawler systems none of the systems could be re-deployed during this cruise.

Preliminary (expected) results

The overall aim of both crawler and lander deployments is to cover a seasonal cycle of settling organic matter on the seafloor with contrasting and changing food supplies and to resolve the impact on the benthic community respiration activity. All in all, deployments during PS126 resulted in 25 oxygen profiles suitable for quantification of the diffusive oxygen uptake (DOU). Diffusive oxygen uptake is calculated from the change in oxygen concentration across the diffusive boundary layer (DBL) or the uppermost sediment layer times the diffusion coefficient *d* (T, S) or based on the derivative of the entire profile.

Combined with sediment trap and seafloor imaging we expect new insights in the benthic oxygen consumption rates over a full seasonal cycle. Long-term deployment of both *in-situ* systems further allows interannual variations to be detected. Images taken during the two-year deployment at EG-I showed a strong temporal variability in the supply of organic matter to the seafloor. The use of new underwater technologies will thereby enhance our capabilities to improve our knowledge on the effects of climate change on the Arctic ecosystem.

Data management

Environmental data will be archived, published and disseminated according to international standards by the World Data Center PANGAEA Data Publisher for Earth & Environmental Science (https://www.pangaea.de) within two years after the end of the cruise at the latest.

Any other data will be submitted to an appropriate long-term archive that provides unique and stable identifiers for the datasets and allows open online access to the data.

In all publications, based on this cruise, the **Grant No. AWI_PS126_06** will be quoted and the following *Polarstern* article will be cited: Alfred-Wegener-Institut Helmholtz-Zentrum für Polar- und Meeresforschung. (2017). Polar Research and Supply Vessel POLARSTERN Operated by the Alfred-Wegener-Institute. Journal of large-scale research facilities, 3, A119. http://dx.doi.org/10.17815/jlsrf-3-163.

References

Hoffmann R, Braeckman U, Hasemann C, Wenzhöfer F (2018) Deep-sea benthic communities and oxygen fluxes in the Arctic Fram Strait controlled by sea-ice cover and water depth. Biogeosciences, 15, 4849-4869.

Wenzhöfer F, Lemburg J, Hofbauer M, Lehmenhecker S, Färber P (2016) TRAMPER - An autonomous crawler for long-term benthic oxygen flux studies in remote deep sea ecosystems. Proceedings OCEANS 2016 MTS/IEEE Monterey, 1-6. doi: 10.1109/OCEANS.2016.7761217.

Lemburg J, Wenzhöfer F, Hofbauer M, Färber P, Meyer V (2018) Benthic crawler NOMAD – Increasing payload by low-density design. Proceedings OCEANS 2018 MTS/IEEE, Kobe, 279-285.

9. PHYSICAL OCEANOGRAPHY

Mario Hoppmann[1], Rebecca A. McPherson[1], Normen Lochthofen[1], Janine Ludszuweit[1], Lennard Frommhold[1], Anabel von Jackowski[2]; Wilken-Jon von Appen[1], Sandra Tippenhauer[1], Anja Engel[2] (not on board)

[1]DE.AWI
[2]DE.GEOMAR

Grant-No. AWI_PS126_07

Objectives

The physical conditions which lead to enhanced primary and export production in the Arctic Ocean remain unclear. And with both, rapid increases in ocean temperatures amplified in the Arctic region and sea ice retreat of the past two decades, the connection between these physical changes and the effect on polar marine ecosystem only increases in importance.

The intermittent presence of sea ice and meltwater affects both the physical and biochemical vertical structure of the water column but also limits *in-situ* observations to summer months when the ice has retreated. The effects of changes in the environmental conditions on the polar marine biodiversity can only be detected through long-term observation of the species and processes. The FRAM multidisciplinary observatory attempts to improve the observations and understanding of the connection between marine biodiversity and environmental conditions using long-term observations of both physical oceanic properties and benthic and pelagic environments.

The HAUSGARTEN observatory includes CTD water sampling stations in the Atlantic-influenced West Spitsbergen Current towards the East of Fram Strait, in the Arctic-influenced East Greenland Current to the West, and in the transition regions in the central and northern parts of the region. The FRAM observatory include moored year-round observations for sensor data and sample collection in representative stations of those contrasting water masses. These observations span the whole water column with an emphasis on the upper euphotic zone.

The overall aim of the mooring recoveries and deployments was to characterize the variability, including seasonal cycles and mesoscale features, of physical properties, biogeochemical cycles, and biological processes in Fram Strait, the main gateway between the Arctic Ocean and the low-latitude seas. In particular, the moorings incorporate dedicated water samplers in conjunction with a physical and biogeochemical sensor package including CTD, pH and pCO_2 sensors, fluorometers, light sensors and nitrate sensors. The combination of these sensors and the water samplers, in combination with the deployment of two profiling winches facilitates the assessment of seasonal stratification and nutrient concentrations above and below the pycnocline. The nutrient drawdown enables an estimate of new production. Furthermore, the samples will be used for DNA sequencing to examine seasonal changes in bacterial community structure. The particle samplers collect and preserve filters for DNA extraction and sequencing that together with the fluorescence sensors allow us to track the progression of phytoplankton biomass and community composition over different seasons. These efforts give us a novel

year-round description of biological, chemical, and physical processes in the Fram Strait, leading to an improved understanding of long-term changes and of physical-biological coupling in the upper ocean in this region. In addition, regularly recorded CTD profiles enable a comparison to previous expeditions (available since the HAUSGARTEN observatory was established in 1999) to allow seasonal, annual and interannual changes in the water masses to be observed. The large range and combination of sensors that the moorings are equipped with (details below) enable these temporal changes to be related to the observed changes in physical, chemical and biological structures in Fram Strait.

Work at sea

CTD

Regular hydrographic measurements were conducted using a combined CTD and water sampling system (CTD/Rosette Water Sampler). A total of 29 CTD profiles were recorded at the standard LTER HAUSGARTEN stations (Fig. 9.1, Table 9.1). These included both full water column profiles and profiles in the upper 250 m to focus on the physical and biogeochemical processes in the upper water column. A SUNA which measured nitrate was also mounted to the frame of the CTD for depths < 2,000 m.

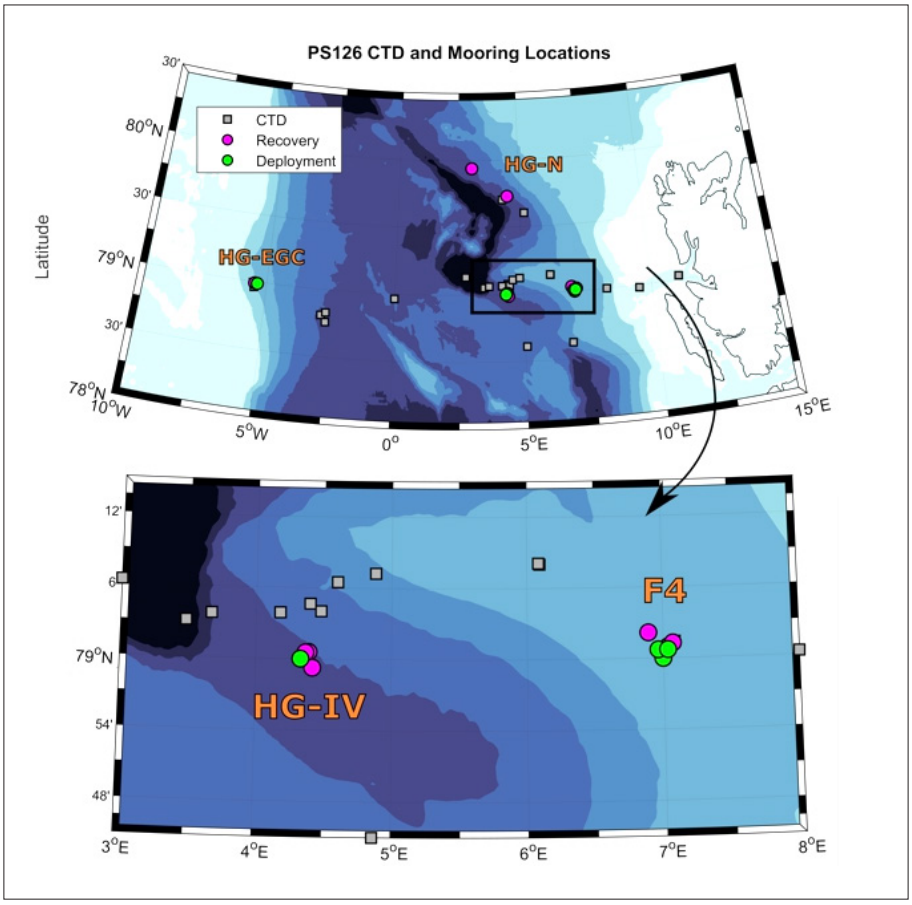

Fig. 9.1: (Top) Map of Fram Strait and HAUSGARTEN region with ship track (blue), CTD stations (grey), mooring recoveries (pink) and deployments (green) from PS126; (bottom) more detailed view of the central HAUSGARTEN stations; the name of each stationcluster is noted below with further details.

Tab. 9.1: List of CTD stations during PS126

The following cast types were performed: S = ”shallow”: cast only to 500 m; D = ”deep”: cast to ~10 m above the bottom; S - D = ”shallow-deep”: cast to a shallow depth for water collection which accompanied a D-cast; Chl *a* = cast to collect large volumes of additional water for biological experiments

Station	Date / Time	Latitude	Longitude	Station	Cast type	CTD depth	Water depth EK80	SUNA
PS126_1-5	20210530 / 11:53	78°37.313‘N	006°48.079‘E	Test	S	500	1774	Y
PS126_2-2	20210530 / 20:37	78°36.538‘N	005°03.921‘E	S3	D	2276	2338	N
PS126_2-11	20210530 / 14:14	78°36.561‘N	005°03.859‘E	S3	S-D	201	2339	Y
PS126_3-1	20210601 / 08:44	79°04.866‘N	004°22.171‘E	HG-IV	D	2221	2279	N
PS126_3-3	20210601 / 11:58	79°04.061‘N	004°10.669‘E	HG-IV	Chl *a*	50	2280	Y
PS126_3-13	20210602 / 05:08	79°03.868‘N	004°10.669‘E	HG-IV	S-D	201	2466	Y
PS126_4-1	20210602 / 19:58	79°06.486‘N	004°35.973‘E	HG-III	S	251	1906	Y
PS126_6-1	20210604 / 17:36	79°07.458‘N	004°52.986‘E	HG-II	S	200	1598	Y
PS126_8-1	20210605 / 10:50	79°08.014‘N	006°05.592‘E	HG-I	S-D	250	1277	Y
PS126_8-9	20210605 / 21:09	79°08.047‘N	006°04.975‘E	HG-I	D	1238	1279	Y
PS126_9-5	20210606 / 14:03	79°01.326‘N	007°04.748‘E	SV-IV	D	1262	1300	Y
PS126_11-1	20210607 / 18:32	78°59.997‘N	008°15.042‘E	SV-III	S	250	898	Y
PS126_12-5	20210608 / 00:16	78°58.812‘N	009°30.917‘E	SV-III	S	200	231	Y
PS126_13-3	20210608 / 04:55	79°01.887‘N	011°05.233‘E	SV-I	S	250	278	Y
PS126_17-2	20210609 / 16:56	79°36.246‘N	005°09.946‘E	N3	S	250	2787	Y
PS126_18-1	20210610 / 03:23	79°44.091‘N	004°28.829‘E	N4	S-D	200	2661	Y
PS126_18-7	20210610 / 10:38	79°42.454‘N	004°16.033‘E	N4	D	2853	2909	N
PS126_19-5	20210611 / 08:17	79°56.122‘N	003°01.929‘E	N5	S	500	2607	Y
PS126_20-2	20210613 / 10:39	79°49.015‘N	002°47.209‘W	EG-IV	D	2533	2592	N
PS126_20-6	20210613 / 19:09	78°45.568‘N	002°36.542‘W	EG-IV	Chl *a*	100	2639	Y
PS126_20-8	20210614 / 02:50	78°49.801‘N	002°37.420‘W	EG-IV	S-D	200	2619	Y
PS126_21-5	20210615 / 10:11	78°59.923‘N	005°30.700‘W	EG-I	D	903	937	Y
PS126_21-12	20210615 / 21:11	78°57.702‘N	005°28.166‘W	EG-I	S-D	200	928	Y
PS126_22-1	20210617 / 03:02	78°57.807’N	000°00.533’W	0°	S	500	2545	Y
PS126_23-1	20210617 / 09:57	79°07.923‘N	002°47.645‘E	HG-IX	S-D	500	5564	Y
PS126_23-8	20210617 / 21:01	79°07.967‘N	002°45.607‘E	HG-IX	D-D	5545	5516	N
PS126_24-1	20210618 / 09:57	79°03.111‘N	003°28.998‘E	HG-VII	S	500	4023	Y
PS126_25-1	20210618 / 18:35	79°03.755‘N	003°40.187‘E	HG-V	S	500	3113	Y
PS126_28-5	20210621 / 01:53	79°03.578‘N	003°35.801‘E	HG-VI	S	500	3382	Y

The CTD (Fig. 9.2) contained dual sensors for temperature, conductivity and oxygen, and one sensor for pressure. Additionally, the system was also equipped with a fluorometer for chlorophyll *a* fluorescence, a transmissiometer, and a downward looking altimeter (Table 9.2). Furthermore, a stand-alone, internally recording, battery-powered Underwater Vision Profiler (UVP, see Chapter 3) was initially also attached to the CTD/Rosette Water Sampler, but was removed later because the battery did not charge properly. The CTD/Rosette Water Samper configuration remained the same throughout the entire duration of the expedition. No major problems with any of the sensors were encountered. The behaviour of the temperature and salinity sensors was monitored by taking value differences between the primary and secondary sensors (secondary minus primary). In general, both temperature and conductivity sensor pairs performed well.

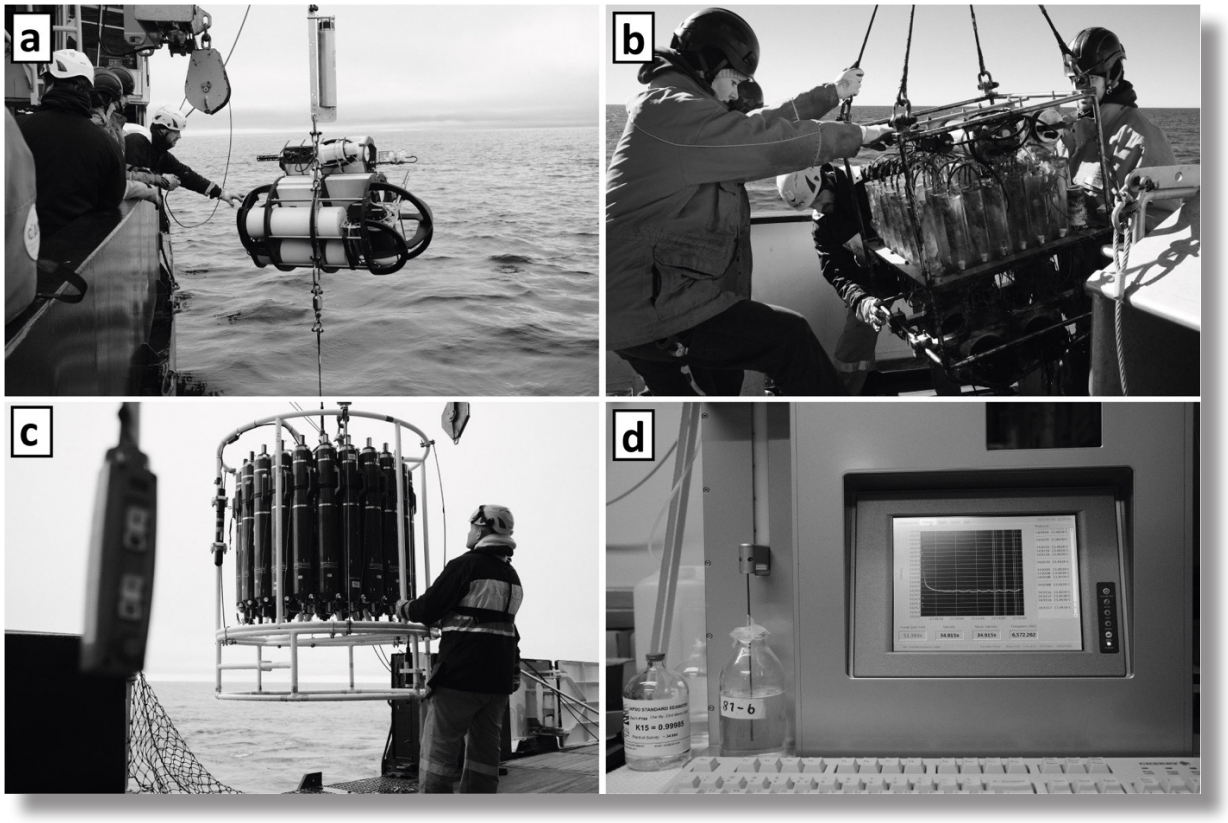

Fig. 9.2: Photographs showing (a) deployment of the winch at mooring F4-W3, (b) recovery of a RAS from one of the moorings, (c) deployment of the CTD, and (d) the salinometer.
used to measure the salinity of the water collected by the CTD. The salinometer was also needed to calibrate the instrument's conductivity sensors.

Tab. 9.2: CTD rosette configuration (remained unchanged during cruise)

Sensor	Instrument	Serial number	Calibration Date
Main datalogger incl. pressure	SBE911+	485	14 Nov. 2017
Primary temperature sensor	SBE3	2417	22 Nov. 2017
Primary conductivity sensor	SBE4	2054	14 Nov. 2017

Sensor	Instrument	Serial number	Calibration Date
Primary oxygen sensor	SBE43	743	17 Oct. 2020
Primary pump	SBE5	1954	–
Secondary temperature sensor	SBE3	2460	23 Nov. 2017
Secondary conductivity sensor	SBE4	2055	14 Nov. 2017
Secondary oxygen sensor	SBE43	48	06 Oct. 2020
Secondary pump	SBE5	8791	–
Chlorophyll fluorometer	WETLabs ECO-AFL/FL	1670	11 Dez. 2009
Transmissiometer	WETLabs C-Star	814	24 Oct. 2011
Altimeter	Benthos PSA916	1228	–
Water sampler	SBE32 Carousel (24 x 12 L)	657	–

The secondary oxygen sensor showed some moderate drift beyond 4,000 m during the deepest CTD cast (PS126_23-8, 5,545 m) but performed well at shallower depths. A drift in temperature with depth was also observed during the deep cast, where the temperature difference between the two sensors increased with depth. However, for all other casts, the difference between the sensors remained small (10^{-3}) and stable.

The sensors were mounted to a rosette water carousel with 24 bottles (12 litres each) for water sampling. There were no issues with any of the OTE (Ocean Test Equipment) bottles, all closed properly and on command, and no misfires occurred. The resulting water samples were mainly used for filtrations and chemical measurements.

The initial transmissiometer calibration according to the corresponding Seabird application note resulted in values slightly >100 %, which needs to be addressed during post-processing.

OPS (Optimare Precision Salinometer) measurements

In order to define the overall data quality (offset and the drift) of the conductivity sensors on the CTD, a total of 60 salinity samples were collected from CTD / Rosette Water Sampler bottles for analysis by means of an Optimare Precision Salinometer (SN007; Fig. 9.2).

Sample analysis was performed following the corresponding manual, and proceeded without any major complications. A mean (± standard deviation) difference of -0.0017 ± 0.0023 was determined between the salinity samples and the primary temperature-conductivity duct, while the mean difference was -0.0055 ± 0.0026 for the secondary temperature-conductivity duct (Table 9.3). The primary conductivity cell therefore seemed to be slightly more accurate and stable. Final data processing and quality control will be done at the Alfred Wegener Institute later on.

Tab. 9.3: Salinity samples overview with CTD casts, bottle numbers, OPS measurements, and differences between CTD sensor measurements and OPS measurements. Values highlighted in red are considered suspicious.

Station	Date	Bottle #	Pressure	Sal00	Sal11	OPS sal	Sal00-OPS	Sal11-OPS
1-5	20210530	13	172	34.967	34.9624	34.9671	-0.0001	-0.0047
1-5	20210530	13	172	34.967	34.9624	34.9671	-0.0001	-0.0047
1-5	20210530	1	507	35.0124	35.0075	35.0125	-0.0001	-0.005
1-5	20210530	1	507	35.0124	35.0075	35.0122	0.0002	-0.0047
2-2	20210530	3	2286	34.9241	34.9196	34.9254	-0.0013	-0.0058
2-2	20210530	3	2286	34.9241	34.9196	34.9254	-0.0013	-0.0058
2-2	20210530	5	2031	34.9141	34.9098	34.9156	-0.0015	-0.0058
2-2	20210530	5	2031	34.9141	34.9098	34.9157	-0.0016	-0.0059
2-2	20210530	10	1318	34.91	34.9065	34.9126	-0.0026	-0.0061
2-2	20210530	10	1318	34.91	34.9065	lost		
3-1	20210601	2	2258	34.9199	34.9158	34.922	-0.0021	-0.0062
3-1	20210601	2	2258	34.9199	34.9158	34.9208	-0.0009	-0.005
3-1	20210601	6	2032	34.9128	34.9089	34.9158	-0.003	-0.0069
3-1	20210601	6	2032	34.9128	34.9089	34.917	-0.0042	-0.0081
3-1	20210601	10	1318	34.9125	34.9093	34.9154	-0.0029	-0.0061
3-1	20210601	10	1318	34.9125	34.9093	34.9163	-0.0038	-0.007
8-9	20210605	1	1255	34.909	34.9076	34.9138	-0.0048	-0.0062
8-9	20210605	1	1255	34.909	34.9076	34.9139	-0.0049	-0.0063
8-9	20210605	7	1013	34.9097	34.9085	34.9133	-0.0036	-0.0048
8-9	20210605	7	1013	34.9097	34.9085	34.9133	-0.0036	-0.0048
9-5	20210606	1	1280	34.9108	34.9073	34.9137	-0.0029	-0.0064
9-5	20210606	1	1280	34.9108	34.9073	34.9137	-0.0029	-0.0064
9-5	20210606	2	861	34.9102	34.9073	34.9136	-0.0034	-0.0063
9-5	20210606	2	861	34.9102	34.9073	34.914	-0.0038	-0.0067
18-7	20210610	1	2903	34.9271	34.9223	34.9269	0.0002	-0.0046
18-7	20210610	1	2903	34.9271	34.9223	34.9274	-0.0003	-0.0051
18-7	20210610	3	2286	34.9197	34.9161	34.9217	-0.002	-0.0056
18-7	20210610	3	2286	34.9197	34.9161	34.9222	-0.0025	-0.0061
18-7	20210610	10	1322	34.9129	34.9098	34.915	-0.0021	-0.0052
18-7	20210610	10	1322	34.9129	34.9098	34.9155	-0.0026	-0.0057
18-7	20210610	18	507	34.9179	34.9157	34.9206	-0.0027	-0.0049
18-7	20210610	18	507	34.9179	34.9157	34.9207	-0.0028	-0.005
20-2	20210613	5	2041	34.914	34.9102	34.9156	-0.0016	-0.0054
20-2	20210613	5	2041	34.914	34.9102	34.9153	-0.0013	-0.0051
20-2	20210613	12	1019	34.902	34.8995	34.9042	-0.0022	-0.0047
20-2	20210613	12	1019	34.902	34.8995	34.9046	-0.0026	-0.0051
20-2	20210613	15	506	34.9266	34.9196	34.9282	-0.0016	-0.0086
20-2	20210613	15	506	34.9266	34.9196	34.9292	-0.0026	-0.0096

Station	Date	Bottle #	Pressure	Sal00	Sal11	OPS sal	Sal00-OPS	Sal11-OPS
20-2	20210613	18	254	34.9423	34.9406	34.9468	-0.0045	-0.0062
20-2	20210613	18	254	34.9423	34.9406	34.9464	-0.0041	-0.0058
21-2	20210615	1	912	34.8833	34.88	34.8848	-0.0015	-0.0048
21-2	20210615	1	912	34.8833	34.88	34.885	-0.0017	-0.005
21-2	20210615	4	760	34.8707	34.8678	34.8723	-0.0016	-0.0045
21-2	20210615	4	760	34.8707	34.8678	34.8725	-0.0018	-0.0047
21-2	20210615	9	405	34.9404	34.9384	34.9413	-0.0009	-0.0029
21-2	20210615	9	405	34.9404	34.9384	34.9409	-0.0005	-0.0025
22-1	20210617	2	202	34.961	34.9532	34.9539	0.0071	-0.0007
22-1	20210617	2	202	34.961	34.9532	34.9545	0.0065	-0.0013
22-1	20210617	10	50	34.1481	34.1367	34.1537	-0.0056	-0.017
22-1	20210617	10	50	34.1481	34.1367	34.1532	-0.0051	-0.0165
23-1	20210617	1	506	34.9558	34.9531	34.9578	-0.002	-0.0047
23-1	20210617	1	506	34.9558	34.9531	34.9578	-0.002	-0.0047
23-1	20210617	3	203	34.9768	34.9752	34.9772	-0.0004	-0.002
23-1	20210617	3	203	34.9768	34.9752	34.9772	-0.0004	-0.002
23-8	20210617	3	5115	34.9273	34.9213	34.925	0.0023	-0.0037
23-8	20210617	3	5115	34.9273	34.9213	34.9252	0.0021	-0.0039
23-8	20210617	6	2031	34.9159	34.9126	34.9161	-0.0002	-0.0035
23-8	20210617	6	2031	34.9159	34.9126	34.9162	-0.0003	-0.0036
23-8	20210617	9	1015	34.9052	34.9032	34.9071	-0.0019	-0.0039
23-8	20210617	9	1015	34.9052	34.9032	34.9069	-0.0017	-0.0037
						mean	-0.0017	-0.0055
						std dev	0.0023	0.0026

Winkler titration for oxygen

Oxygen concentrations were determined by iodometric titration according to the Winkler method (Grasshoff et al. 1999). The Winkler method is based on the premise that the oxidation of iodide to iodine does not directly occur in seawater and can be performed in a series of oxidation reactions to colourimetrically determine dissolved oxygen.

Dissolved oxygen was the second parameter (after salinity) sampled from the CTD (see also Chapter 3 for more parameters). Seawater was slowly filled into a calibrated glass bottle without turbulences or bubbles. Then 1 mL of manganese chloride ($Mn(II)Cl_2$) and 1 mL of alkaline iodide (KOH) solution were dispensed into the glass bottle. The glass bottle was sealed without trapping air bubbles and then vigorously shaken for 30 seconds. The resultant iodine precipitate was stored in the dark at 4° C until further processing.

After storage, a magnetic stirrer and 1 ml of sulphuric acid were added to the glass bottle. Then the magnetic plate was switched on to stir up the precipitate until the iodine was fully dissolved. After that, the iodine was titrated with a 0.02 M sodium thiosulphate solution and 1 mL of starch solution until the sample turned colourless. The factor from the calibrated bottle and the volume of sodium thiosulphate were used to calculate the final concentration of oxygen in the given depth. Table 9.4 gives an overview of the stations where such measurements were taken.

Tab. 9.4: Station list of Winkler titrations for dissolved oxygen.

Station ID	Shallow CTDs	Deep CTDs
HG-I		x
HG-II	x	
HG-V	x	
HG-VI	x	
HG-IX	x	
N4		x
N5	x	
EG-I	x	
EG-IV	x	x
SV-I	x	
SV-IV	x	
0°	x	
Test station		x

In addition to the regularly performed oxygen titrations, extra water samples for oxygen were taken from CTD bottles at selected calibration stops (see below) for recovered mooring instrumentation (Table 9.5). The results from the calibration stops suggest that there is a generally moderate discrepancy (~0.3 ml/l) between sensor measurements and titration data for most stops, with a much higher discrepancy for the N4 samples (up to 1 ml/l). However, a more detailed analysis incorporating the entire oxygen titration and CTD datasets is necessary in order to assess what kind of correction has to be applied to the sensors.

Tab. 9.5: Results of extra oxygen titrations for calibration casts

Station	Date	CTD Cast	Depth [m]	Niskin Bottle	Mean (µmol/L)	SD	O2 (mL/L)
HG-I	05.06.2021	PS126_08-09	1000	7	306.97	0.71	6.87
HG-I	05.06.2021	PS126_08-09	1238	3	303.84	0.81	6.8
N4	10.06.2021	PS126_18-07	500	18	351.35	0.58	7.87
N4	10.06.2021	PS126_18-07	1300	10	338.85	0.26	7.59
N4	10.06.2021	PS126_18-07	2250	3	333.40	0.79	7.47
EG-IV	13.06.2021	PS126_20-02	1000	12	304.99	1.4	6.83
EG-IV	13.06.2021	PS126_20-02	2000	5	305.14	0.53	6.83

Underway measurements

During PS126, standard oceanographic underway measurements by means of a thermo-salinograph (TSG) with a double sensor configuration, as well as a vessel-mounted ADCP, were continuously recorded. The TSG data were validated using water samples taken from the keel water inlet, which were later analysed using the OPS lab salinometer.

Mooring deployments

A total of five moorings were redeployed (Table 9.6) with minor modifications in the placement of sensors compared to PS121, particularly in the upper 50 m to better resolve the physical and biological structure of the upper water column. Details of each mooring and the setup are documented in the mooring diagrams below (Fig. 9.3).

Tab. 9.6: List of moorings recovered and deployed during PS126

Name	Longitude		Latitude		Depth	Top	Deployment time					Station
	Degrees	Minutes	Degrees	Minutes	Meters	Meters	Year	Month	Day	Hour	Minute	
Recoveries												
F4-19	6	59.98‘E	78	59.98‘N	1212	53	2019	8	22	7	49	PS121_13-1
F4-S-4	6	57.81‘E	79	00.71‘N	1222	16	2019	8	22	10	36	PS121_13-2
F4-W-2	7	02.14‘E	79	00.70‘N	1236	125	2019	8	22	13	19	PS121_13-3
HG-IV-W-2	4	23.97‘E	79	01.37‘N	2473	25	2019	8	26	7	41	PS121_26-1
HG-IV-S-4	4	15.75‘E	79	01.34‘N	2539	18	2019	8	26	10	21	PS121_26-2
HG-IV-FEVI-40	4	19.92‘E	79	00.00‘N	2542	64	2019	8	26	14	28	PS121_26-3
HG-EGC-6	5	23.78‘W	78	59.75‘N	996	47	2019	8	29	10	56	PS121_31-1
HG-N-S-1	3	07.19‘E	79	56.64‘N	2500	14	2019	9	6	14	7	PS121_44-1
HG-N-FEVI-39	4	30.36‘E	79	44.35‘N	2657	57	2019	9	7	10	28	PS121_46-3
Deployments												
F4-20	6	59.967‘E	79	59.974‘N	1241	51	2021	6	8	15	3	PS126_14-1
F4-S-5	6	57.81‘E	79	0.709‘N	1260	17	2021	6	8	17	29	PS126_14-2
F4-W-3	7	02.05‘E	79	0.71‘N	1241	115	2021	6	8	19	37	PS126_14-3
HG-IV-FEVI-42	4	19.89‘E	78	59.979‘N	2556	56	2021	6	3	11	21	PS126_3-23
HG-EGC-7	5	21.588‘W	78	59.276N	1041	34	2021	6	16	9	10	PS126_21-17

The conditions for mooring deployments were favourable with a generally calm sea state and low sea ice coverage in the central and eastern sites (Fig. 9.1). Towards the West for the deployment of EGC-7, the sea ice was thicker and more prevalent and the deployment was delayed for one hour, waiting for the wind to move a field of large ice floes away from the deployment location where a lead developed. This worked well though the dense and dynamic ice field did add a time pressure to the deployment.

All 5 of the moorings were deployed successfully, though a number of incidents should be noted. While deploying EGC-7 on 16 June 2021, the rope at ~600 m (total depth 997 m) snapped and the bottom part of the mooring (4 floats, one Seaguard, the two acoustic releases

and the anchor) was lost overboard. It appears that the splice failed and became disconnected from the eye and shackle. The acoustic releasers were manually triggered and the bottom 460 m of EGC-7 recovered. The mooring was then reassembled with a second anchor, the acoustic releasers were reset and EGC-7 was redeployed successfully. Two more rope segments had to be replaced upon deployment due to damage (moorings FEVI-42 and F4-20), but these were spotted before they went over the capstan.

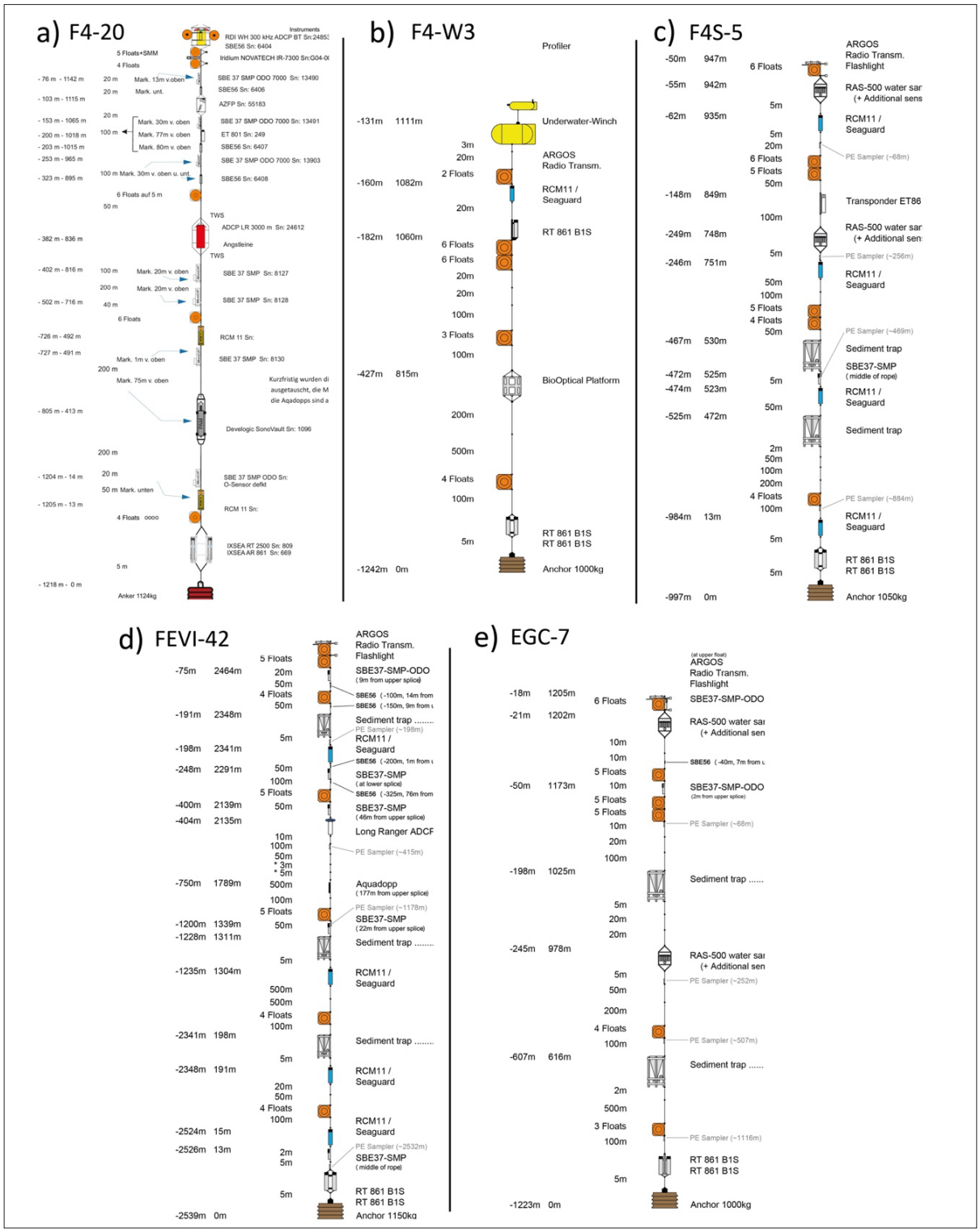

Fig. 9.3: Moorings deployed during PS126

Mooring recoveries

During expedition PS121 in summer 2019, nine moorings were deployed in the HAUSGARTEN area. During PS126, all of those moorings were successfully recovered without any major complications or losses (Table 9.6, Fig. 9.4). A total of 104 sensors were retrieved, while only two were lost (see results section below for details). The recoveries of the moorings to the north and east were a little more challenging due to the prevalent ice conditions. The sea state for the eastern mooring (outside of the ice) was generally very calm.

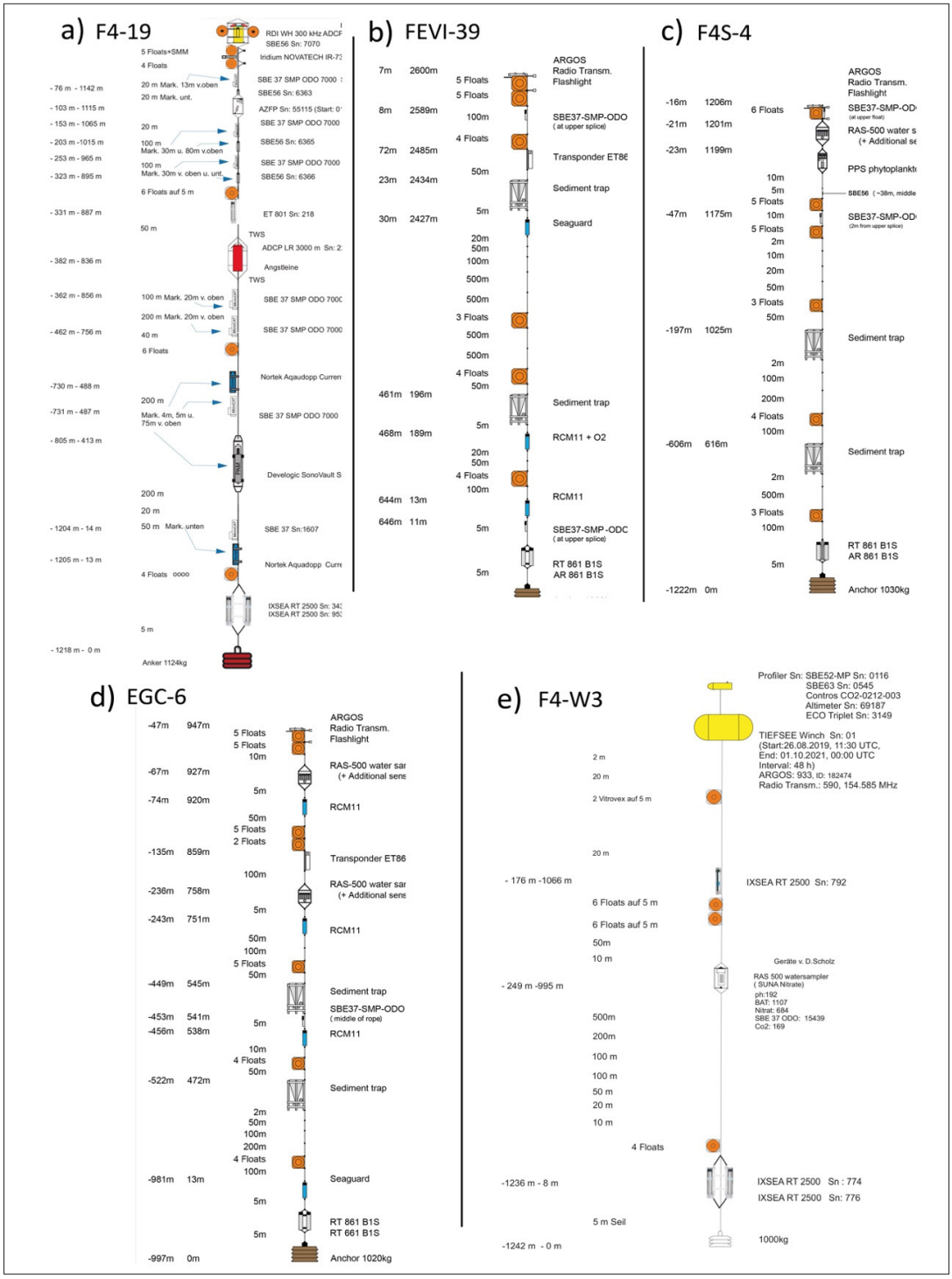

Fig. 9.4: Moorings recovered during PS126 (Part I)

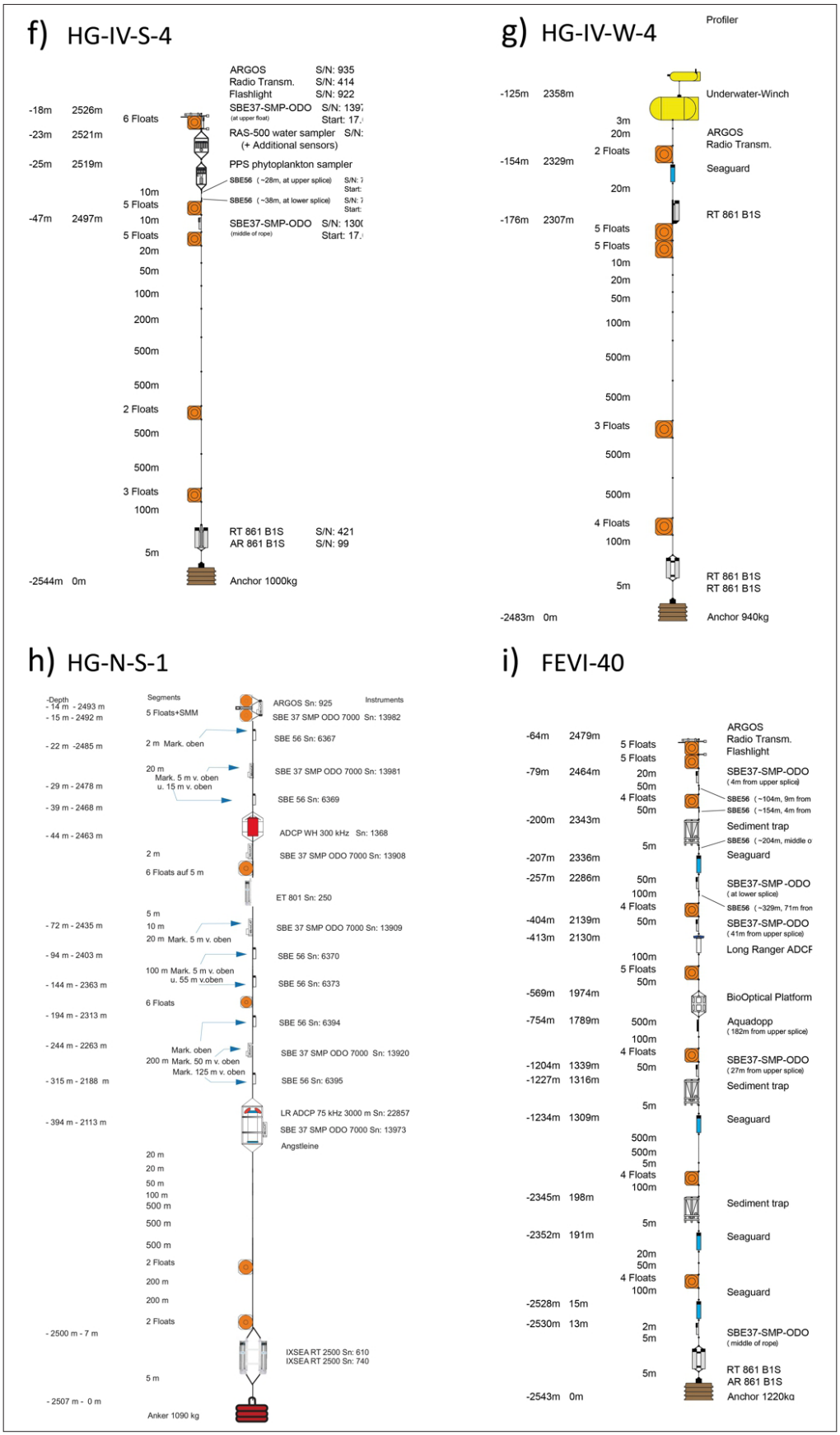

Fig. 9.4: Moorings recovered during PS126 (Part II)

Calibration Casts

After each mooring recovery and after the data had been downloaded from the instruments, the SBE37s and SBE56s were attached to the CTD for calibration. In total, four calibration casts were conducted, with further details in Table 9.7. Each instrument can be compared to the CTD measurements (pressure, temperature, salinity and oxygen) to determine the accuracy and drift of each sensor over the course of the two-year deployment. During the upcast, the CTD was paused between one to three depths in well-mixed layers of water below 1,000 m for up to 20 minutes to allow a direct comparison between sensors. The potentially drifted value can then be considered during post-processing and when analysing the data from the moorings, generally using a linear fit over the whole time series.

Tab. 9.7: Details of calibration casts for SBE37 and SBE56 sensors on recovered moorings

Date of CTD	Station Number	Mooring	Stops
06.06.2021	PS126_8-9	HG-IV-S-4 and FEVI-40	2
10.10.2021	PS126_18-7	F4-19 and F4-S4	3
13.06.2021	PS126_20-2	HG-N-S-1	2
18.06.2021	PS126_24-1	F4-W2 and HG-EGC-6	1

Preliminary (expected) results

CTD

A section of CTD profiles from across the Fram Strait, from the East Greenland continental shelf edge to Svalbard, confirmed the expected distribution of water masses (Fig. 9.5). The warm (>3° C) and saline water of the West Spitsbergen Current can be observed from the surface to below 400 m along the Eastern shelf, with maximum temperatures >4° C. Towards the West and East Greenland, this warm Atlantic water is subducted below cold and fresh Polar Water (<0° C), forming the East Greenland Current. Oxygen and Fluorescence tend to peak in the upper 50 m, with particularly high values in the central Fram Strait region, between 0° to 6° E. Below 50 m, both decrease and tend towards a constant value.

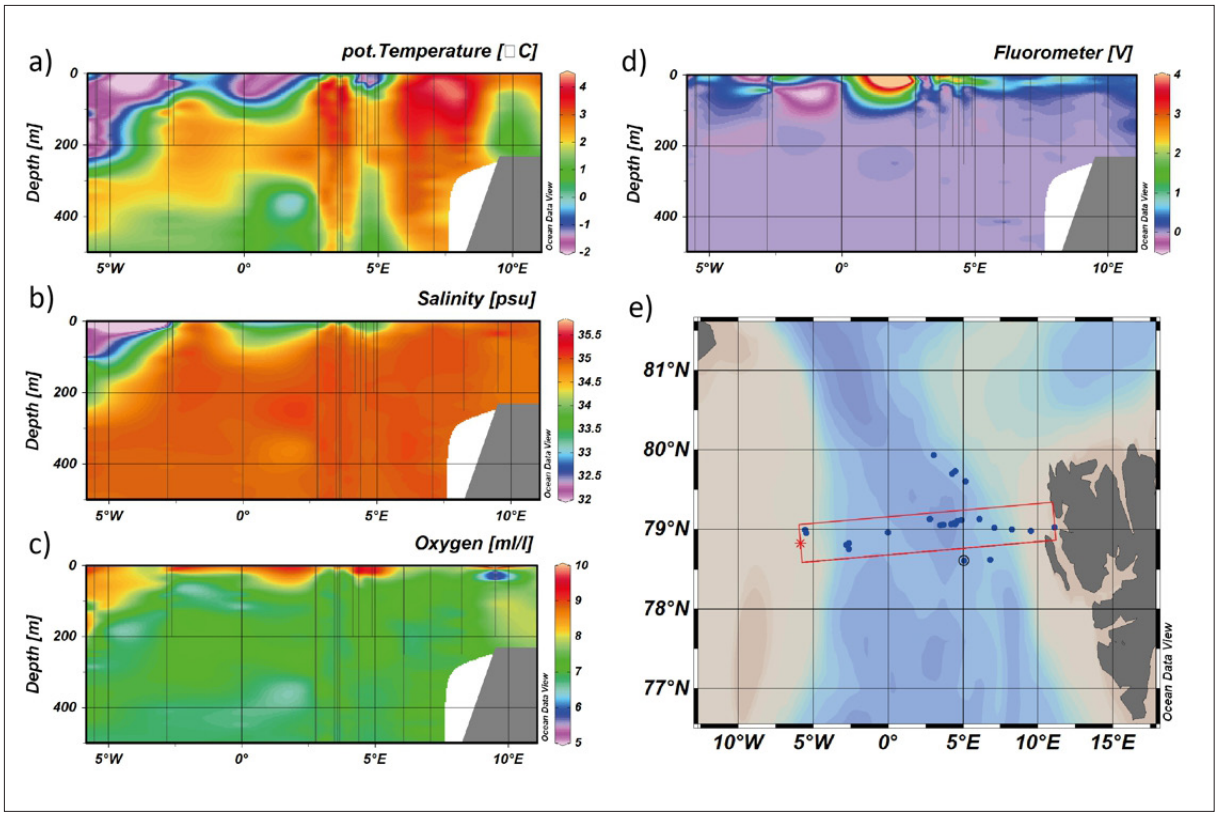

Fig. 9.5: Preliminary results of a) potential temperature, b) practical salinity, c) oxygen, and d) Chl a fluorescence obtained from CTD casts inside of the red box in e) across Fram Strait

Calibration casts

One segment from each of the calibration casts is presented in Figure 9.6, giving an overview of the accuracy of each instrument. Generally, there was a good agreement between the CTD and the recovered instruments, particularly in pressure and temperature, with variability of less than 5 m and 0.05° C respectively. There was a good agreement despite of the greater variability between salinity and oxygen measurements, with the moored instruments generally overestimating oxygen when compared to the CTD sensors (see also next section). A number of instruments recorded salinity and oxygen values that were significantly different to the CTD and other instruments on the same cast, and care needs to be taken when post-processing the data.

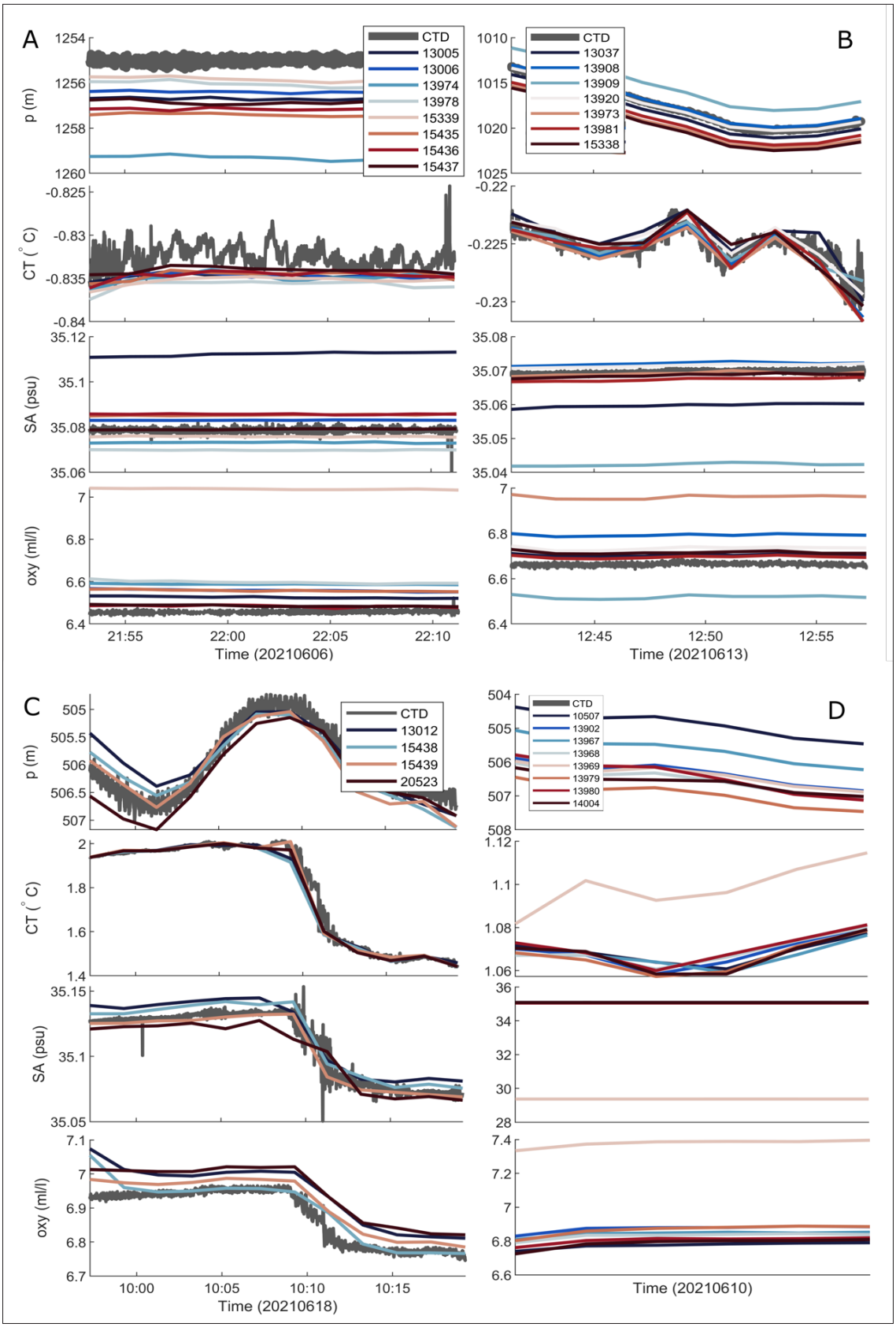

Fig. 9.6: Results of calibration casts for all SBE37s recovered from all moorings compared to the CTD (grey); during the CTD upcast at a certain depth the series corresponds to a 10 – 15 minutes pause each time.

Oxygen Titration

Preliminary results for the general dissolved oxygen concentrations based on Winkler titrations are shown in Figure 9.7.

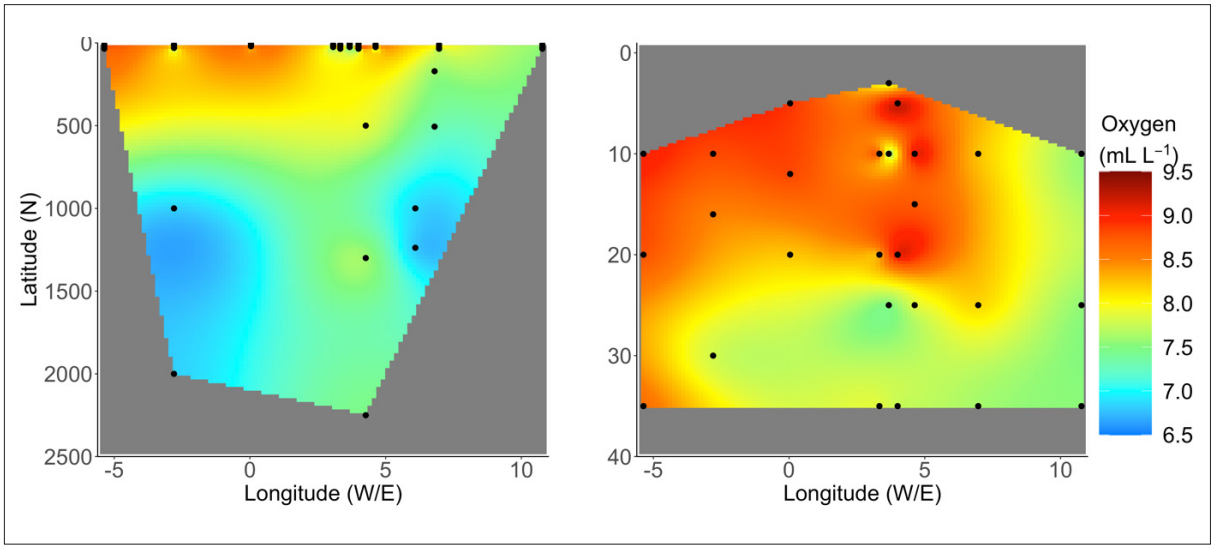

Fig. 9.7: Oxygen concentration throughout the water column (left) and in the upper 40 m (right) of a west-east transect through Fram Strait

Moorings

The top float and attached SBE37 (SN 13982) from HG-N-S-1 were lost a few months after deployment, presumably pulled upon by a large ridge keel or iceberg, or damaged by strong wave action. The rest of the instrumentation was retrieved with no damage. However, the lack of the top float meant that upper 50 m of line, including one SBE37, two SBE56s and the 300 kHz ADCP (SN 1368) was not held taught and fell below the second floats at 50 m. This was particularly unfortunate for the ADCP, whose data could not be used after the top float was lost. The other instruments on this line may still have delivered useful data, but they were not at their intended depths. One SBE56 attached at 194 m (SN 6394) was also lost due to a failure of the plastic attachment.

For the recovered sensors, a preliminary look at the data suggests that they are generally functioning as planned, with some exceptions for individual parameters especially towards the end of the 2-year measurement period. In particular, none of the RCM 11 current meters recorded a complete data set. Instead, data collection stopped between September 2020 and February 2021 for reasons still unknown.

Neither of the winches on HG-IV-W4 or F4-W-2 worked over the planned 2-year deployment period. The profiler on F4-W-2 was lost and the data could not be downloaded from the main controller due to a corrupt SD card, which needs to be sent in for data recovery. The winch on HG-IV-W4 only delivered useful profiling data during the first 2 months, albeit at a higher frequency than originally planned.

The upwards-facing 300 kHz ADCP at 53 m on F4-19 stopped recording after 3 months. The reason for this remains unclear, but most probably it was a battery failure.

Exemplary results from most physical oceanography sensors and selected bio-optical sensors collected by the mooring cluster at HG-IV are illustrated in Figure 9.8. The time series highlights the seasonality of seawater characteristics with very warm surface water in summer, as well as the development and decay of algal blooms in spring and summer.

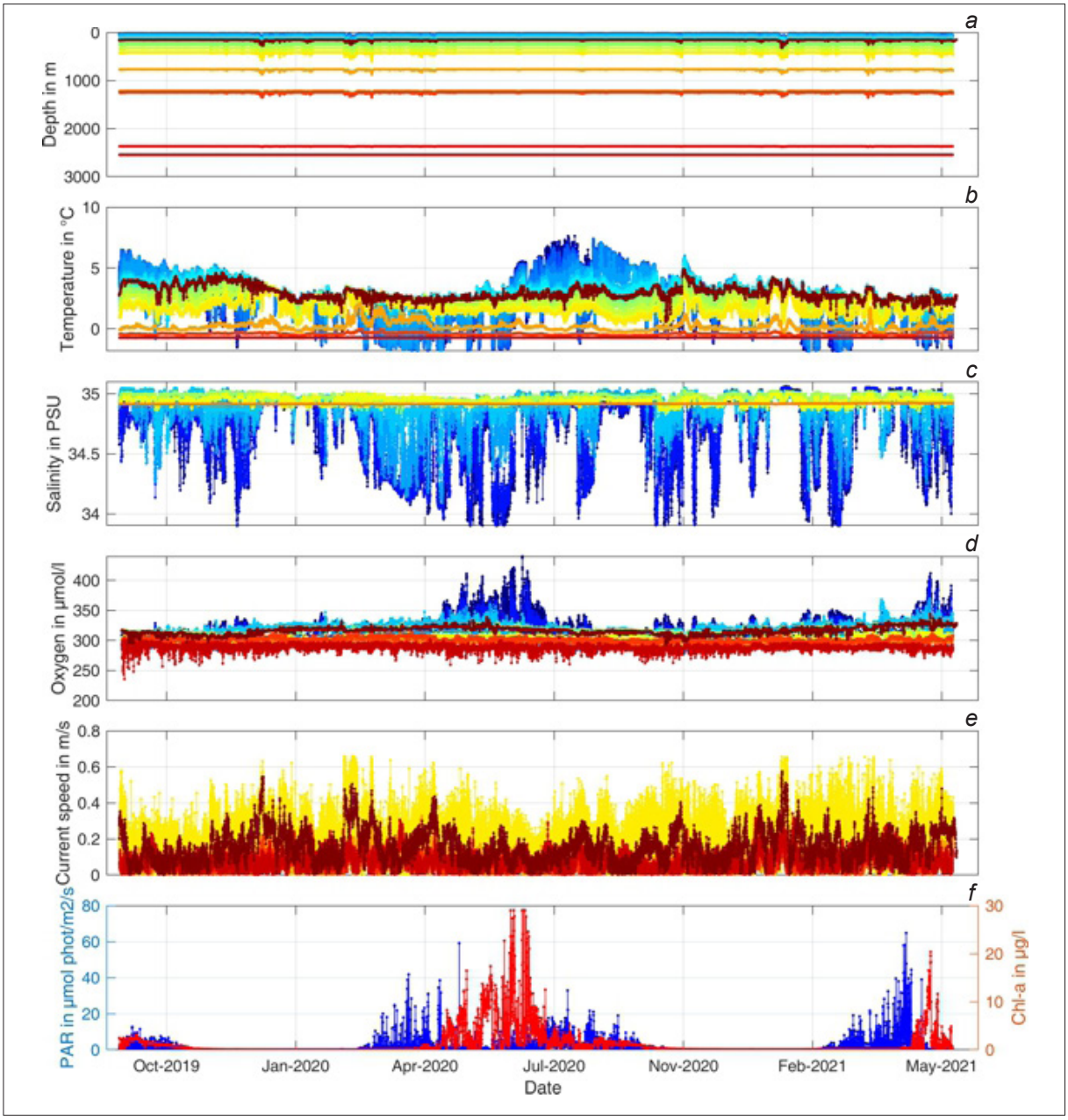

Fig. 9.8: Exemplary physical (a – e) and bio-optical data (f) obtained from the mooring cluster at the central HAUSGARTEN site HG-IV

Data management

Upon return to shore, the raw data collected on PS126 (CTD, moorings, TSG, VMADCP) will be archived, published and disseminated according to international standards by the World Data Center PANGAEA Data Publisher for Earth & Environmental Science (https://www.pangaea.de). The processed and quality-controlled CTD dataset will be finalized and archived

in PANGAEA within one year after the expedition. The physical measurements of the moorings (temperature, salinity, velocity) will also be processed and published within a year, followed by the biogeochemical data shortly after.

In all publications, based on this cruise, the Grant No. AWI_PS126_07 will be quoted and the following Polarstern article will be cited: Alfred-Wegener-Institut Helmholtz-Zentrum für Polar- und Meeresforschung. (2017). Polar Research and Supply Vessel POLARSTERN Operated by the Alfred-Wegener-Institute. Journal of large-scale research facilities, 3, A119. http://dx.doi.org/10.17815/jlsrf-3-163.

References

Grashoff K, Kremling K, Ehrhard M (1999) Methods of Seawater Analysis. 3d, Completely Revised and Extended Edition (WILEY-VCH, Weinheim).

10. FRAM POLLUTION OBSERVATORY – MONITORING LITTER AND MICROPLASTIC AT HAUSGARTEN

Melanie Bergmann[1], Autun Purser[1], [1]DE.AWI
Deonie Allen[2]; Ulrich Hoge[1] (not on board) [2]UK.USTRAT

Grant-No. AWI_PS126_08

Outline and Objectives

Marine litter or marine debris has long been on the political and public agenda as it has been recognized as a rising pollution problem affecting all oceans and coastal areas of the world and more than 1,300 species (Bergmann et al. 2017a). Over time, larger plastic litter items fragment into smaller particles termed 'microplastics' (<5 mm), which have recently received increasing attention (Ryan 2015) as they can be taken up more easily by a wider range of biota and humans.

Previous analysis of seafloor photographs taken for the epibenthic megafauna time series at three stations of the HAUSGARTEN observatory (Fig. 10.1) indicate that litter rose almost 30-fold between 2004 and 2017 at the northernmost station and reached densities similar to those reported from a canyon near the Portuguese capital Lisbon (Parga Martínez et al. 2020). This increase has prompted research on litter and microplastic pollution in different ecosystem compartments and repeated sampling campaigns to observe temporal trends.

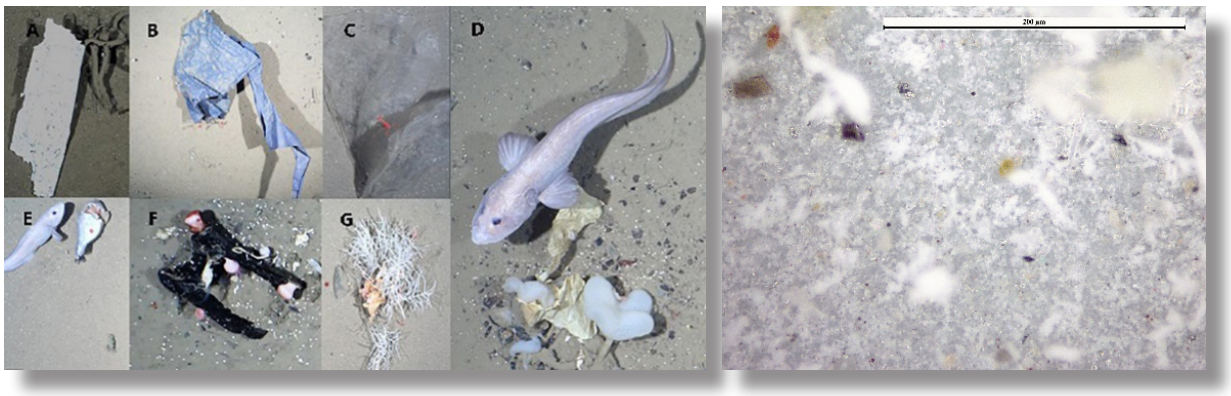

Fig. 10.1: Examples of marine litter and faunal interactions photographed by OFOS at HAUSGARTEN observatory (from Parga-Martinez et al. 2020) and atmospheric microplastics (from Allen et al. 2019)

This research is embedded in FRAM infrastructure under the header FRAM Pollution Observatory and has highlighted that Arctic sea ice, sea surface, water column and deep-sea sediments harbour high levels of microplastic pollution, especially the seafloor, with up to ~13,000 microplastic particles per kg sediment at the northernmost station (Bergmann et al. 2017b; Peeken et al. 2018; Tekman et al. 2020). Plastic has also invaded the Arctic food web (Trevail et al. 2015; Kühn et al. 2018) including sea ice-associated zooplankton (Amélineau et al. 2016). Significant quantities of microplastic in Arctic snow samples indicate that atmospheric

transport plays an important role (Bergmann et al. 2019). Recent data even suggest that the sea surface acts as a source of airborne microplastic (Allen et al. 2020). Still, on the whole, the role and processes of atmospheric transport of microplastics have not yet received the merited scientific attention although they are considered to play a key role (Zhang et al. 2020).

Work at sea

Litter and microplastic pollution on the seafloor

Five surveys (S3, HG-IV, N3, HG-I, EG-IV) were undertaken with the Ocean Floor Observation Bathymetry system to continue the megafauna time series (see Chapter 3, Table 3.2). In addition, sediment samples (top 5 cm) were taken from multiple corer deployments and frozen for assessments of microplastic concentrations (EG-IV, HG-I, HG-IV, N5, N3, S3, SV-I).

Quantification of airborne microplastic

The air sampling activities commenced as *Polarstern* left the harbour of Bremerhaven. The microplastic (MP) scientists efficiently build up and implemented the sampling equipment so that the first sample included the harbour and land air from Bremerhaven out into the open ocean. Sampling continued uninterrupted throughout the expedition until *Polarstern* returned to Bremerhaven, providing a full mainland-passage-Arctic-passage-mainland dataset. This allows an effective comparison of atmospheric MP concentrations in the Arctic with air concentrations in the passage / North Sea and concentrations on the mainland coast.

The sampling equipment was set up in the “crow’s nest”, 29 m above sea level (Fig. 10.2). This is the ideal elevated position away from ship’s operating activities that could potentially contaminate the samples and a position that provided the most direct and open access to air from the marine environment that had not been influenced by the ship. Samples were collected daily and comprised atmospheric deposition and air concentration samples from the air mass the ship had navigated through over in the previous 24 hours. These samples were collected on filters and transported to the microplastic laboratory on the mainland for analysis using µ-Raman spectroscopy.

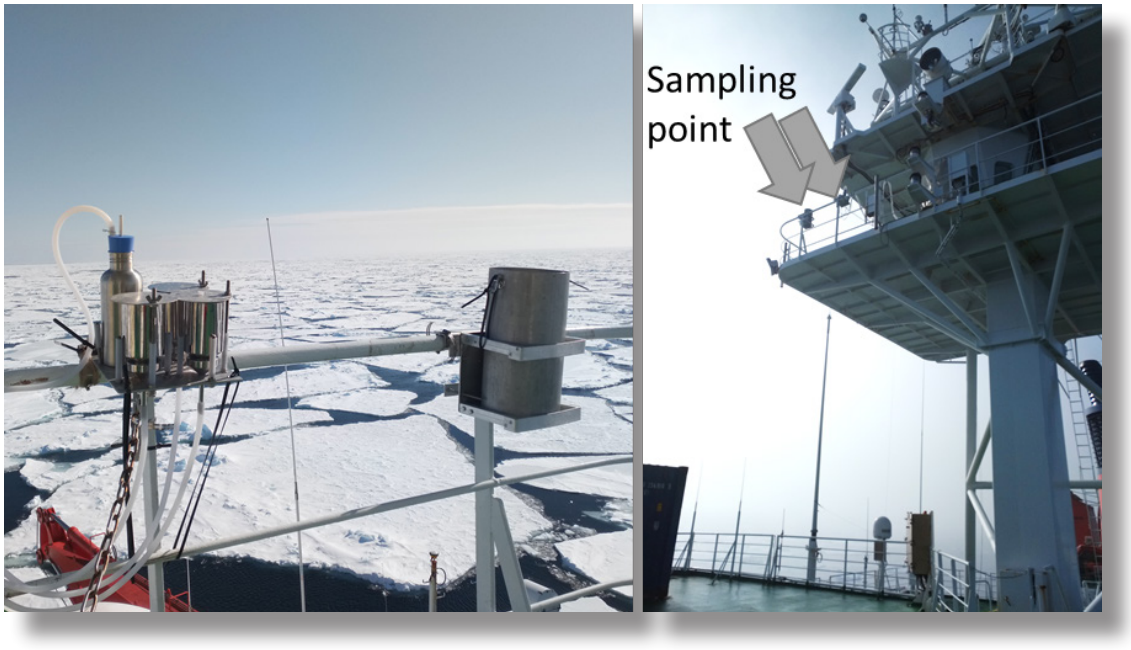

Fig. 10.2: Atmospheric sampling position on the Polarstern

Complementary weather data were provided by the Deutsche Wetterdienst for the entire expedition. This includes 10-minute recordings of true and relative wind velocity, daily and modelled air mass ceiling (planetary boundary layer and inversion level) and direction alongside the ship's course and heading. This enables the calculation of periods of sampling of air reaching the samples from the forward part of the ship (i.e. uncontaminated by ship or stack activities due to wind direction and strength). The majority of the samples show negligible potential for ship or stack contamination due to the elevation of the sampling platform, the wind direction and strength, and the course or heading of the ship. Station work in the HAUSGARTEN area was generally carried out by ship downwind.

Assessments of microplastics in sea water, snow and ice

In conjunction with the continuous air sampling, seawater, snow, melt pond and ice samples were collected during 10 helicopter-based visits to nearby ice floes and icebergs (Fig. 10.3, Table 10.1). These activities were undertaken to quantify and characterise the MP deposited in the Arctic marine environment via snow deposition, MP in the meltwater entering the marine environment, and MP concentrations in the seawater surface. Seawater and snow samples were taken with 2-L stainless steel Ecotanka containers from outside the zone of potential ship contamination via zodiac in open water or from the edge of visited ice floes (Table 10.1). In total, 16 separate 4-L surface seawater samples (including location-specific blank samples) were collected, which enable comparison to the atmospheric MP samples. Eleven ice cores were taken at eight stations with a 9 cm diameter corer (Kovacs Enterprise, Roseburg, USA) and transferred to plastic bags (LDPE polyethylene tube films by Rische and Herfurth). Upon return to the ship, the ice cores were stored at –20° C. The snow, seawater and melt pond samples were vacuum pumped onto sterilised Whatman quartz fibre filters (WHA1851047, 2.2 µm pore size) for MP analysis in the mainland laboratory.

Fig. 10.3: Ice, snow and melt pond sampling on the Arctic ice floes in the HAUSGARTEN area; trajectory of one of the sampled ice floes suggesting its origin off Severnaja Zemlya (source: T. Krumpen, AWI)

Assessment of microplastics in mesopelagic Arctic food webs

Although evidence suggest that microplastic is prevalent in Arctic ecosystems, we scarcely know to what extent it infiltrates food webs. To fill this gap, a Bongo net was used at HAUSGARTEN stations HG-IV and HG-VI (PS126-08-4, PS126-28-4; 0 to ~500 m water depth) to sample mesopelagic zooplankton species that form an integral part of the Arctic food web. Specimens

of the most abundant mesopelagic organisms present in the samples (Table 10.1) other than previously studied calanoid copepods were thoroughly rinsed individually with Milli-Q water, transferred into pre-rinsed glass vials and stored at –20° C for further analysis.

Tab. 10.1: List of deployments and samples taken for microplastic and litter assessments

Gear and / or platform	Date	Position (dec)	Matrix and samples collected
Ice Floe 1 (Helicopter)	01.06.2021	79.0076667 004.3801667	snow (4 samples) melt pond (2 L)
Ice Floe 2 (Helicopter)	04.06.2021	79.0190500 004.4106167	snow (4 samples) melt pond (2 L) ice core (2 cores) seawater (4 L)
Ice Floe 3 (Helicopter)	05.06.2021	79.1930167 005.1965667	snow (4 samples) melt pond (2 L) ice core (2 cores)
Ice Floe 4 (Helicopter)	09.06.2021	79.4235000 004.7899167	snow (4 samples) melt pond (2 L) seawater (4 L)
Ice Floe 5 (Helicopter)	10.06.2021	79.7203333 004.3232333	snow (4 samples) melt pond (2 L) ice core (1 core) seawater (4 L)
Ice Floe 6 (Helicopter)	12.06.2021	80.1910000 003.0619500	snow (4 samples) melt pond (2 L) 2 ice cores seawater (4 L)
Ice Floe 7 (Helicopter)	13.06.2021	78.9019444 -003.1566667	snow (4 samples) melt pond (2 L) ice core (1 core) seawater (4 L) *Melosira*
Ice Floe 8 (Iceberg) (Helicopter)	14.06.2021	78.5943333 -003.5486667	snow (4 samples) ice core (1 core) seawater (4 L) *Melosira*
Ice Floe 9 (Helicopter)	15.06.2021	79.0240000 -005.7083333	snow (4 samples) melt pond (2 L) ice core (1 core) seawater (4 L) *Melosira*
Ice Floe 10 (Iceberg) (Helicopter)	18.06.2021	79.04222222 002.97250000	snow (4 samples) melt pond (2 L) ice core (1 core)

Gear and / or platform	Date	Position (dec)	Matrix and samples collected
Grab sample (Zodiac)	30.05.2021	78.69916667 006.98416667	seawater (4 L)
Bongo net PS126-08-7 0 – 450 m	05.06.2021	79.180127 005.917138 HG-I	*Beroe cucumis* (6 x 1 ind./sample) Chaetognatha (6 x 5 ind./sample) *Thysanoessa inermis* (4 x 1 ind./sample) *Themisto abyssorum* (6 x 5 ind./sample) *Clione limacina* (4 x 1 ind./sample) *Aglantha digitale* (6 x 5 ind./sample)
Bongo net PS126-28-4 0 – ~500 m	20.06.2021–21.06.2021	78.986958 003.614526 HG-VI	*Sarsia tubulosa* (2 x 1 ind./sample) *Clione limacina* (6 x 1 ind./sample) *Themisto abyssorum* (6 x 5 ind./sample) *Thysanoessa longicaudata* (6 x 5 ind./sample) Chaetognatha (6 x 5 ind./sample) *Beroe cucumis* (10 x 1 ind./sample) *Aglantha digitale* (6 x 5 ind./sample) *Thysanoessa inermis* (10 x 1 ind./sample)

Preliminary (expected) results

During five OFOBS transects, various items were observed including fishery-related debris and fragments of plastic film (Fig. 10.4). However, only a detailed analysis of the imagery will enable us to determine the spatial variability in litter densities on the seafloor and temporal trends by comparison with previous data (Parga Martinez et al. 2020). Sediment samples will be analysed for MP concentrations and compared with previous results to assess temporal trends.

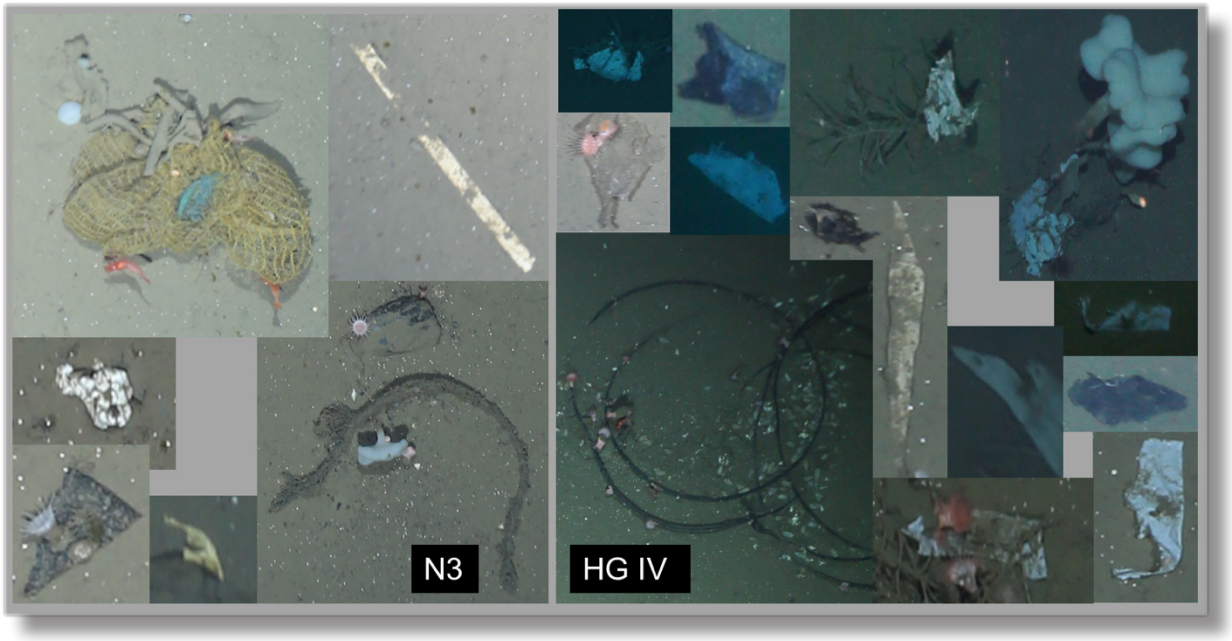

Fig. 10.4: Examples of OFOBS images with plastic debris from HAUSGARTEN stations N3 and HG-IV at ~2,500 m water depth

During PS126, a total of 53 air concentration samples (including blanks) and 39 deposition samples were collected. 45 snow, melt pond and sea ice samples were collected from ice floes within helicopter reach of the vessel in the HAUSGARTEN area at 10 unique locations with corresponding field blank samples (Table 10.1). Two of these were of glacial origin, i.e. icebergs. Analysis of the 82 faunal samples from two locations will show to what degree MP has infiltrated the mesopelagic Arctic food web (Table 10.1).

Analysis of potential MP particles was not possible on board because of potential contamination of samples during microplastic analysis and because spectroscopic analysis by laser is not currently possible on a vibrating vessel. However, visual inspection of the filters suggests that there may be an interesting MP dataset unfolding within this sample set. After microplastic analysis by µ-Raman in dedicated MP laboratories, expected results will comprise a quantitative polymer characterization for each of the samples, creating a detailed and composite picture of MP in the atmosphere and ocean-atmosphere exchange during the Arctic summer season.

Calculation of ice floe drift trajectories via analysis of satellite imagery allows us to determine the region of ice formation, i.e. where MP was entrained (Peeken et al. 2018). The trajectory of one of the sampled ice floes suggests its origin off Severnaja Zemlya (Fig. 10.3). The western ice floes likely originated and drifted from further east, from an area near Cape Baranova, or even from the central Laptev Sea (T. Krumpen, pers. comm.). Some of the ice floes may be of coastal origin, whereas others could stem from freeze-up over deep waters.

Data management

Environmental data and imagery will be archived, published and disseminated according to international standards by the World Data Center PANGAEA Data Publisher for Earth & Environmental Science (https://www.pangaea.de) within two years after the end of the cruise at the latest. By default, the CC-BY license will be applied after publication of the results. The seafloor imagery will also be uploaded to the online image database BIIGLE to enable access by other parties. Any other data will be submitted to an appropriate long-term archive that provides unique and stable identifiers for the datasets and allows open online access to the data.

In all publications, based on this cruise, the **Grant No. AWI_PS126_08** will be quoted and the following *Polarstern* article will be cited: Alfred-Wegener-Institut Helmholtz-Zentrum für Polar- und Meeresforschung. (2017). Polar Research and Supply Vessel POLARSTERN Operated by the Alfred-Wegener-Institute. Journal of large-scale research facilities, 3, A119. http://dx.doi.org/10.17815/jlsrf-3-163.

References

Allen S, Allen D, Moss K, Le Roux G, Phoenix VR, Sonke JE (2020) Examination of the ocean as a source for atmospheric microplastics. PLOS ONE, 15, e0232746.

Allen S, Allen D, Phoenix V, Le Roux G, Durantez Jimenez P, Simonneau A, Binet S, Galop D (2019) Atmospheric transport and deposition of microplastics in a remote mountain catchment. Nature Geosciences, 12, 339-344.

Amélineau F, Bonnet D, Heitz O, Mortreux V, Harding AMA, Karnovsky N, Walkusz W, Fort J, Grémillet D (2016) Microplastic pollution in the Greenland Sea: Background levels and selective contamination of planktivorous diving seabirds. Environmental Pollution, 219, 1131-1139.

Bergmann M, Mützel S, Primpke S, Tekman MB, Trachsel J, Gerdts G (2019) White and wonderful? Microplastics prevail in snow from the Alps to the Arctic. Science Advances, 5, eaax1157.

Bergmann M, Tekman MB, Gutow L (2017a) Marine litter: Sea change for plastic pollution. Nature, 544, 297-297.

Bergmann M, Wirzberger V, Krumpen T, Lorenz C, Primpke S, Tekman MB et al. (2017b) High Quantities of Microplastic in Arctic Deep-Sea Sediments from the HAUSGARTEN Observatory. Environmental Science and Technology, 51, 11000–11010.

Kühn S, Schaafsma FL, van Werven B, Flores H, Bergmann M, Egelkraut-Holtus M et al. (2018) Plastic ingestion by juvenile polar cod (*Boreogadus saida*) in the Arctic Ocean. Polar Biology, 41, 1269-1278.

Liu K, Wu T, Wang X, Song Z, Zong C, Wei N, Li D (2019) Consistent transport of terrestrial microplastics to the ocean through atmosphere. Environmental Science and Technology, 53(18), 10612-10619.

Parga Martínez KB, Tekman MB, Bergmann M (2020) Temporal trends in marine litter at three stations of the HAUSGARTEN observatory in the Arctic deep sea. Frontiers in Marine Science, 7, 321.

Peeken I, Primpke S. Beyer B, Gütermann J, Katlein C, Krumpen T et al. (2018) Arctic sea ice is an important temporal sink and means of transport for microplastic. Nature Communications, 9, 1505.

Ryan PG (2015) A Brief History of Marine Litter Research. In: Marine Anthropogenic Litter (eds. Bergmann M, Gutow L, Klages M). Springer Berlin, pp. 1-25.

Tekman MB, Wekerle C, Lorenz C, Primpke S, Hasemann C, Gerdts G et al. (2020) Tying up loose ends of microplastic pollution in the Arctic: Distribution from the sea surface, through the water column to deep-sea sediments at the HAUSGARTEN observatory. Environmental Science and Technology, 54, 4079-4090.

Trevail AM, Gabrielsen GW, Kühn S, Van Franeker JA (2015) Elevated levels of ingested plastic in a high Arctic seabird, the northern fulmar (*Fulmarus glacialis*). Polar Biology, 38, 975-981.

Wang X, Li C, Liu K, Zhu L, Song Z, Li D (2020) Atmospheric microplastic over the South China Sea and East Indian Ocean: abundance, distribution and source. Journal of Hazardous Materials, 121846.

Zhang Y, Kang S, Allen S, Allen D, Gao T, Sillanpää M (2020) Atmospheric microplastics: A review on current status and perspectives. Earth-Science Reviews, 203, 103118.

11. FRAMJELLY – GELATINOUS ZOOPLANKTON IN THE GATEWAY TO THE ARCTIC: ADVANCED METHODS TO STUDY THEIR DIVERSITY, DISTRIBUTION AND ROLE IN THE FRAM STRAIT FOOD WEB

Charlotte Havermans[1], Annkathrin Dischereit[1], Hendrik Hampe[2], Véronique Merten[2], Dmitrii Pantiukhin[1], Gerlien Verhaegen[3]; Henk-Jan Hoving[2] (not on board)

[1]DE.AWI
[2]DE.GEOMAR
[3]JP.JAMSTEC

Grant-No. AWI_PS126_09

Outline

Gelatinous zooplankton, comprising ctenophores, cnidarians and tunicates, are generally understudied, despite their increase recently hypothesized in biomass throughout the World Ocean, also known as “jellification” of the ocean, as a result of the complex interplay of climate change, overfishing and other anthropogenic factors. In the Arctic Ocean, an increase in advected boreal-Atlantic species is anticipated with the growing Atlantification of the pelagic system, however, reliable datasets on gelatinous zooplankton diversity and abundances are still missing to detect such changes. Despite the LTER (Long-Term Ecological Research) HAUSGARTEN area being one of the most elaborately and intensively sampled pelagic and deep-sea time series, it currently lacks a component targeting the gelatinous zooplankton community, despite its regionally high abundances and biomass. Therefore, we aimed to obtain reliable data on gelatinous zooplankton diversity, distribution patterns, and abundances by using a combination of various traditional net catches with advanced methods including optics and environmental DNA based on high-throughput sequencing.

Objectives

Gelatinous zooplankton, hereafter also referred to as jellies, are fragile, soft-bodied organisms grouping together a number of phylogenetically unrelated taxa: ctenophores, scyphozoans (true jellyfish), hydrozoans (including the colonial siphonophores and hydromedusae), and pelagic tunicates (salps and appendicularians). Despite their diversity, most of them have in common the alternance between sexual and asexual reproduction, taking advantage of favourable environmental conditions by growing and multiplying rapidly. Because of their fragile bodies, they are easily fragmented or destroyed with traditional net sampling, which is why jellies are often neglected in pelagic studies, or when considered, their biomass and diversity are greatly underestimated (Hosia et al. 2017). Jellies are known to be major drivers of ecosystem changes. Many species cope well with environmental change (warming, eutrophication, oxygen reduction, overfishing) and an increase in jelly biomass, or “jellification” has been observed in several marine ecosystems worldwide (e.g. Richardson et al. 2009). Such gelatinous shifts can affect food web dynamics and cause the collapse of commercially important fish stocks (Purcell 2012).

Because of the significant impacts of climate warming on the Arctic marine ecosystem, a large-scale assessment of its biodiversity is particularly pressing. However, reliable data on the abundance, species boundaries and trophic roles of Atlantic and Arctic jellies are virtually inexistent. Hence, despite their importance in both Atlantic and Arctic ecosystems, jellies have been completely ignored in scenarios of species interactions and range shifts (Licandro et al. 2015; Mánko et al. 2020). Nonetheless, with the growing Atlantification of the pelagic system an increase in advected boreal-Atlantic species is anticipated. This is illustrated by the recent increase in biomass of the scyphozoan *Periphylla periphylla* in the Barents Sea (Tiller et al. 2017) and its recent first-time appearance in a high-Arctic Svalbard fjord (Geoffroy et al. 2018). The HAUSGARTEN LTER observarory is one of the most elaborately and intensively sampled pelagic and deep-sea time series and its location at the Atlantic gateway to the Arcticis is a harbinger of ongoing changes in the Arctic. Yet it currently lacks a component that targets the gelatinous zooplankton community despite their high abundances observed in Fram Strait's surface waters (Havermans, pers. obs.) and their likelihood to undergo community changes.

Not only do Jellies belong to different taxonomic lineages, they also differ greatly in feeding ecology. Trophic roles can be classified into (a) filter feeders and grazers such as tunicates, (b) passive trappers feeding on diverse prey types, such as siphonophores, and (c) active hunters like ctenophores, feeding on zooplankton, ichthyoplankton and other jellies. Many species, such as the dominant ctenophore *Mertensia ovum*, are known to exert a major influence on lower trophic levels, rarely becoming satiated at natural prey densities. However, little is known so far on the variation in feeding habits and spatio-temporal trophic flexibility of jelly populations. Considering that jellies will become more important in many oceans, their impact on the ecosystem as predators and prey will similarly increase. Until recently, the contribution of gelatinous zooplankton to predators' energy budgets was greatly underestimated. Jellies have a low energy density in comparison to other plankton (Doyle et al. 2007) and have therefore been considered a "trophic dead-end". Since their watery tissues are rapidly digested in predator's stomachs, conventional microscopic analyses have often overlooked the presence of jellies in the diets of predators, leading to an oversimplified view of their role in the food web. Even though the importance of jellies as prey is still difficult to quantify, evidence from molecular diet analyses and *in-situ* observations have proven their top-down control to be much more important than previously assumed. Indeed, many fish, birds, turtles, cephalopods and other invertebrates target jellies as part of their diet (Hays et al. 2018). The concept that jellies act as an "energy roundabout" – transporting energy through a range of trophic levels, from zooplankton to top consumers (Robinson et al. 2014) – deserves further validation for polar ecosystems.

Jellies may also be important carbon transporters to the deep-sea floor. Due to presumably low predation pressure after a bloom, sinking jellies may provide export mechanisms for carbon to the seafloor in the form of "jelly-falls" (Lebrato et al. 2012). Appendicularians produce several new houses per day, of which the discarded ones sink at fast rates, significantly contributing to the biological carbon pump, which also holds for Arctic regions (Deibel et al. 2005). Once on the seafloor, jelly carcasses may sustain a diverse benthic scavenging community, including bentho-pelagic amphipods (Havermans and Smetacek 2018).

The overarching goal of the FramJelly project is to establish a comprehensive baseline knowledge of jelly diversity, abundance and distributional patterns and their link to oceanography and primary production. Our integrative jelly surveys will consist of a combination of various net sampling, *in-situ* optical observations and environmental DNA (eDNA) studies. Optimization of eDNA methods will establish a cost-effective monitoring tool, allowing to detect incoming jelly species and changes in community composition based on water sampling. The trophic role of key jelly species in the pelagic food web will be explored as well as the role of jelly-falls sustaining the benthic food web. This knowledge will serve to evaluate potential distribution

shifts of Atlantic and Arctic gelatinous zooplankton species and their consequences for the Arctic food web.

The objectives of the FRAMJELLY project are:

- Study gelatinous species diversity and abundances and link these data to environmental parameters. These data will be used for modelling efforts to better understand habitat preference and predicting future niches under warming scenarios (net catches, optics and eDNA sampling, Species and Community Distribution Modelling);
- Elucidate the trophic role of jellies in the Fram Strait food web. Asses of the feeding ecology of dominant jelly species and their role as prey for pelagic predators (net sampling, biomarker and molecular diet analyses);
- Evaluate the role of jelly-falls as food for benthic scavengers (lander deployments with baited traps, molecular diet analyses);
- Characterize the molecular diversity of jelly species encountered in different water masses and the connectivity of Arctic populations by comparison with specimens collected during other Arctic cruises (e.g. Central-Arctic, Svalbard, Greenland) (net sampling, DNA barcoding and phylogeographic analyses);
- Optimize eDNA methods for assessing jelly, cephalopod and fish diversity in the water column and in the deep-sea sediments. DNA calibration and degradation experiments will be carried out with different species composition and abundances of jellies (water and sediment sampling, in-vitro experiments, molecular analyses).

Work at sea

At ten HAUSGARTEN stations (S3, SV-II, SV-IV, HG-I, HG-IV, HG-IX, N4, N5, EG-I, EG-IV), we conducted various net deployments including vertical net casts with the Maxi-Multi net, as well as towed and vertically deployed Bongo and jelly nets (see Table 11.1). At three of these stations (HG-IV, S3, EG-IV), we conducted a towed video survey with the camera system PELAGIOS II in addition to the aforementioned net sampling. The planned PELAGIOS station at N4 could not be achieved due to heavy sea ice cover. At each of the ten stations, we sampled water from the CTD rosette for eDNA for assessing jelly, cephalopod and fish species diversity. At all of these stations where nets were deployed and water was sampled for eDNA, we also sampled sediment from the multiple corer (MUC) for eDNA studies aiming to detect potential jelly, cephalopod and fish “food falls”. At two stations (SV-I and EG-I), we deployed a free-fall lander equipped with baited traps to sample bentho-pelagic scavenging amphipods.

At the stations S3, HG-IV and EG-IV, we obtained an integrative survey on species diversity and vertical species distributions that allowed us to compare video surveys, depth-stratified net hauls and water sampling for eDNA from the CTD, at a range of different depths. Net sampling at the same depths as the PELAGIOS imaging transects will allow us to capture the observed organisms and to validate the *in-situ* identifications morphologically and genetically. These results on species diversity and abundances will then also be compared to the community composition revealed with eDNA analyses at the different depths.

Tab. 11.1: FramJelly deployments on board PS126

Site	Station	Deployment	Max. depth (m)
S3	2-6	Multi net-Maxi vertical	1500
	2-7	Bongo net towed	600
	2-8	Jelly-net vertical	48
	2-9	PELAGIOS	1600
HG-IV	3-9	Multi net-Maxi vertical	1500
	3-10	Bongo net towed	600
	3-11	Jelly-net vertical	100
	3-12	Bongo net towed	353
	3-20	PELAGIOS	1600
HG-I	8-6	Bongo net towed	250
	8-7	Bongo net towed	450
	8-8	Multi net-Maxi vertical	1200
SV-IV	9-8	Multi net-Maxi vertical	1160
	9-9	Bongo net towed	600
	9-10	Bongo net towed	224
SV-I	10-1	Free-fall lander	900
SV-II	12-2	Multi net-Maxi vertical	200
	12-3	Bongo net towed	741
	12-4	Bongo net towed	100
N4	18-3	Multi net-Maxi vertical	1500
	18-4	Bongo net vertical	600
	18-5	Bongo net vertical	150
N5	19-3	Multi net-Maxi vertical	1200
EG-IV	20-4	Multi net-Maxi vertical	1500
	20-5	Bongo net towed	620
	20-7	PELAGIOS	2000
EG-I	21-1	Free-fall lander	900
	21-10	Multi net-Maxi vertical	900
	21-11	Bongo net towed	500
	21-12	Bongo net towed	225
HG-IX	23-6	Multi net-Maxi vertical	2500
	23-7	Bongo net towed	177

Zooplankton sampling

Samples of gelatinous zooplankton for species identification, abundance data, molecular analyses and experimental work were collected using Multi nets, Bongo nets and jelly nets. The Maxi-Multi net (mesh sizes 330 µm) was deployed vertically through the water column at a speed of 0.5 m/s using nine different opening and closing nets for depth-stratified sampling.

The Bongo net (mesh sizes 335 and 500 µm) was equipped with a large non-filtering cod-end and a V-Fin depressor. At all stations but N4, it was towed obliquely at a ship's speed of 2 knots. At N4, vertical Bongo net hauls were carried out due to heavy ice cover. The jelly net was deployed vertically and hauled with a speed of 0.2 m/s through the water column. The nets were equipped with a depth logger and CTD to measure environmental conditions and the maximum depth reached *in situ*. During the net deployments, we switched on the EK80 onboard echosounder in order to compare the obtained acoustic profiles with the net catches.

On board, all catches were sorted into different taxonomic groups. Gelatinous zooplankton specimens were photographed individually, where possible, identified up to species level, and frozen at –80° C or preserved in 96 % undenatured ethanol. Abundances will be calculated based on the volume of water sampled and the number of jellies counted per species. Other macrozooplankton species, including amphipods, pteropods and decapods were also sorted, counted and subsequently preserved in ethanol. Some species (e.g. *Themisto* spp., *Cyclocaris guilelmi*) were collected for trophic analyses (molecular diet and biomarker analyses), and preserved in ethanol or frozen at –80° C.

Experiments with live jellies

We performed several experiments to determine the shedding of DNA by jelly individuals and its detectability over time for different amounts of a particular hydrozoan species. We also composed a "mock" community of known jelly species in different numbers to test the efficiency of different primer sets in recovering all species present in the tank. To keep the jellies under optimal conditions, we used four large Kreisel tanks, that were circular in shape and created uniform water pressure throughout the tank, enabling the jellies to swim freely but also to stay away from the sides of the tank. These tanks were placed in a cold container with a stabilized room temperature of 2° C and filled with filtered seawater. Salinity and temperature of the tanks were measured at the start or end of the experiments. The candidate for the eDNA experiments was the hydrozoan *Aglantha digitale*, which was very abundant in the catches and allowed us to sort out enough individuals in good condition for keeping them alive for several days. As one of the most abundant hydrozoan jellies in the open ocean of the Arctic, this is an interesting target taxon for eDNA calibration and optimization, in order to accurately interpret our *in-situ* eDNA studies. For experiment 1, we kept 6 individuals of *A. digitale* of similar sizes in each of three Kreisel tanks, the fourth Kreisel tank served as a control tank without animals. To detect changes in eDNA concentrations over time and a potential peak of eDNA shedding, we kept them for 36 hours in the tanks, and took triplicate water samples of 500 ml each for each of the four tanks after 2, 10, 18, 24 and 36 h. These water samples were filtered over 0.2 µm Sterivex filters and a blank with MilliQ water was included to detect contamination. Then, all 18 individuals were removed, their bell heights were measured and they were frozen in bulk, separately for each tank. The air flow in the Kreisel tanks was stopped in order to account for DNA degradation over time, and 500 ml water were filtered again in triplicate per tank. Step by step the individuals were removed after 24, 48, 72 and 96 h. For the second experiment, we kept different numbers of *A. digitale* in each tank. In Kreisel tank 1, we kept one individual of *A. digitale*, in the second tank 5, and in the third tank 10 individuals. The fourth tank again served as a control. To monitor eDNA shedding in the tank water over time, and to test whether we were able to characterize quantitatively eDNA for different numbers of individuals, we took 500 ml water samples in triplicates per tank at the beginning of the incubation, after 12, 24, 36, 48, 60, 72, 84 and 96 h. These samples were filtered over 0.2 µm Sterivex filters, with a MilliQ blank included at each time interval. After the experiment, the individuals were measured for bell height and frozen at –80° C in bulk samples per tank. Finally, the third experiment was conducted with a diverse assemblage of jellyfish caught with the Maxi-Multi net at station HG-

IX. We placed 2 individuals of *Atolla tenella*, 2 individuals of *Aglantha digitale*, 3 individuals of *Sminthea arctica*, 2 individuals of *Botrynema brucei*, 4 individuals of *Dimophyes arctica* (2 eudoxid and 2 polygastric stages), 4 individuals of an unidentified ctenophore species, and 1 individual of *Solmundella bitentaculata* in a normal non-circulating tank with 14 L of filtered seawater. At the beginning of the experiment, 500 ml of the seawater from the tank were filtered as a control sample. The assemblage was kept in the tank for about 40 hours. Then 2 L were filtered in triplicate over 0.2 µm Sterivex filters.

Water and sediment sampling for eDNA studies

At each of the ten aforementioned stations, we sampled water from the CTD rosette for eDNA analyses to study the species diversity of jelly, cephalopod and fish. At the stations HG-I, SV IV, SV-II, N5, and EG-I, watersamples were collectd from four different depths: surface, Chl max layer, 50 and 100 m. At the stations S3, HG-IV, N4, EG-IV and HG-IX, we sampled water from the following depths: surface, Chl max layer, ca. 50, 100, 200, 400, 500, 750, 1,000, 1,300, 1,600, 2,000, 2,500 m and above bottom, to examine the eDNA throughout the water column and compare this with Multi net catches and PELAGIOS transects at the different depths. For each depth, the triplicate of 2 L was sampled and filtered over 0.2 µm Sterivex filters. To test the potential contamination a blank sample of MilliQ water was included during each filtration. Sediment samples were also collected from the MUC at all of the aforementioned stations for eDNA studies aiming to detect potential jelly, cephalopod and fish "food falls".

Optical surveys

To study biodiversity, vertical distribution and abundances of gelatinous zooplankton (and other elusive fauna like cephalopods), we deployed the towed camera system PELAGIOS II to perform pelagic video transects down to 2,000 m water depth. This system was towed horizontally via a fibre optic cable at low ships speed (1 knot) at various depths from 20 m to 2,000 m. The PELAGIOS II consists of both, a 4 k and HD camera, a depth sensor with current meters, and a CTD. The water column in front of the camera is illuminated by LED lights. It was deployed at the stations S3, HG-IV, and EG-IV, but could not be deployed at N4 as planned due to heavy ice cover. The maximum depths reached with the PELAGIOS dives are listed in Table 11.1.

Deployment of baited trap lander

At two stations (SV-I and EG-I), we deployed a free-fall lander. This lander was equipped with four traps containing mackerel bait wrapped in mesh and placed in a Kautex vial with holes, to attract scavengers with an odour plume. Scavenging bentho-pelagic amphipods were able to enter the traps through small funnels of various diameters (1 – 4 cm). The first lander deployment had a residence time of approx. 18 h on the seafloor, whereas the second had a residence time of approx. 8 h.

Preliminary (expected) results

Diversity, abundances and distribution patterns of gelatinous zooplankton from net catches

We sampled gelatinous zooplankton using three types of nets at ten different stations. The total number of individuals caught with the different net deployments carried out at each station, and species richness based on our preliminary morphological identification at sorting, are listed in Table 11.2. After verifying the morphological identifications in the home laboratory, and validating the uncertain identifications with molecular barcoding, we will calculate abundances based on the number of individuals per volumes of water filtered with the different nets. These

will then be compared between stations and associated with environmental factors. The most abundant species encountered during this cruise at almost each station were the hydrozoan *Aglantha digitale*, the hydrozoan *Sminthea arctica* and the siphonophore *Dimophyes arctica* (eudoxid and polygastric life stages) (see Fig. 11.1). More than 2,100 individuals of gelatinous zooplankton were collected during this cruise, the majority of which was photographed and frozen or preserved individually. Based on our preliminary data, station SV-IV appeared to be particularly abundant and characterized by a high species diversity. SV-II was the shallowest shelf station (ca. 300 m water depth), closest to Svalbard shelf stations and harboured a distinct gelatinous zooplankton assemblage, with species only encountered at this station (e.g. *Sarsia tubulosa*). At station HG-IX, we sampled the highest species richness (18 different species). This is the deepest stations (water depth > 5,500 m) and we conducted the deepest Multi net haul, up to 2,500 m instead of 1,500 m at other stations. Hence, we found several true deep-sea jellies at this station, such as *Crossota norvegica*, which was only found in the nets at this station but was also reported from the deepest PELAGIOS transect at EG-IV. Species composition and abundance data will be linked to oceanographic features, primary productivity and sea ice concentration, and key drivers for distribution patterns will be determined. The results on diversity and abundances from net catches will be compared with those obtained from PELAGIOS II video transects and eDNA analyses.

Tab. 11.2: Gelatinous zooplankton sampled with net deployments at the different PS126 stations. The number of individuals recovered at each station and the species richness are listed.

Site	Number of individuals	Species richness
S3	79	9
HG-IV	142	11
HG-IV	253	8
SV-IV	532	12
SV-II	31	10
N4	119	8
N5	146	11
EG-IV	268	11
EG-IV	277	12
HG-IX	322	18
Total	2159	ca. 27

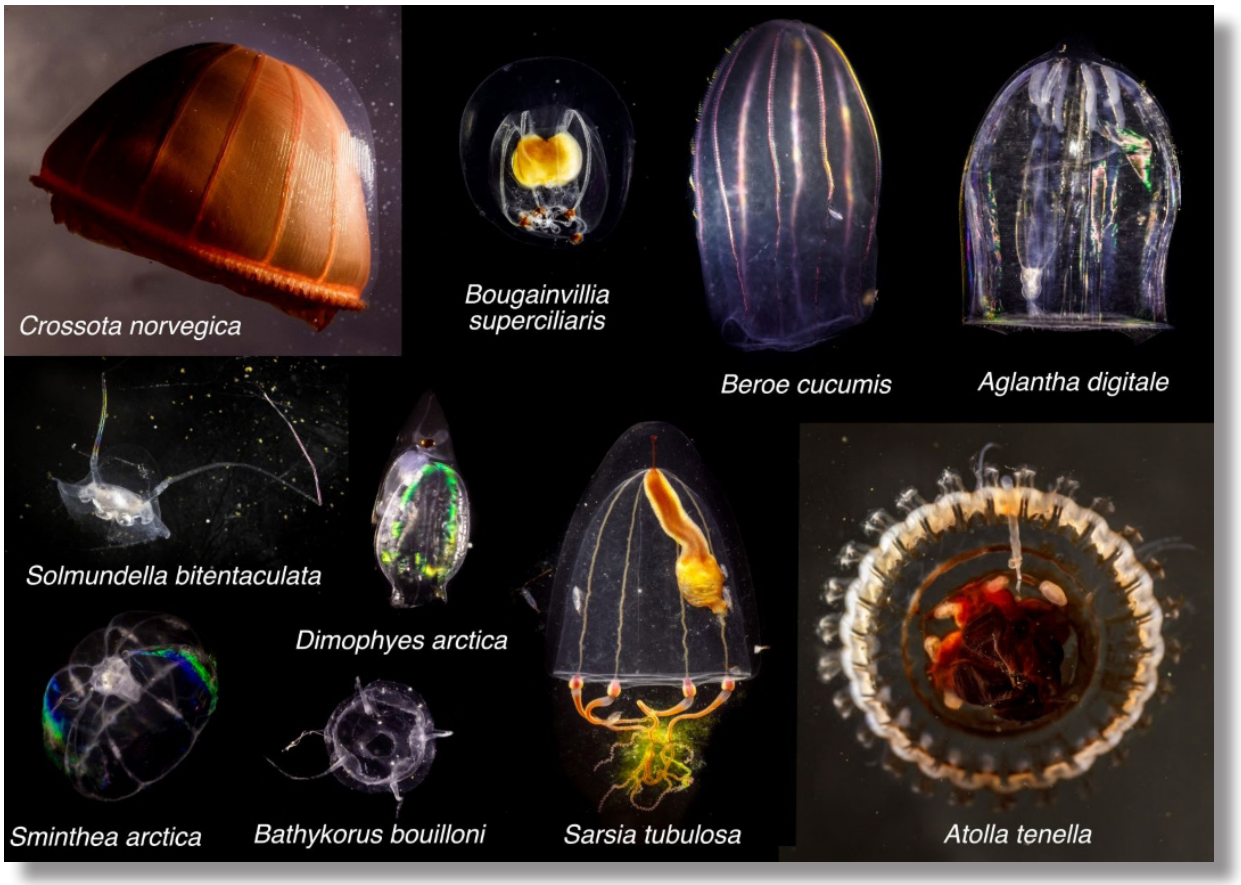

Fig. 11.1: Photographs of several species of gelatinous zooplankton sampled during PS126; images were taken by Mario Hoppmann

For the dominant species *Aglantha digitale*, we measured the sizes at different depth ranges, from which we obtained individuals with the depth-stratified Maxi-Multi net sampling. Figure 11.2 shows *Aglantha*'s size distribution at one example station (EG-IV) over several depth ranges. For the different depth ranges, samples sizes differed, due to the uneven distribution of *Aglantha digitale* at different depths in the Arctic Ocean, which we could also observe with other gear used during this cruise, e.g. PELAGIOS II (results see below). The boxplots show the differences in size linked to a certain depth range. Only a few specimens were available for size measurements from surface waters as well as in the deep depth range (600 – 700 m). In medium depths (i.e. 100 – 300 m and 300 – 500 m), most specimens were caught. A difference in size ranges per depth could be stated: organisms from depth between 300 – 500 m were generally larger than those sampled between 100 – 300 m. Further analyses will be conducted on with the complete dataset from all stations including all sampled individuals of *A. digitale*.

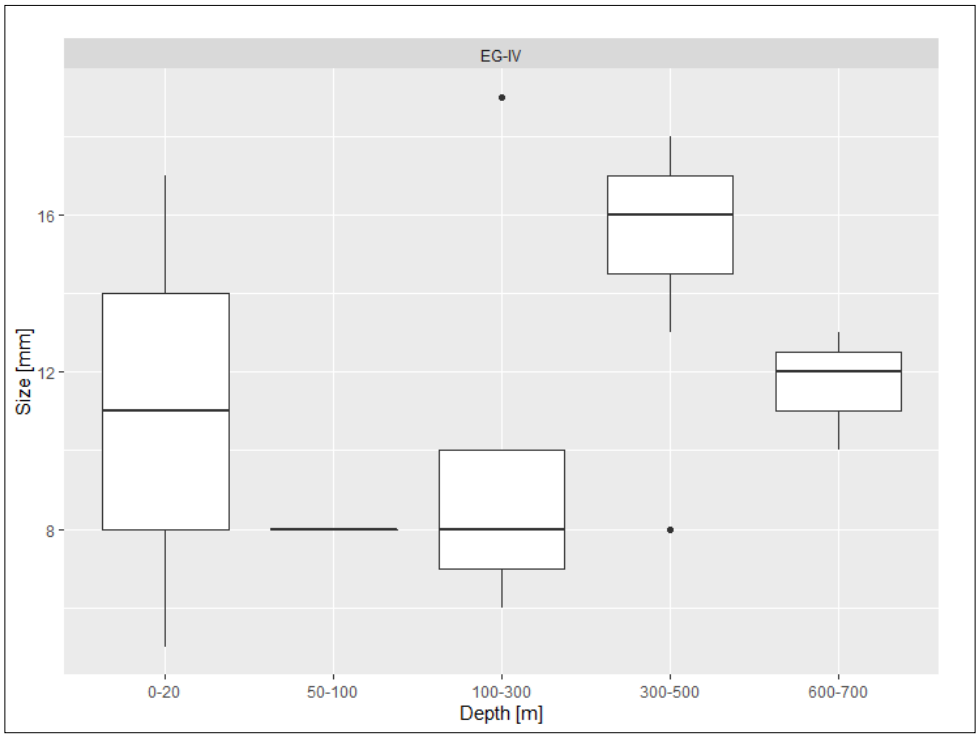

Fig. 11.2: Size distribution of the hydrozoan Aglantha digitale over different depth ranges. Sample size: 0 – 20 m (2), 50 – 100 m (1), 100 – 300 m (5), 300 – 500 m (7), 600 – 700 m (3)

Species distribution and abundance patterns based on PELAGIOS II video annotations

Pelagic video transects were obtained at three stations, S3, HG-IV and EG-IV. The majority of the obtained videos was annotated on board. At station S3, we recorded approximately 300 encounters with jellies, more than twice as many as at HG-IV, and the dive at EG-IV yielded a record of species number and abundance, probably because it was the deepest dive of three stations. Here we present the data from the first dive of PELAGIOS II at S3, where it was deployed up to 1,600 m. Video annotations were used to study the abundance of 14 taxa of gelatinous zooplankton observed at different depths. The most abundant species belonged to the family of Rhopalonematidae, mainly consisting of *Aglantha digitale* and *Sminthea arctica*, followed by the order Trachymedusae (incl. *Botrynema* spp.) and the suborder of Physonectae (incl. *Rudjakovia pilicata)*. The results confirm the need to combine different methods (net sampling, optics) for recovering the entire species diversity of gelatinous zooplankton, as dominant species detected with video transects were not found at all with net catches (e.g. *Rudjakovia pilicata*), or were found in lower abundance. The opposite was true in net catches: the abundant but small polygastric and eudoxid stages of *Dimophyes arctica* could not be visualized with the optical surveys. The depth distributions occupied by the different taxa are displayed in Figure 11.3. The two species of the Rhopalonematidae family occupy distinctively different depth/temperature niches, with *Aglantha digitale* displaying the highest abundance at 300 m and *Rudjakovia pilicata* at 600 m. The highest abundance and diversity of the gelatinous species were observed at 600 m depth. The variance partitioning among the explanatory effects of the pilot Poisson Joint Species Distribution Model (following Ovaskainen et al. 2020). Figure 11.4 shows that the temperature is the most important factor causing variation in species abundances. On the contrary, salinity plays only a very minor role, which can be explained by the fact that salinity does not vary strongly at this station. Similar analyses, including more

environmental parameters such as dissolved oxygen, sea ice concentration and productivity, will be performed on the complete dataset of video annotations from all three dives.

Based on these data, (joint) species distribution models will be run using the "HMSC" (Hierarchical modelling of Species Communities) package following Ovaskainen et al. (2020). These models will be used to generate ecological niche predictions of species for the Fram Strait region and projections under future climate change scenarios (based on CMIP6 models). The annotated datasets will be integrated into the Oceanic Biodiversity Observation Database (OBOD) at GEOMAR.

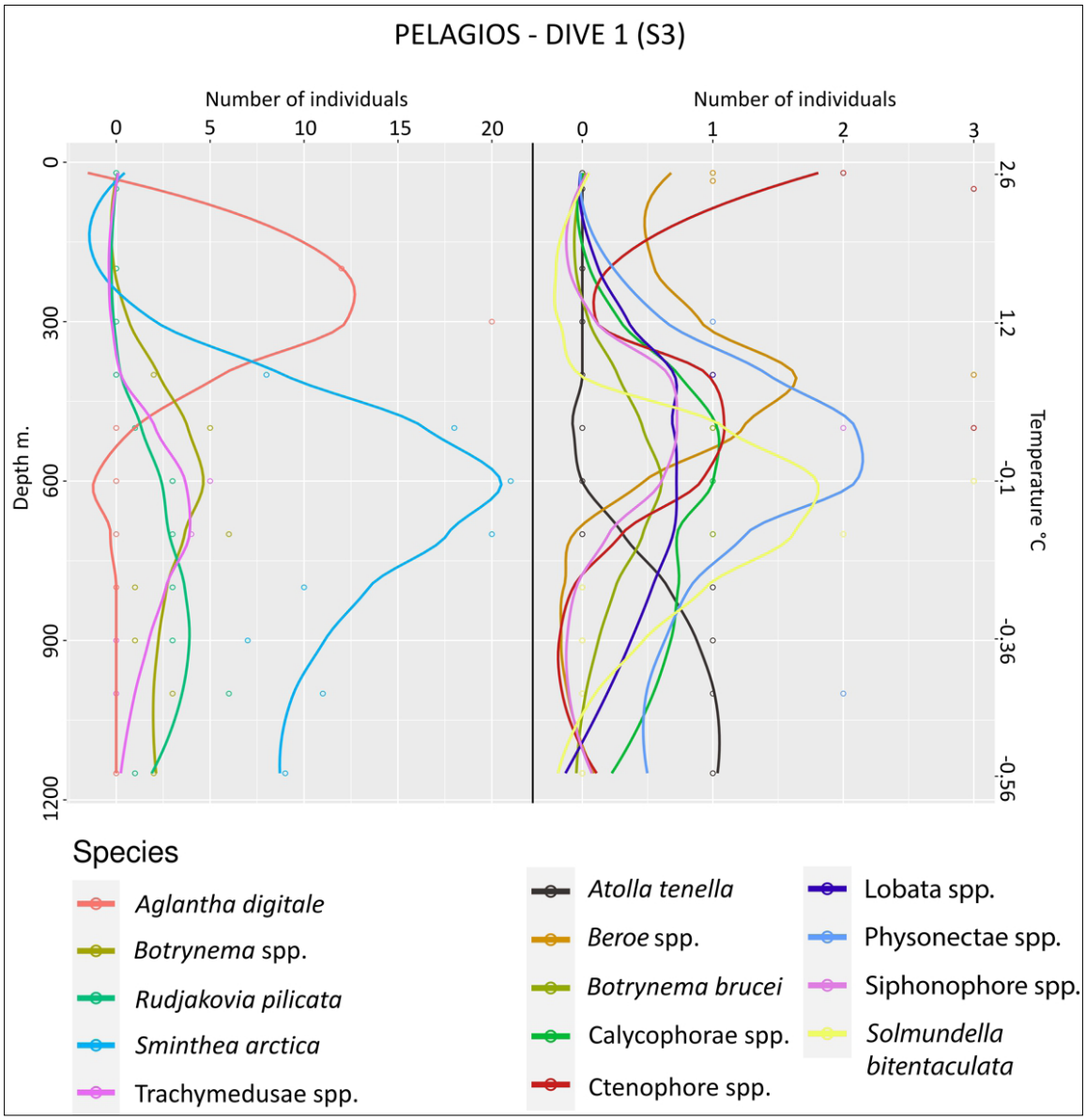

Fig. 11.3: Distribution profiles according to depth and temperature of the 14 taxa of gelatinous zooplankton encountered during the PELAGIOS II dive at station S3. On the left side, the most abundant species are plotted, with the number of individuals annotated in function of depth (left Y-axis) and temperature (right Y-axis). On the right side, the distribution curves of the less abundant species are displayed

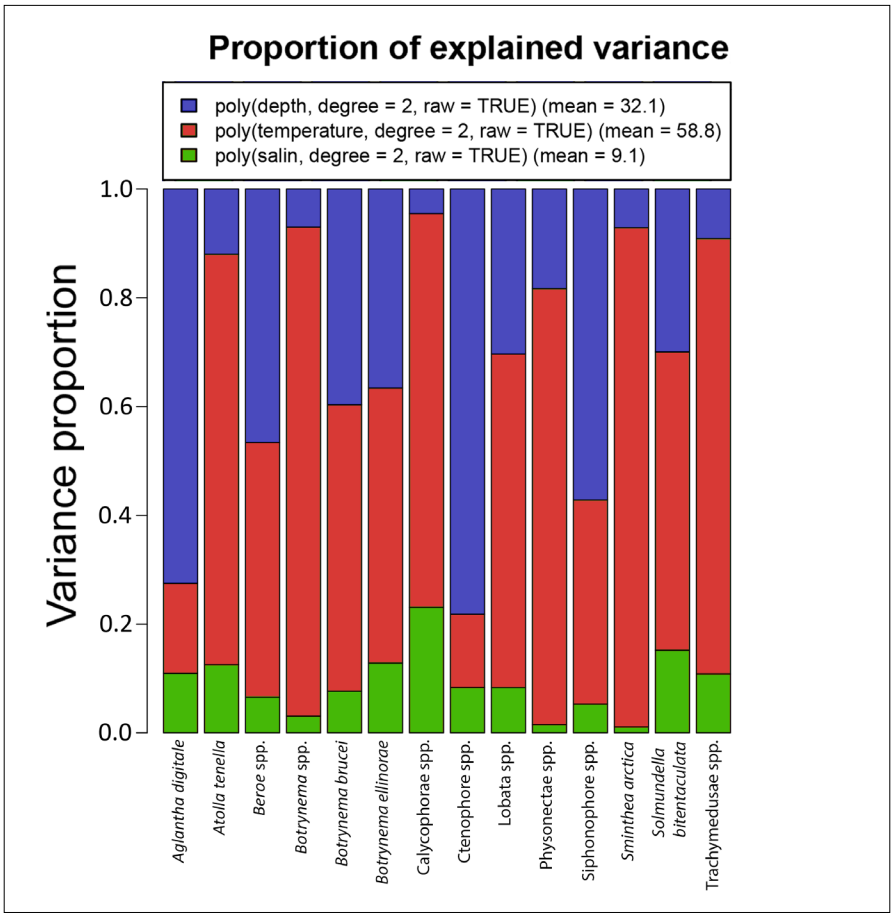

Fig. 11.4: Variance partitioning among the explanatory effects (depth in blue, temperature in red, salinity in green) from the pilot model of the joint Poisson species distribution (Ovaskainen et al. 2020)

DNA barcoding and phylogeography

A subset of the gelatinous zooplankton specimens sampled will be genetically characterized (or "barcoded") by sequencing different markers, depending on the taxon, such as the cytochrome c oxidase sub-unit I (COI), 16S rDNA and 18S rDNA. In this way, we will complement existing reference databases and assess the regional genetic variability of morphospecies. For widespread species, we will combine these sequence datasets with sequences from species collected during previous sampling campaigns in the Arctic region e.g. during the HE560 expedition targeting Svalbard fjords, and PS122 (MOSAiC) in the central Arctic.

Molecular diet analyses

Aglantha digitale is one of the most abundant hydrozoans in the Fram Strait region but its feeding habits have not been studied. Hence, in order to characterize the regional variation in diet composition, we sampled the stomachs of 107 individuals of *A. digitale*. At each of the stations HG-I, SV-IV, N4, N5, EG-I, and EG-IV stations, we dissected 10 – 20 individuals and removed their stomachs, which were immediately frozen at –80° C to prevent further digestion of dietary items. In the home laboratory, DNA will be isolated from the stomach contents and analyzed with DNA metabarcoding using universal primers.

To characterize the occurrence of jelly predation in the diet of pelagic carnivorous zooplankton, we sampled different species of pelagic amphipods (e.g. *Themisto* spp., *Cyclocaris guilelmi*, *Lanceola clausii*). In the laboratory, we will isolate the stomach content from these species and

extract their DNA. These samples will also be investigated by DNA metabarcoding, combining universal and jelly-specific primers.

Finally, we will investigate the diet of bentho-pelagic scavenging amphipods collected with the lander deployments to investigate the role of "jelly-falls" and nekton carcasses (cephalopods, fish) sustaining benthic communities. A large number of amphipods belonging to different species (*Eurythenes gryllus sensu stricto*, lysianassoid spp.) was collected during the two baited-trap lander deployments. For a subset of samples per species, DNA will be isolated from their stomach contents and amplifications will be carried out using general and taxon-specific primers (e.g. 18S for cephalopods, de Jonge et al. 2021).

eDNA analyses

eDNA metabarcoding will be used to investigate the diversity of jelly, cephalopod and fish based on *in-situ* water samples from different depths, as well as sediment samples collected at various stations. DNA will be isolated from the Sterivex filters used for water filtrations, and from directly from sediment fractions. Amplifications will be carried out using general and taxon-specific primers (e.g. 18S for cephalopods; de Jonge et al. 2021). The efficiency of eDNA to provide quantitative estimates of species will also be assessed, by comparing the relative read abundances of the metabarcoding analyses with abundance data obtained from video transects and net casts for different depths. For dominant jelly species, we will also assess the relative abundances using quantitative real-time PCR (qPCR) after developing species-specific primer sets.

For eDNA experiments carried out on board with *Aglantha digitale*, we will develop species-specific primer sets for qPCR assays for quantitatively monitoring the DNA molecules shed over time, and their decay after removal of the specimens. For the third eDNA experiment, we will use DNA metabarcoding with universal and taxon-specific primer sets, in order to test which primer sets are most efficient at detecting all taxa present in the sample. This will also allow us to define whether certain species shed more DNA than others over time and dominate the sample in terms of read abundance.

Data management

Samples of zooplankton and bentho-pelagic amphipods will be archived and stored at the AWI and GEOMAR. DNA extracts from jellies and other plankton, eDNA filters and sediment will be stored at –80° C in the AWI and/or GEOMAR for up to ten years after publication of the results (according to the DFG guidelines for good scientific practice). A voucher specimen collection of jelly samples preserved in ethanol and linked to their DNA extracts by unique sample identifiers, will be kept in a repository at the AWI. Georeferenced datasets including species inventories, distribution records and abundance data of macrozooplankton from net catches will be submitted to the World Data Center PANGAEA Data Publisher for Earth & Environmental Science (https://www.pangaea.de) as soon as the data are available (within two years after the cruise at the latest), possibly with an embargo period until publications are completed. By default, the CC-BY license will be applied.

Video footages will be archived in the GEOMAR and AWI IT storage infrastructures and metadata will be accessible via the Ocean Science Information System (OSIS, https://portal.geomar.de/osis) within six months after the completion of the expedition. After quality assessment and annotation, the annotated datasets with screenshots of the observations will be submitted to PANGAEA, and released as soon as the results are published (max. two years after the expedition, with a potential embargo period of one additional year).

Molecular data (DNA sequences, metabarcoding reads) will be archived, published and disseminated within GenBank during the publication process, and metabarcoding project results will be deposited in the National Center for Biotechnology Information (NCBI).

Results of the PS126 expedition will be published in peer-reviewed journals within three years after the end of the cruise. In all publications, based on this cruise, the **Grant No. AWI_PS126_09** will be quoted and the following *Polarstern* article will be cited: Alfred-Wegener-Institut Helmholtz-Zentrum für Polar- und Meeresforschung. (2017). Polar Research and Supply Vessel POLARSTERN Operated by the Alfred-Wegener-Institute. Journal of large-scale research facilities, 3, A119. http://dx.doi.org/10.17815/jlsrf-3-163.

References

Deibel D, Saunders PA, Acuna JL, Bochdansky AB, Shiga N, Rivkin RB (2005) The role of appendicularian tunicates in the biogenic carbon cycle of three Arctic polynyas. In: Gorsky G, Youngbluth MJ, Deibel D (eds) Reponse of marine ecosystems to global change: Ecological impact of appendicularians. Gordon and Breach, Paris, pp. 327-356.

De Jonge DSW, Merten V, Bayer T, Puebla O, Reusch TBH, Hoving H-JT (2021) A novel metabarcoding primer pair for environmental DNA analysis of Cephalopoda (Mollusca) targeting the nuclear 18S rRNA region. Royal Society Open Science, 8, 201388.

Doyle TK, Houghton JDR, McDevitt R, Davenport J, Hays GC (2007) The energy density of jellyfish: estimates from bomb-calorimetry and proximate consumption. Journal of Experimental Marine Biology and Ecology, 343, 239-252.

Geoffroy M, Berge J, Majaneva S, Johnsen G, Langbehn TJ, Cottier F, Mogstad AA, Zolich A, Last K (2018) Increased occurrence of the jellyfish *Periphylla periphylla* in the European high Arctic. Polar Biology, 41, 2615-2619.

Havermans C, Smetacek V (2018) Bottom-up and top-down triggers of diversification: A new look at the evolutionary ecology of scavenging amphipods in the deep sea. Progress in Oceanography, 164, 37-51.

Hays GC, Doyle TK, Houghton JD (2018) A paradigm shift in the trophic importance of jellyfish? Trends in Ecology and Evolution, 33, 874-884.

Hosia A, Falkenhaug T, Baxter EJ, Pagès F (2017) Abundance, distribution and diversity of gelatinous predators along the northern Mid-Atlantic Ridge: A comparison of different sampling methodologies. PLoS ONE, 12, e0187491.

Lebrato M, Pitt KA, Sweetman AK, Jones DOB, Cartes JE, Oschlies A, Condon RH, Molinero JC, Adler L, Gaillard C, Lloris D, Billett DSM (2012) Jelly-falls historic and recent observations: a review to drive future research directions. Hydrobiologia, 690, 227-245.

Licandro P, Blackett M, Fischer A, Hosia A, Kennedy J, Kirby RR, Raab K, Stern R, Tranter P (2015) Biogeography of jellyfish in the North Atlantic, by traditional and genomic methods. Earth System Science Data, 7, 173-191.

Mánko MK, Gluchowska M, Weydmann-Zwolicka A (2020) Footprints of Atlantification in the vertical distribution and diversity of gelatinous zooplankton in the Fram Strait (Arctic Ocean). Progress in Oceanography, 189, 102414.

Ovaskainen O, Abrego N (2020) Joint species distribution modelling: with applications in R. Cambridge University Press.

Purcell JE (2012) Jellyfish and ctenophore blooms coincide with human proliferations and environmental perturbations. Annual Review of Marine Science, 4, 209-235.

Richardson AJ, Bakun A, Hays G, Gibbons M (2009). The jellyfish joyride: causes, consequences and management responses to a more gelatinous future. Trends in Ecology and Evolution, 24, 312-322.

Robinson KL, Ruzicka JJ, Decker MB, Brodeur RD, Hernandez FJ, Quinones J, Ancha EM, Uye SI, Mianzan H, Graham WM (2014) Jellyfish, forage fish, and the world's major fisheries. Oceanography, 27, 104-115.

Tiller RG, Borgersen AL, Knutsen Ø, Bailey J, Vanhauwaert H, Bjelland JM, Eisenhauer L, Liu Y (2017) Coming soon to a fjord near you: future jellyfish scenarios in a changing climate. Coastal Management, 45, 1-23.

APPENDIX

A.1 Teilnehmende Institute / Participating Institutions

A.2 Teilnehmer / Cruise Participants

A.3 Schiffsbesatzung / Ship's Crew

A.4 Stationsliste / Station List

A.1 TEILNEHMENDE INSTITUTE / PARTICIPATING INSTITUTIONS

Institution	Address
DE.AWI	Alfred-Wegener-Institut Helmholtz-Zentrum für Polar- und Meeresforschung Am Handelshafen 12 27570 Bremerhaven Germany
DE.DWD	Deutscher Wetterdienst Geschäftsbereich Wettervorhersage Seeschifffahrtsberatung Bernhard-Nocht-Straße 76 20359 Hamburg Germany
DE.GEOMAR	GEOMAR Helmholtz-Zentrum für Ozeanforschung Wischhofstraße 1-3 24148 Kiel Germany
DE.HeliService	HeliService International GmbH Gorch-Fock-Straße 105 26721 Emden Germany
JP.JAMSTEC	Japan Agency for Marine Earth Science and Technology 2-15, Natsushimacho Yokosuka Kanagawa 237-0061 Japan
DE.MPIMM	Max-Planck-Institut für Marine Mikrobiologie Celsiusstraße 1 28359 Bremen Germany
DE.UBONN	Rheinische Friedrich-Wilhelms-Universität Bonn Meckenheimer Allee 169 Poppelsdorfer Schloß 53115 Bonn Germany

Institution	Address
UK.USTRAT	University of Strathclyde Department of Civil and Environmental Engineering 16 Richmond Street Glasgow G1 1XQ United Kingdom
US.WHOI	Woods Hole Oceanographic Institution 266 Woods Hole Road Woods Hole MA 02543-1050 USA

A.2 FAHRTTEILNEHMER / CRUISE PARTICIPANTS

Name / Last name	Vorname / First name	Institut / Institute	Beruf / Profession	Fachrichtung / Discipline
Allen	Deonie	UK.USTRAT	Scientist	Microplastic
Bergmann	Melanie	DE.AWI	Scientist	Biology
Busack	Michael	DE.AWI	Technician	AUV
Dannheim	Jennifer	DE.AWI	Scientist	Biology
Dischereit	Annkathrin	DE.AWI	Scientist	YIG FramJelly
Enriquez Garcia	Alberto	HeliService	Technician	Helicopter Service
Escalle	Simon	DE.AWI	Technician	Lander/Crawler
Frommhold	Lennard	DE.AWI	Technician	Moorings
Golde	Sandra	DE.GEOMAR	Student	Biology
Gotterbarm	Katharina	DE.AWI	Volunteer	Biology
Hagemann	Jonas	DE.AWI	Technician	AUV
Hampe	Hendrik	DE.GEOMAR	Technician	YIG FramJelly
Hasemann	Christiane	DE.AWI	Scientist	Biology
Havermans	Charlotte	DE.AWI	Scientist	YIG FramJelly
Hohe	Christian	DE.AWI	Technician	Marine Optics
Hoppmann	Mario	DE.AWI	Scientist	Phys. Oceanography
Jager	Harold	HeliService	Pilot	Helicopter Service
John	Uwe	DE.AWI	Scientist	Ecological Chemistry
Kim	Dong-gyun	DE.AWI	Scientist	Biology
Klüver	Tania	DE.GEOMAR	Technician	Biology
Knüppel	Nadine	DE.AWI	Technician	Biology
Köhler	Klara	DE.AWI	Student	Biogeochemistry
Konrad	Christian	DE.AWI	Technician	Biology
Kraberg	Alexandra	DE.AWI	Scientist	Biology
Lehmenhecker	Sascha	DE.AWI	Engineer	AUV
Lochthofen	Normen	DE.AWI	Engineer	Moorings
Ludszuweit	Janine	DE.AWI	Technician	Moorings
McPherson	Rebecca	DE.AWI	Scientist	Phys. Oceanography
Merten	Véronique	DE.GEOMAR	Scientist	YIG FramJelly
Metfies	Katja	DE.AWI	Scientist	Biology
Meyer-Kaiser	Kirstin	US.WHOI	Scientist	Biology
Nicolaus	Anja	DE.AWI	Technician	Biology
Nordhausen	Axel	DE.MPIMM	Technician	Lander/Crawler
Otte	Frank	DWD	Technician	Meteorology
Pallentin	Malte	DE.AWI	Technician	Lander / Crawler

Name / Last name	Vorname / First name	Institut / Institute	Beruf / Profession	Fachrichtung / Discipline
Pantiukhin	Dmitrii	DE.AWI	Scientist	YIG FramJelly
Picard	Xavier	HeliService	Technician	Helicopter Service
Purser	Autun	DE.AWI	Scientist	AUV
Richter	Roland	HeliService	Engineer	Helicopter Service
Schiller	Elena	DE.AWI	Technician	Lander/Crawler
Schnier	Jannik	DE.AWI	Scientist	Biology
Scholz	Daniel	DE.AWI	Technician	Biogeochemistry
Schrage	Kharis	US.WHOI	Student	Biology
Soltwedel	Thomas	DE.AWI	Scientist	Chief Scientist
Strickmann	Tobias	DE.AWI	Student	Biology
Suter	Patrick	DWD	Scientist	Meteorology
Uthoff	Antonia	DE.AWI	Scientist	Ecological Chemistry
Verhaegen	Gerlien	JP.JAMSTEC	Scientist	YIG FramJelly
von Jackowski	Anabel	DE.GEOMAR	Scientist	Biology
Weiss	Josefine	DE.UBONN	Scientist	Biology
Wenzel	Julia	DWD	Scientist	Meteorology
Wenzhöfer	Frank	DE.AWI	Scientist	Lander/Crawler
Xi	Hongyan	DE.AWI	Scientist	Marine Optics

A.3 SCHIFFSBESATZUNG / SHIP'S CREW

No.	Name / Last name	Vorname / First name	Rang / Rank
1	Schwarze	Stefan	Master
2	Spielke	Steffen	Chiefmate
3	Heuck	Sören Hinnerk	Chief
4	Buchholz	Conrad	2nd Mate
5	Fallei	Holger	2nd Mate
6	Langhinrichs	Jacob	2nd Mate
7	Hofmann	Jörg Walter	CommOffc
8	Gößmann-Lange	Petra	Ships doc
9	Brose	Thomas Christian	2nd. Eng.
10	Haack	Michael Detlev	2nd. Eng.
11	Kästner	Manfred Andre	2nd. Eng.
12	Redmer	Jens Dirk	E-Eng.
13	Dimmler	Werner	ELO
14	Frank	Gerhard Ansgar	ELO
15	Krüger	Lars	ELO
16	Nasis	Ilias	ELO
17	Sedlak	Andreas Enrico	Bosun
18	Neisner	Winfried	Carpen.
19	Grünwald	Marlin	MP Rat.
20	Klinger	Dana Maria	MP Rat.
21	Kreutzmann	Lennart	MP Rat.
22	Meier	Jan	MP Rat.
23	Möller	Falko	MP Rat.
24	Bäcker	Andreas	AB
25	Burzan	Gerd-Ekkehard	AB
26	Wende	Uwe	AB
27	Preußner	Jörg	Storek.
28	Gebhardt	Norman	MP Rat.
29	Hilliger	Maik	MP Rat.
30	Rhau	Lars-Peter	MP Rat.
31	Schwarz	Uwe	MP Rat.
32	Teichert	Uwe	MP Rat.
33	Marquardt	Geron	Cook
34	Silinski	Frank	Cooksm.
35	Zahn	Maren	Cooksm.
36	Czyborra	Bärbel	Chief Stew.
37	Braun	Maja Alexandra	Nurse

38	Arendt	René	2nd Stew.
39	Chen	Quan Lun	2nd Stew.
40	Krause	Tomasz	2nd Stew.
41	Pieper	Daniel	2nd Stew.
42	Silinski	Carmen	2nd Stew.
43	Hu	Guoyong	Laundrym.
44	Lenz	Julian Alexander	Apprent.
45	Stellamanns	Thies Christian	Apprent.

A.4 STATIONSLISTE / STATION LIST PS126

Tab. A.4: Station list of expedition PS126 from Bremerhaven to Bremerhaven; the list details the action log for all stations along the cruise track.

See https://www.pangaea.de/expeditions/events/PS126 to display the station (event) list for expedition PS126.
This version contains Uniform Resource Identifiers for all sensors listed under https://sensor.awi.de.
See https://www.awi.de/en/about-us/service/computing-centre/data-flow-framework.html for further information about AWI's data flow framework from sensor observations to archives (O2A).

Event label	Date/Time	Latitude	Longitude	Depth [m]	Gear	Action	Comment
PS126_0_Underway-28	2021-05-24T09:28:40	53.56699	8.55514		SWEAS	max depth	
PS126_0_Underway-26	2021-05-26T07:26:12	60.76380	3.15063	257.0	UWS	max depth	
PS126_0_Underway-25	2021-05-26T07:27:07	60.76621	3.14962	257.0	UAS	max depth	
PS126_0_Underway-24	2021-05-26T07:27:25	60.76694	3.14930	256.0	TSG	Station start	
PS126_0_Underway-24	2021-05-26T07:27:25	54.85775	6.87467	20.3	TSG	Station end	
PS126_0_Underway-23	2021-05-26T07:28:08	60.76882	3.14850	258.0	TSG	Station start	
PS126_0_Underway-23	2021-05-26T07:28:08	54.85912	6.87361	20.7	TSG	Station end	
PS126_0_Underway-22	2021-05-26T07:28:33	60.76994	3.14796	258.0	SNDVELPR	Station start	
PS126_0_Underway-22	2021-05-26T07:28:33	53.71721	8.28554	7.0	SNDVELPR	Station end	
PS126_0_Underway-18	2021-05-26T07:31:40	60.77840	3.14431	262.0	pCO2	Station start	
PS126_0_Underway-18	2021-05-26T07:31:40	53.71788	8.28379	6.6	pCO2	Station end	
PS126_0_Underway-17	2021-05-26T07:32:30	60.78072	3.14333	264.0	pCO2	Station start	
PS126_0_Underway-17	2021-05-26T07:32:30	53.71898	8.28094	6.7	pCO2	Station end	
PS126_0_Underway-14	2021-05-26T07:40:03	60.79886	3.13552	268.0	NEUMON	max depth	
PS126_0_Underway-12	2021-05-26T07:40:32	60.80009	3.13507	269.0	GRAV	max depth	
PS126_0_Underway-9	2021-05-26T07:40:55	60.80104	3.13472	270.0	HVAIR	max depth	
PS126_0_Underway-7	2021-05-26T07:42:32	60.80517	3.13296	272.0	FBOX	Station start	
PS126_0_Underway-7	2021-05-26T07:42:32	54.86216	6.87124	21.3	FBOX	Station end	

Event label	Date/Time	Latitude	Longitude	Depth [m]	Gear	Action	Comment
PS126_0_Underway-6	2021-05-26T07:42:54	60.80619	3.13252	273.0	MYON	max depth	
PS126_0_Underway-2	2021-05-26T07:45:03	60.81187	3.13016	274.0	AFIM	Station start	
PS126_0_Underway-2	2021-05-26T07:45:03	53.71977	8.27879	6.7	AFIM	Station end	
PS126_0_Underway-1	2021-05-26T07:45:33	60.81324	3.12962	274.0	ADCP	Station start	
PS126_0_Underway-1	2021-05-26T07:45:33	54.86353	6.87013	21.6	ADCP	Station end	
PS126_0_Underway-27	2021-05-26T07:46:41	60.81636	3.12847	275.0	W-RADAR	Station start	
PS126_0_Underway-27	2021-05-26T07:46:41	68.30450	3.66865	1896.3	W-RADAR	Station end	
PS126_0_Underway-11	2021-05-26T08:36:34	60.94702	3.10305	332.0	MAG	max depth	
PS126_1-1	2021-05-30T06:13:23	78.62036	6.80082	1786.5	B_LANDER	Station start	Larvae-Lander 1
PS126_1-1	2021-05-30T06:13:23	78.62435	6.78493	1772.5	B_LANDER	Station end	Larvae-Lander 1
PS126_1-2	2021-05-30T06:42:17	78.62159	6.80238	1776.7	AUV_lab	Station start	AUV Paul
PS126_1-2	2021-05-30T06:42:17	78.62098	6.76136	1808.8	AUV_lab	Station end	AUV Paul
PS126_1-3	2021-05-30T09:16:01	78.62186	6.80503	1771.8	HN	Station start	
PS126_1-3	2021-05-30T09:16:01	78.62160	6.80255	1774.6	HN	Station end	
PS126_1-4	2021-05-30T10:58:24	78.62166	6.80137	1775.5	OFOBS	max depth	
PS126_1-5	2021-05-30T12:08:24	78.62191	6.80008	1774.9	CTD-RO	max depth	
PS126_1-6	2021-05-30T13:39:39	78.62183	6.80118	1774.8	TVMUC	max depth	
PS126_1-7	2021-05-30T14:30:11	78.62185	6.80388	1773.3	RAMSES	Station start	
PS126_1-7	2021-05-30T14:30:11	78.62198	6.80858	1770.0	RAMSES	Station end	
PS126_1-8	2021-05-30T16:19:46	78.62423	6.75348	1798.7	MSN	max depth	
PS126_1-9	2021-05-30T16:46:01	78.62659	6.75401	1782.5	FTRW-P	max depth	
PS126_2-1	2021-05-30T20:11:41	78.60900	5.06614	2338.0	B_LANDER	Station start	Larvae Lander
PS126_2-1	2021-05-30T20:11:41	78.60502	5.07437	2338.2	B_LANDER	Station end	Larvae Lander
PS126_2-2	2021-05-30T21:38:03	78.60905	5.06539	2338.1	CTD-RO	max depth	
PS126_2-3	2021-05-30T23:02:26	78.60895	5.06570	2338.5	PARCA	Station start	
PS126_2-3	2021-05-30T23:02:26	78.60877	5.06388	2338.7	PARCA	Station end	
PS126_2-4	2021-05-30T23:59:09	78.60883	5.06432	2342.4	LOKI	Station start	

Event label	Date/Time	Latitude	Longitude	Depth [m]	Gear	Action	Comment
PS126_2-4	2021-05-30T23:59:09	78.60807	5.02315	2357.3	LOKI	Station end	
PS126_2-5	2021-05-31T01:17:16	78.60863	5.06346	2339.5	MSN	max depth	
PS126_2-6	2021-05-31T03:37:11	78.60845	5.06278	2340.2	MSN	max depth	
PS126_2-7	2021-05-31T05:42:18	78.60905	5.06522	2339.3	BONGO	Station start	
PS126_2-7	2021-05-31T05:42:18	78.64029	5.20315	2337.1	BONGO	Station end	
PS126_2-8	2021-05-31T07:22:57	78.63935	5.20153	2336.2	EBS	max depth	
PS126_2-9	2021-05-31T08:27:15	78.60661	5.06680	2338.5	OFOS	max depth	
PS126_2-10	2021-05-31T12:37:44	78.56090	5.45508	2079.5	RAMSES	Station start	
PS126_2-10	2021-05-31T12:37:44	78.56204	5.45572	2085.6	RAMSES	Station end	
PS126_2-11	2021-05-31T14:33:27	78.60884	5.06448	2339.2	CTD-RO	max depth	
PS126_2-12	2021-05-31T16:07:26	78.61073	5.06435	2339.2	PC	max depth	
PS126_2-13	2021-05-31T19:24:56	78.60506	5.07355	2337.8	TVMUC	max depth	
PS126_2-14	2021-05-31T21:31:31	78.60457	5.07502	2337.8	BC	max depth	
PS126_2-15	2021-06-01T00:27:00	78.61681	5.00018	2363.0	OFOBS	Station start	
PS126_2-15	2021-06-01T00:27:00	78.61677	5.16035	2349.7	OFOBS	Station end	
PS126_3-1	2021-06-01T09:40:49	79.07740	4.39906	2280.8	CTD-RO	max depth	
PS126_3-2	2021-06-01T11:01:10	79.07148	4.44107	2276.9	RAMSES	Station start	
PS126_3-2	2021-06-01T11:01:10	79.06832	4.46357	2278.1	RAMSES	Station end	
PS126_3-3	2021-06-01T12:06:50	79.06711	4.47867	2282.7	CTD-RO	max depth	
PS126_3-4	2021-06-01T13:13:02	79.02336	4.26923	2599.6	MOOR	Station start	HG-IV-S-4; recovery
PS126_3-4	2021-06-01T13:13:02	79.00906	4.36775	2588.4	MOOR	Station end	HG-IV-S-4; recovery
PS126_3-5	2021-06-01T15:56:19	79.00290	4.33341	2608.8	MOOR	Station start	FEVIE-40; recovery
PS126_3-5	2021-06-01T15:56:19	78.98761	4.41907	2599.1	MOOR	Station end	FEVIE-40; recovery
PS126_3-6	2021-06-01T19:31:33	79.06482	4.18052	2463.4	PARCA	Station start	
PS126_3-6	2021-06-01T19:31:33	79.06486	4.18619	2458.6	PARCA	Station end	
PS126_3-7	2021-06-01T20:25:14	79.06504	4.18309	2460.0	LOKI	Station start	
PS126_3-7	2021-06-01T20:25:14	79.06486	4.18489	2460.0	LOKI	Station end	

Event label	Date/Time	Latitude	Longitude	Depth [m]	Gear	Action	Comment
PS126_3-8	2021-06-01T21:37:35	79.06470	4.18479	2460.1	MSN	Station start	
PS126_3-8	2021-06-01T21:37:35	79.06439	4.19168	2457.1	MSN	Station end	
PS126_3-9	2021-06-01T23:59:36	79.06483	4.19004	2455.7	MSN	max depth	
PS126_3-10	2021-06-02T02:08:30	79.06326	4.19828	2459.0	BONGO	Station start	
PS126_3-10	2021-06-02T02:08:30	79.03174	4.18335	2619.3	BONGO	Station end	
PS126_3-11	2021-06-02T03:15:25	79.03086	4.18394	2620.6	PLA	max depth	
PS126_3-12	2021-06-02T03:35:37	79.02786	4.18410	2623.8	BONGO	Station start	
PS126_3-12	2021-06-02T03:35:37	79.00064	4.16057	2688.9	BONGO	Station end	
PS126_3-13	2021-06-02T05:18:51	79.06440	4.17702	2467.6	CTD-RO	max depth	
PS126_3-14	2021-06-02T06:44:54	79.06477	4.17816	2463.9	TVMUC	max depth	
PS126_3-15	2021-06-02T08:58:51	79.06471	4.17838	2463.8	PC	max depth	
PS126_3-16	2021-06-02T11:37:03	79.06461	4.18189	2462.0	BC	max depth	
PS126_3-17	2021-06-02T12:53:44	79.06516	4.18345	2458.3	B_LANDER	Station start	FLUX Lander
PS126_3-17	2021-06-02T12:53:44	79.06351	4.19219	2460.8	B_LANDER	Station end	FLUX Lander
PS126_3-18	2021-06-02T15:18:47	79.06403	4.11337	2527.1	B_LANDER	Station start	LARVAE-Lander 2
PS126_3-18	2021-06-02T15:18:47	79.06015	4.15773	2501.5	B_LANDER	Station end	LARVAE-Lander 2
PS126_3-19	2021-06-02T17:52:33	79.04570	4.12652	2605.5	GKG	max depth	
PS126_3-20	2021-06-02T19:18:21	79.06282	4.22545	2447.2	OFOS	max depth	
PS126_3-21	2021-06-03T00:16:11	79.03585	4.17103	2616.7	OFOBS	Station start	
PS126_3-21	2021-06-03T00:16:11	79.07263	4.31304	2340.8	OFOBS	Station end	
PS126_3-22	2021-06-03T05:45:17	79.06916	4.16832	2463.2	B_LANDER	Station start	Long Term Lander
PS126_3-22	2021-06-03T05:45:17	79.06729	4.17062	2464.1	B_LANDER	Station end	Long Term Lander
PS126_3-23	2021-06-03T07:48:39	79.00020	4.33415	2611.5	MOOR	Station start	FEVI-42; deployed
PS126_3-23	2021-06-03T07:48:39	79.00006	4.33113	2612.3	MOOR	Station end	FEVI-42; deployed
PS126_3-24	2021-06-03T13:00:50	78.99048	4.31748	2635.3	TVMUC	max depth	
PS126_4-1	2021-06-03T20:11:41	79.10812	4.59970	1904.3	CTD-RO	max depth	
PS126_4-2	2021-06-03T20:45:07	79.10807	4.59940	1899.3	RAMSES	Station start	

Event label	Date/Time	Latitude	Longitude	Depth [m]	Gear	Action	Comment
PS126_4-2	2021-06-03T20:45:07	79.10823	4.59962	1896.3	RAMSES	Station end	
PS126_4-3	2021-06-03T21:29:42	79.10819	4.59979	1906.2	FLU	Station start	
PS126_4-3	2021-06-03T21:29:42	79.10830	4.61168	1918.3	FLU	Station end	
PS126_4-4	2021-06-03T23:07:13	79.10785	4.60246	1913.7	TVMUC	max depth	
PS126_4-5	2021-06-04T01:16:11	79.10787	4.60233	1912.1	PC	max depth	
PS126_4-6	2021-06-04T03:12:16	79.10844	4.60728	1914.3	GKG	max depth	
PS126_5-1	2021-06-04T04:48:58	79.06800	4.15673	2476.0	AUV_lab	Station start	AUV Paul
PS126_5-1	2021-06-04T04:48:58	79.03307	4.31933	2543.3	AUV_lab	Station end	AUV Paul
PS126_5-2	2021-06-04T07:47:27	79.07203	4.18298	2443.3	OFOBS	max depth	
PS126_5-3	2021-06-04T14:17:39	79.02183	4.40082	2541.2	MOOR	Station start	HG-IV-W4; recovery
PS126_5-3	2021-06-04T14:17:39	79.00972	4.39063	2575.5	MOOR	Station end	HG-IV-W4; recovery
PS126_6-1	2021-06-04T17:51:49	79.12078	4.88210	1620.2	CTD-RO	max depth	
PS126_6-2	2021-06-04T19:02:06	79.13528	4.92835	1502.0	RAMSES	Station start	
PS126_6-2	2021-06-04T19:02:06	79.13111	4.93511	1516.9	RAMSES	Station end	
PS126_6-3	2021-06-04T19:42:37	79.13088	4.93277	1520.0	MSN	max depth	
PS126_6-4	2021-06-04T21:13:13	79.12562	4.91905	1559.5	LOKI	Station start	
PS126_6-4	2021-06-04T21:13:13	79.12310	4.91939	1572.6	LOKI	Station end	
PS126_6-5	2021-06-04T22:33:04	79.12604	4.91656	1560.7	PARCA	Station start	
PS126_6-5	2021-06-04T22:33:04	79.12553	4.91645	1562.2	PARCA	Station end	
PS126_6-6	2021-06-05T00:20:46	79.12509	4.93459	1549.1	TVMUC	max depth	
PS126_6-7	2021-06-05T01:44:43	79.12586	4.93511	1544.6	PC	max depth	
PS126_6-8	2021-06-05T03:16:46	79.12577	4.92304	1556.1	BC	max depth	
PS126_7-1	2021-06-05T05:09:58	79.10549	4.55193	1803.5	B_LANDER	Station start	Larvae Lander 2
PS126_7-1	2021-06-05T05:09:58	79.09239	4.51115	2216.1	B_LANDER	Station end	Larvae Lander 2
PS126_8-1	2021-06-05T11:05:04	79.13359	6.09323	1277.9	CTD-RO	max depth	
PS126_8-2	2021-06-05T11:50:32	79.13501	6.09219	1278.8	RAMSES	Station start	
PS126_8-2	2021-06-05T11:50:32	79.13497	6.09187	1278.2	RAMSES	Station end	

Event label	Date/Time	Latitude	Longitude	Depth [m]	Gear	Action	Comment
PS126_8-3	2021-06-05T12:28:18	79.13489	6.09146	1278.6	PARCA	Station start	
PS126_8-3	2021-06-05T12:28:18	79.13360	6.09375	1277.3	PARCA	Station end	
PS126_8-4	2021-06-05T13:31:23	79.13353	6.09297	1279.0	LOKI	Station start	
PS126_8-4	2021-06-05T13:31:23	79.13469	6.08363	1278.7	LOKI	Station end	
PS126_8-5	2021-06-05T14:45:51	79.13448	6.08499	1277.1	MSN	max depth	
PS126_8-6	2021-06-05T16:25:58	79.13387	6.09394	1278.6	BONGO	Station start	
PS126_8-6	2021-06-05T16:25:58	79.14269	6.03485	1296.3	BONGO	Station end	
PS126_8-7	2021-06-05T17:15:29	79.16475	5.96932	1351.3	BONGO	Station start	
PS126_8-7	2021-06-05T17:15:29	79.19410	5.90336	1439.5	BONGO	Station end	
PS126_8-8	2021-06-05T18:28:45	79.19247	5.90139	1435.4	MSN	max depth	
PS126_8-9	2021-06-05T21:55:25	79.13502	6.08475	1278.6	CTD-RO	max depth	
PS126_8-10	2021-06-06T00:06:31	79.13521	6.08744	1278.9	TVMUC	max depth	
PS126_8-11	2021-06-06T01:19:10	79.13536	6.08696	1278.4	PC	max depth	
PS126_8-12	2021-06-06T02:40:24	79.13652	6.07425	1281.1	BC	max depth	
PS126_8-13	2021-06-06T04:11:18	79.13183	6.26222	1318.7	OFOBS	Station start	
PS126_8-13	2021-06-06T04:11:18	79.13408	6.11270	1276.6	OFOBS	Station end	
PS126_9-1	2021-06-06T09:01:02	79.02995	6.99321	1302.4	B_LANDER	Station start	arcFOCE-Lander
PS126_9-1	2021-06-06T09:01:02	79.03564	6.98186	1309.7	B_LANDER	Station end	arcFOCE-Lander
PS126_9-2	2021-06-06T09:34:22	79.01510	6.97272	1272.3	MOOR	Station start	F4-S-4; deployed
PS126_9-2	2021-06-06T09:34:22	79.03600	6.89193	1297.4	MOOR	Station end	F4-S-4; deployed
PS126_9-3	2021-06-06T12:23:39	79.00395	7.01343	1259.8	MOOR	Station start	F4-19
PS126_9-3	2021-06-06T12:23:39	79.01587	7.03599	1284.4	MOOR	Station end	F4-19
PS126_9-4	2021-06-06T14:18:20	79.01410	7.04464	1282.4	MOOR	Station start	F4-W-2; recovery
PS126_9-4	2021-06-06T14:18:20	79.02107	7.07070	1297.0	MOOR	Station end	F4-W-2; recovery
PS126_9-5	2021-06-06T16:53:47	79.02332	7.08376	1302.2	CTD-RO	max depth	
PS126_9-6	2021-06-06T17:48:38	79.02274	7.08440	1301.3	RAMSES	Station start	
PS126_9-6	2021-06-06T17:48:38	79.02188	7.09012	1300.3	RAMSES	Station end	

Event label	Date/Time	Latitude	Longitude	Depth [m]	Gear	Action	Comment
PS126_9-7	2021-06-06T18:26:08	79.02181	7.09156	1301.1	FLU	Station start	
PS126_9-7	2021-06-06T18:26:08	79.02054	7.09571	1298.8	FLU	Station end	
PS126_9-8	2021-06-06T18:59:32	79.02025	7.09490	1298.1	MSN	max depth	
PS126_9-9	2021-06-06T20:26:03	79.02070	7.09367	1298.8	BONGO	Station start	
PS126_9-9	2021-06-06T20:26:03	78.98001	7.04712	1221.2	BONGO	Station end	
PS126_9-10	2021-06-06T22:12:29	78.98187	7.04652	1219.9	BONGO	Station start	
PS126_9-10	2021-06-06T22:12:29	79.01368	7.07700	1285.7	BONGO	Station end	
PS126_9-11	2021-06-06T23:18:43	79.02085	7.08441	1298.0	PARCA	Station start	
PS126_9-11	2021-06-06T23:18:43	79.02125	7.08440	1298.8	PARCA	Station end	
PS126_9-12	2021-06-07T00:51:17	79.02084	7.08389	1298.0	TVMUC	max depth	
PS126_9-13	2021-06-07T02:14:24	79.02158	7.08608	1299.2	PC	max depth	
PS126_9-14	2021-06-07T03:39:34	79.02449	7.06877	1302.3	BC	max depth	
PS126_10-1	2021-06-07T17:46:48	78.99995	7.99810	1099.9	B_LANDER	Station start	Foodfall-Lander
PS126_10-1	2021-06-07T17:46:48	78.99899	7.97880	1108.8	B_LANDER	Station end	Foodfall-Lander
PS126_11-1	2021-06-07T18:53:03	78.99980	8.25025	898.1	CTD-RO	max depth	
PS126_11-2	2021-06-07T19:33:09	78.99998	8.25128	897.9	RAMSES	Station start	
PS126_11-2	2021-06-07T19:33:09	79.00038	8.25358	897.3	RAMSES	Station end	
PS126_12-1	2021-06-07T21:58:32	78.98022	9.51587	231.4	RAMSES	Station start	
PS126_12-1	2021-06-07T21:58:32	78.98023	9.51581	231.7	RAMSES	Station end	
PS126_12-2	2021-06-07T22:27:27	78.98032	9.51594	231.4	MSN	max depth	
PS126_12-3	2021-06-07T23:12:17	78.98077	9.50862	230.3	BONGO	Station start	
PS126_12-3	2021-06-07T23:12:17	78.98446	9.47639	232.8	BONGO	Station end	
PS126_12-4	2021-06-07T23:34:44	78.98421	9.48229	233.6	BONGO	Station start	
PS126_12-4	2021-06-07T23:34:44	78.98022	9.52531	232.0	BONGO	Station end	
PS126_12-5	2021-06-08T00:27:45	78.98023	9.51543	231.2	CTD-RO	max depth	
PS126_12-6	2021-06-08T01:22:59	78.98022	9.51487	230.7	TVMUC	max depth	
PS126_13-1	2021-06-08T03:46:13	79.03119	11.08813	0.0	RAMSES	Station start	

Event label	Date/Time	Latitude	Longitude	Depth [m]	Gear	Action	Comment
PS126_13-1	2021-06-08T03:46:13	79.03067	11.08826	0.0	RAMSES	Station end	
PS126_13-2	2021-06-08T04:22:34	79.03023	11.08871	0.0	FLU	Station start	
PS126_13-2	2021-06-08T04:22:34	79.03109	11.08837	0.0	FLU	Station end	
PS126_13-3	2021-06-08T05:10:37	79.03030	11.08761	0.0	CTD-RO	max depth	
PS126_13-4	2021-06-08T05:46:27	79.03033	11.08823	0.0	PARCA	Station start	
PS126_13-4	2021-06-08T05:46:27	79.03029	11.08788	230.7	PARCA	Station end	
PS126_13-5	2021-06-08T06:33:05	79.03075	11.08770	0.0	TVMUC	max depth	
PS126_14-1	2021-06-08T12:54:04	78.99992	7.00024	1243.8	MOOR	Station start	F4-20; deployed
PS126_14-1	2021-06-08T12:54:04	78.99962	6.99802	1241.2	MOOR	Station end	F4-20; deployed
PS126_14-2	2021-06-08T15:32:55	79.01220	6.96389	1261.5	MOOR	Station start	F4-S-5 N; deployed
PS126_14-2	2021-06-08T15:32:55	79.01181	6.96341	1259.9	MOOR	Station end	F4-S-5 N; deployed
PS126_14-3	2021-06-08T17:53:33	79.01205	7.03618	1276.9	MOOR	Station start	F4-W3; deployed
PS126_14-3	2021-06-08T17:53:33	79.01183	7.03416	1276.5	MOOR	Station end	F4-W3; deployed
PS126_15-1	2021-06-08T22:21:17	79.13463	6.05840	1283.3	BC	max depth	
PS126_16-1	2021-06-09T02:04:43	78.83331	6.66575	1779.8	B_LANDER	Station start	arcFOCE-Lander
PS126_16-1	2021-06-09T02:04:43	78.83831	6.66260	1782.9	B_LANDER	Station end	arcFOCE-Lander
PS126_17-1	2021-06-09T15:11:01	79.60399	5.16993	2784.6	B_LANDER	Station start	LARVAE-Lander 1, rescue mission failed
PS126_17-1	2021-06-09T15:11:01	79.59734	5.16343	2789.5	B_LANDER	Station end	LARVAE-Lander 1, rescue mission failed
PS126_17-2	2021-06-09T17:10:05	79.60369	5.15855	2793.4	CTD-RO	max depth	
PS126_17-3	2021-06-09T17:46:37	79.60147	5.14501	2803.4	RAMSES	Station start	
PS126_17-3	2021-06-09T17:46:37	79.60040	5.13912	2807.0	RAMSES	Station end	
PS126_17-4	2021-06-09T19:24:56	79.60100	5.14047	2807.0	TVMUC	max depth	
PS126_17-5	2021-06-09T21:38:23	79.60094	5.17600	2785.0	PC	max depth	
PS126_17-6	2021-06-09T23:58:57	79.59800	5.17168	2786.5	BC	max depth	
PS126_18-1	2021-06-10T03:34:48	79.73246	4.47650	2683.2	CTD-RO	max depth	

Event label	Date/Time	Latitude	Longitude	Depth [m]	Gear	Action	Comment
PS126_18-2	2021-06-10T04:08:44	79.72778	4.45578	2702.0	RAMSES	Station start	
PS126_18-2	2021-06-10T04:08:44	79.72261	4.42987	2724.0	RAMSES	Station end	
PS126_18-3	2021-06-10T04:52:53	79.72143	4.42264	2730.8	MSN	max depth	
PS126_18-4	2021-06-10T06:43:55	79.71255	4.33242	2801.0	BONGO	Station start	
PS126_18-4	2021-06-10T06:43:55	79.71076	4.29333	2865.6	BONGO	Station end	
PS126_18-5	2021-06-10T07:37:40	79.71077	4.29695	2862.5	BONGO	Station start	
PS126_18-5	2021-06-10T07:37:40	79.71072	4.29148	2868.9	BONGO	Station end	
PS126_18-6	2021-06-10T08:07:13	79.71033	4.28226	2878.7	B_LANDER	Station start	FLUX-Lander
PS126_18-6	2021-06-10T08:07:13	79.70889	4.23162	2931.0	B_LANDER	Station end	FLUX-Lander
PS126_18-7	2021-06-10T11:46:14	79.70420	4.27553	2916.0	CTD-RO	max depth	
PS126_18-8	2021-06-10T14:52:20	79.73921	4.50599	2652.3	MOOR	Station start	FEVI-39; recovery
PS126_18-8	2021-06-10T14:52:20	79.73027	4.48523	2718.2	MOOR	Station end	FEVI-39; recovery
PS126_18-9	2021-06-10T19:36:10	79.72890	4.50164	2752.9	TVMUC	max depth	
PS126_18-10	2021-06-10T21:41:53	79.73004	4.48591	2723.7	PC	max depth	
PS126_18-11	2021-06-11T00:10:15	79.73084	4.51595	2782.3	BC	max depth	
PS126_18-12	2021-06-11T07:44:28	79.74041	4.48656	2616.2	PARCA	Station start	
PS126_18-12	2021-06-11T07:44:28	79.74051	4.47124	2618.8	PARCA	Station end	
PS126_19-1	2021-06-12T00:45:27	79.93917	3.05493	2593.5	LOKI	Station start	
PS126_19-1	2021-06-12T00:45:27	79.93940	3.05279	2593.8	LOKI	Station end	
PS126_19-2	2021-06-12T02:10:17	79.93931	3.05293	2593.8	MSN	max depth	
PS126_19-3	2021-06-12T04:04:36	79.94387	3.03447	2596.1	MSN	max depth	
PS126_19-4	2021-06-12T05:45:25	79.94099	3.12188	2566.2	MOOR	Station start	HG-N-S-1; recovery
PS126_19-4	2021-06-12T05:45:25	79.94016	3.03514	2600.7	MOOR	Station end	HG-N-S-1; recovery
PS126_19-5	2021-06-12T08:40:13	79.93272	3.01406	2618.3	CTD-RO	max depth	
PS126_19-6	2021-06-12T09:59:35	79.94138	3.09218	2575.5	RAMSES	Station start	
PS126_19-6	2021-06-12T09:59:35	79.93683	3.05633	2594.9	RAMSES	Station end	
PS126_19-7	2021-06-12T11:34:12	79.93160	2.98079	2634.6	TVMUC	max depth	

Event label	Date/Time	Latitude	Longitude	Depth [m]	Gear	Action	Comment
PS126_19-8	2021-06-12T13:59:15	79.94348	3.03186	2597.3	BC	max depth	
PS126_19-9	2021-06-12T15:04:46	79.94714	2.99805	2606.8	FLU	Station start	
PS126_19-9	2021-06-12T15:04:46	79.94669	2.98987	2613.4	FLU	Station end	
PS126_20-1	2021-06-13T07:54:01	78.81384	-2.75891	2599.0	B_LANDER	Station start	Flux Lander; Rescue mission aborted
PS126_20-1	2021-06-13T07:54:01	78.78638	-2.85288	2594.3	B_LANDER	Station end	Flux Lander; Rescue mission aborted
PS126_20-2	2021-06-13T11:42:41	78.80911	-2.81069	2593.8	CTD-RO	max depth	
PS126_20-3	2021-06-13T14:25:47	78.81049	-2.69978	2611.2	RAMSES	Station start	
PS126_20-3	2021-06-13T14:25:47	78.80097	-2.73224	2611.5	RAMSES	Station end	
PS126_20-4	2021-06-13T15:06:29	78.79963	-2.73726	2611.4	MSN	max depth	
PS126_20-5	2021-06-13T18:05:34	78.75880	-2.61910	2638.0	BONGO	Station start	
PS126_20-5	2021-06-13T18:05:34	78.76193	-2.60174	2640.5	BONGO	Station end	
PS126_20-6	2021-06-13T19:18:43	78.75832	-2.61829	2638.0	CTD-RO	max depth	
PS126_20-7	2021-06-13T20:10:49	78.72152	-2.52709	2667.0	OFOS	max depth	
PS126_20-8	2021-06-14T03:00:47	78.82921	-2.62405	2620.3	CTD-RO	max depth	
PS126_20-9	2021-06-14T04:29:49	78.81072	-2.64271	2623.9	TVMUC	max depth	
PS126_20-10	2021-06-14T06:28:41	78.77274	-2.70552	2621.1	PC	max depth	
PS126_20-11	2021-06-14T09:09:35	78.74222	-2.87938	2576.8	BC	max depth	
PS126_20-12	2021-06-14T17:40:08	78.87674	-3.03461	2515.6	OFOBS	Station start	
PS126_20-12	2021-06-14T17:40:08	78.79573	-3.19740	2469.1	OFOBS	Station end	
PS126_21-1	2021-06-15T04:18:27	79.00096	-5.49112	983.7	B_LANDER	Station start	FOODFALL-LANDER
PS126_21-1	2021-06-15T04:18:27	78.99374	-5.56462	911.8	B_LANDER	Station end	FOODFALL-LANDER
PS126_21-2	2021-06-15T04:22:48	79.00044	-5.49471	981.0	B_LANDER	Station start	Long Term Lander, recovery
PS126_21-2	2021-06-15T04:22:48	79.00175	-5.46019	1004.8	B_LANDER	Station end	Long Term Lander, recovery
PS126_21-3	2021-06-15T05:28:24	78.99618	-5.44162	1001.1	TRAMPER	max depth	

Event label	Date/Time	Latitude	Longitude	Depth [m]	Gear	Action	Comment
PS126_21-4	2021-06-15T08:23:35	78.99442	-5.40263	1023.3	MOOR	Station start	EGC 6; recovery
PS126_21-4	2021-06-15T08:23:35	78.99022	-5.46501	973.9	MOOR	Station end	EGC 6; recovery
PS126_21-5	2021-06-15T10:37:24	78.99491	-5.53628	937.0	CTD-RO	max depth	
PS126_21-6	2021-06-15T13:00:33	78.99016	-5.58688	888.8	RAMSES	Station start	
PS126_21-6	2021-06-15T13:00:33	78.98548	-5.64008	836.3	RAMSES	Station end	
PS126_21-7	2021-06-15T13:40:53	78.98558	-5.64714	829.4	LOKI	Station start	
PS126_21-7	2021-06-15T13:40:53	78.98417	-5.72337	767.3	LOKI	Station end	
PS126_21-8	2021-06-15T15:40:18	78.98919	-5.33773	1060.7	MSN	max depth	
PS126_21-9	2021-06-15T16:57:55	78.98602	-5.38162	1021.6	MSN	max depth	
PS126_21-10	2021-06-15T18:35:24	78.94871	-5.42832	942.8	BONGO	Station start	
PS126_21-10	2021-06-15T18:35:24	78.98441	-5.44257	979.1	BONGO	Station end	
PS126_21-11	2021-06-15T20:20:36	78.92604	-5.43247	890.6	BONGO	Station start	
PS126_21-11	2021-06-15T20:20:36	78.94536	-5.45876	911.8	BONGO	Station end	
PS126_21-12	2021-06-15T21:23:10	78.96053	-5.47868	919.5	CTD-RO	max depth	
PS126_21-13	2021-06-15T21:59:54	78.95429	-5.51310	884.9	PARCA	Station start	
PS126_21-13	2021-06-15T21:59:54	78.96012	-5.56005	855.3	PARCA	Station end	
PS126_21-14	2021-06-15T23:25:06	78.96646	-5.54157	878.8	TVMUC	max depth	
PS126_21-15	2021-06-16T01:06:25	79.01769	-5.62406	902.5	PC	max depth	
PS126_21-16	2021-06-16T02:12:25	79.01320	-5.65896	869.2	BC	max depth	
PS126_21-17	2021-06-16T04:34:44	78.99323	-5.29086	1104.9	MOOR	Station start	EGC-7 N; deployed
PS126_21-17	2021-06-16T04:34:44	78.98794	-5.35980	1041.1	MOOR	Station end	EGC-7 N; deployed
PS126_22-1	2021-06-17T03:02:11	78.96346	-0.00889	2545.3	CTD-RO	max depth	
PS126_22-2	2021-06-17T03:40:10	78.96397	0.00119	2548.7	RAMSES	Station start	
PS126_22-2	2021-06-17T03:40:10	78.96458	0.01398	2554.7	RAMSES	Station end	
PS126_23-1	2021-06-17T09:56:42	79.13206	2.79409	5556.0	CTD-RO	max depth	
PS126_23-2	2021-06-17T10:40:44	79.13345	2.76115	5524.4	RAMSES	Station start	
PS126_23-2	2021-06-17T10:40:44	79.13388	2.74918	5515.3	RAMSES	Station end	

Event label	Date/Time	Latitude	Longitude	Depth [m]	Gear	Action	Comment
PS126_23-3	2021-06-17T11:18:25	79.13486	2.74424	5522.2	FLU	Station start	
PS126_23-3	2021-06-17T11:18:25	79.13533	2.72272	5508.4	FLU	Station end	
PS126_23-4	2021-06-17T12:03:53	79.13544	2.71477	5488.4	LOKI	Station start	
PS126_23-4	2021-06-17T12:03:53	79.13632	2.68714	5475.2	LOKI	Station end	
PS126_23-5	2021-06-17T13:18:50	79.13673	2.68518	5476.2	MSN	max depth	
PS126_23-6	2021-06-17T15:36:53	79.13405	2.84166	5570.6	MSN	max depth	
PS126_23-7	2021-06-17T18:09:03	79.13094	2.84521	5566.8	BONGO	Station start	
PS126_23-7	2021-06-17T18:09:03	79.14896	2.77050	5576.8	BONGO	Station end	
PS126_23-8	2021-06-17T21:01:22	79.13279	2.76011	5511.4	CTD-RO	max depth	
PS126_23-9	2021-06-17T23:12:48	79.12177	2.67398	5465.4	PARCA	Station start	
PS126_23-9	2021-06-17T23:12:48	79.12031	2.64107	5441.6	PARCA	Station end	
PS126_23-10	2021-06-18T02:25:09	79.13329	2.75682	5516.1	TVMUC	max depth	
PS126_23-11	2021-06-18T06:03:33	79.13688	2.85089	5572.9	GKG	max depth	
PS126_24-1	2021-06-18T09:57:17	79.05185	3.48330	4023.0	CTD-RO	max depth	
PS126_24-2	2021-06-18T11:03:30	79.04042	3.50105	3800.3	RAMSES	Station start	
PS126_24-2	2021-06-18T11:03:30	79.03863	3.50071	3815.8	RAMSES	Station end	
PS126_24-3	2021-06-18T13:36:34	79.06127	3.46540	4060.1	TVMUC	max depth	
PS126_24-4	2021-06-18T16:19:13	79.06477	3.48381	3945.4	BC	max depth	
PS126_25-1	2021-06-18T18:15:45	79.06311	3.66090	3113.7	CTD-RO	max depth	
PS126_25-2	2021-06-18T19:20:48	79.05731	3.70428	2991.4	RAMSES	Station start	
PS126_25-2	2021-06-18T19:20:48	79.05154	3.73605	2856.8	RAMSES	Station end	
PS126_25-3	2021-06-18T21:29:55	79.06341	3.65728	3126.8	TVMUC	max depth	
PS126_25-4	2021-06-19T00:01:58	79.06471	3.66162	3107.0	PC	max depth	
PS126_25-5	2021-06-19T02:19:25	79.06016	3.67396	3109.1	BC	max depth	
PS126_26-1	2021-06-19T04:41:24	79.07181	4.17990	2445.3	OFOBS	max depth	
PS126_26-2	2021-06-19T11:36:28	79.04592	4.17446	2564.9	B_LANDER	Station start	Longterm Lander
PS126_26-2	2021-06-19T11:36:28	79.04555	4.17444	2567.1	B_LANDER	Station end	Longterm Lander

Event label	Date/Time	Latitude	Longitude	Depth [m]	Gear	Action	Comment
PS126_27-1	2021-06-19T16:36:41	79.59897	5.13246	2808.3	B_LANDER	Station start	LARVAE-Lander 1
PS126_27-1	2021-06-19T16:36:41	79.60138	5.17870	2781.0	B_LANDER	Station end	LARVAE-Lander 1
PS126_27-2	2021-06-20T01:24:46	79.56955	5.25157	2659.9	OFOBS	Station start	
PS126_27-2	2021-06-20T01:24:46	79.60249	5.15324	2797.0	OFOBS	Station end	
PS126_27-3	2021-06-20T06:47:51	79.59942	5.13275	2808.6	BC	max depth	
PS126_28-1	2021-06-20T16:19:36	79.05964	3.59702	3381.1	MUC	max depth	
PS126_28-2	2021-06-20T18:48:32	79.05763	3.58704	3432.5	PC	max depth	
PS126_28-3	2021-06-20T21:43:03	79.05938	3.58347	3468.6	BC	max depth	
PS126_28-4	2021-06-20T23:45:59	78.99883	3.67207	2943.8	BONGO	Station start	
PS126_28-4	2021-06-20T23:45:59	78.97915	3.56158	2589.3	BONGO	Station end	
PS126_28-5	2021-06-21T01:53:28	79.05961	3.59678	3381.8	CTD-RO	max depth	
PS126_28-6	2021-06-21T02:39:37	79.06030	3.58238	3451.7	PARCA	Station start	
PS126_28-6	2021-06-21T02:39:37	79.05630	3.62175	3260.5	PARCA	Station end	
PS126_28-7	2021-06-21T03:44:56	79.06237	3.52491	3757.2	RAMSES	Station start	
PS126_28-7	2021-06-21T03:44:56	79.06291	3.56333	3546.8	RAMSES	Station end	

** Comments are limited to 130 characters. See https://www.pangaea.de/expeditions/events/PS126 to show full comments in conjunction with the station (event) list for expedition PS126*

Abbreviation	Method/Device
ADCP	Acoustic Doppler Current Profiler
AFIM	AutoFim
AUV_lab	Autonomous underwater vehicle Polar Autonomous Underwater Laboratory
BC	Box corer
BONGO	Bongo net
B_LANDER	Bottom lander
CTD-RO	CTD/Rosette
EBS	Epibenthic sledge
FBOX	FerryBox
FLU	Fluorometer
FTRW-P	Pelagic fish trawl
GKG	Giant box corer
GRAV	Gravimetry
HN	Hand net
HVAIR	High volume air sampler
LOKI	Light frame on-sight keyspecies investigation
MAG	Magnetometer
MOOR	Mooring
MSN	Multiple opening/closing net
MUC	MultiCorer
MYON	DESY Myon Detector
NEUMON	Neutron monitor
OFOBS	Ocean Floor Observation and Bathymetry System
OFOS	Ocean Floor Observation System
PARCA	Particle camera
PC	Piston corer
PLA	Plankton net
RAMSES	RAMSES hyperspectral radiometer
SNDVELPR	Sound velocity probe
SWEAS	Ship Weather Station
TRAMPER	TRAMPER
TSG	Thermosalinograph
TVMUC	Multicorer with television

Abbreviation	Method/Device
UAS	Underway air sampling
UWS	Underway water sampling
W-RADAR	Wave Radar System
pCO2	pCO2 sensor

Die **Berichte zur Polar- und Meeresforschung** (ISSN 1866-3192) werden beginnend mit dem Band 569 (2008) als Open-Access-Publikation herausgegeben. Ein Verzeichnis aller Bände einschließlich der Druckausgaben (ISSN 1618-3193, Band 377-568, von 2000 bis 2008) sowie der früheren **Berichte zur Polarforschung** (ISSN 0176-5027, Band 1-376, von 1981 bis 2000) befindet sich im electronic Publication Information Center **(ePIC)** des Alfred-Wegener-Instituts, Helmholtz-Zentrum für Polar- und Meeresforschung (AWI); see https://epic.awi.de. Durch Auswahl “Reports on Polar- and Marine Research“ (via “browse”/”type”) wird eine Liste der Publikationen, sortiert nach Bandnummer, innerhalb der absteigenden chronologischen Reihenfolge der Jahrgänge mit Verweis auf das jeweilige pdf-Symbol zum Herunterladen angezeigt.

The **Reports on Polar and Marine Research** (ISSN 1866-3192) are available as open access publications since 2008. A table of all volumes including the printed issues (ISSN 1618-3193, Vol. 377-568, from 2000 until 2008), as well as the earlier **Reports on Polar Research** (ISSN 0176-5027, Vol. 1-376, from 1981 until 2000) is provided by the electronic Publication Information Center **(ePIC)** of the Alfred Wegener Institute, Helmholtz Centre for Polar and Marine Research (AWI); see URL https://epic.awi.de. To generate a list of all Reports, use the URL http://epic.awi.de and select “browse”/ ”type” to browse ”Reports on Polar and Marine Research”. A chronological list in declining order will be presented, and pdf-icons displayed for downloading.

Zuletzt erschienene Ausgaben:

Recently published issues:

757 (2021) The Expedition PS126 of the Research Vessel POLARSTERN to the Fram Strait in 2021, edited by Thomas Soltwedel with contributions of the participants

756 (2021) Russian-German Cooperation: Expeditions to Siberia in 2020, edited by Boris K. Biskaborn, Dmitry Yu. Bolshiyanov, Mikhail N. Grigoriev, Anne Morgenstern, Luidmila A. Pestryakova, Leonid V. Tsibizov, and Antonia Dill

755 (2021) The Expedition PS124 of the Research Vessel POLARSTERN to the southern Weddell Sea in 2021, edited by Hartmut H. Hellmer and Moritz Holtappels with contributions of the participants

754 (2021) MOSAiC Expedition: Airborne Surveys with Research Aircraft POLAR 5 and POLAR 6 in 2020, edited by Andreas Herber, Sebastian Becker, Hans Jakob Belter, Jörg Brauchle, André Ehrlich, Marcus Klingebiel, Thomas Krumpen, Christof Lüpkes, Mario Mech, Manuel Moser, and Manfred Wendisch

753 (2021) The Expedition PS123 of the Research Vessel POLARSTERN to NEUMAYER STATION III in 2020/2021, edited by Tim Heitland with contributions of the participants

752 (2021) Expeditions to Fennoscandia in 2020, edited by Matthias Fuchs, Lona van Delden, Nele Lehmann, and Torben Windirsch

751 (2021) The MOSES Sternfahrt Expeditions of the Research Vessels ALBIS, LITTORINA, LUDWIG PRANDTL, MYA II and UTHÖRN to the Elbe River, Elbe Estuary and German Bight in 2020, edited by Ingeborg Bussmann, Norbert Anselm, Holger Brix, Philipp Fischer, Götz Flöser, Felix Geissler, Norbert Kamjunke

750 (2021) International Online Symposium: Focus Siberian Permafrost – Terrestrial Cryosphere and Climate Change, editorial board: Pfeiffer EM, Vybornova O, Kutzbach L, Fedorova I, Knoblauch C, Tsibizov L & Beer C

749 (2021) Russian-German Cooperation: Expeditions to Siberia in 2019, edited by Matthias Fuchs, Dmitry Bolshiyanov, Mikhail Grigoriev, Anne Morgenstern, Luidmila Pestryakova, Leonid Tsibizov, and Antonia Dill

ALFRED-WEGENER-INSTITUT
HELMHOLTZ-ZENTRUM FÜR POLAR-
UND MEERESFORSCHUNG

BREMERHAVEN

Am Handelshafen 12
27570 Bremerhaven
Telefon 0471 4831-0
Telefax 0471 4831-1149
www.awi.de

HELMHOLTZ